NASA TECHNICAL NOTE

NASA TN D-3166

NASA TN D-3166

JET-INDUCED LIFT LOSSES ON VTOL CONFIGURATIONS HOVERING IN AND OUT OF GROUND EFFECT

by Garl L. Gentry and Richard J. Margason

Langley Research Center
Langley Station, Hampton, Va.

NATIONAL AERONAUTICS AND SPACE ADMINISTRATION • WASHINGTON, D. C. • FEBRUARY 1966

NASA TN D-3166

JET-INDUCED LIFT LOSSES ON VTOL CONFIGURATIONS HOVERING IN AND OUT OF GROUND EFFECT

By Garl L. Gentry and Richard J. Margason

Langley Research Center
Langley Station, Hampton, Va.

NATIONAL AERONAUTICS AND SPACE ADMINISTRATION

For sale by the Clearinghouse for Federal Scientific and Technical Information
Springfield, Virginia 22151 – Price $3.00

JET-INDUCED LIFT LOSSES ON VTOL CONFIGURATIONS HOVERING IN AND OUT OF GROUND EFFECT

By Garl L. Gentry and Richard J. Margason
Langley Research Center

SUMMARY

The effects of the pressure ratio, of the ratio of planform area to jet area, and of the wing height on the lift loss due to the suction pressures induced on the lower surface of the fuselage and wings of a VTOL aircraft by the entrainment action of the vertical efflux from the lifting jets have been investigated at small scale. The induced loads were found to amount to approximately 1 percent of the thrust for single-jet VTOL configurations and 3 to 4 percent of the thrust for multiple jets out of ground effect. The jet-induced loads were found to be a function of the square root of the ratio of planform area to jet area and were strongly influenced by the rate at which the jet entrained the surrounding air and by the distance between the area of maximum entrainment and the lower surface of the fuselage. An empirical expression for calculating the jet-induced loads was derived.

INTRODUCTION

The design of jet VTOL aircraft requires a detailed knowledge of the losses in thrust due to the jet engines installed in the aircraft. These losses include those common to conventional jet aircraft such as the inlet losses, nozzle losses, and lift losses – plus losses due to hot-gas reingestion and a different type of lift loss which is peculiar to VTOL configurations.

The present investigation is related only to the lift loss caused by the entrainment of ambient air by the exiting jets when hovering, a loss peculiar to VTOL configurations. The entrainment of the surrounding air causes a reduction in pressure on the lower surface of the fuselage and wings. This pressure loss differs from the lift loss that is encountered in conventional engine installations primarily because of the much greater extent of surface area surrounding the exit of the vertically oriented jets in VTOL aircraft and also because of the number of possible arrangements and the disposition of the jets.

Very little is currently known about the magnitude of the lift losses caused by the jets in VTOL aircraft. Some pressure-distribution investigations preliminary to the present study as well as the theory and experimental data of reference 1 indicated that the

lift loss due to a single jet would generally be less than 1 percent of the total thrust for the ratios of planform area to jet area representative of jet VTOL aircraft. The four-jet configuration of reference 2, however, indicated that lift losses of between 3 and 4 percent could be encountered for multiple-jet configurations. Losses of this magnitude can significantly affect the performance of the aircraft and must be properly allowed for in the design of the airplane. The present investigation was therefore undertaken to determine the factors influencing the magnitude of the static base loss for single- and multiple-jet configurations.

SYMBOLS

Measurements for this investigation were taken in the U.S. Customary System of Units. Equivalent values are indicated herein parenthetically in the International System (SI) in the interest of promoting use of this system in future NASA reports. Details concerning the use of SI, together with physical constants and conversion factors, are given in reference 3.

A_j	jet-exit area, $in.^2$ (cm^2)
b	wing span or plate width, in. (cm)
C_p	pressure coefficient, $\frac{p_l - p}{p_{t,p} - p}$
c_r	root chord, in. (cm)
D	diameter of jet exit, in. (cm)
D_e	effective diameter, diameter of a circle equivalent in area to total jet-exit area of a given configuration, in. (cm)
h	height from jet exit to ground, in. (cm)
l	length of jet exit, in. (cm)
ΔL	load induced on plate, lb (N)
p	ambient static pressure, lb/ft^2 (N/m^2)
p_l	local static pressure, lb/ft^2 (N/m^2)
$p_{t,p}$	plenum-chamber total pressure, lb/ft^2 (N/m^2)
q_N	jet impact pressure at exit, lb/ft^2 (N/m^2)

q_x maximum impact pressure measured at distance x downstream from jet exit, lb/ft^2 (N/m^2)

r radius of any point from center of jet exit, in. (cm)

R radius of jet or plate, in. (cm)

S plate or wing-plus-fuselage planform area, in.^{2} (cm^2)

T jet thrust, lb (N)

x distance normal to jet exit, in. (cm)

z jet exit projection beyond lower surface of fuselage or plates, in. (cm)

Subscripts:

i point of maximum rate of change of decay parameter

max maximum

MODELS, APPARATUS, TESTS, AND PROCEDURES

Models and Apparatus

Most of the data of this investigation were obtained for the airplane-type configurations shown in figures 1, 2, and 3. This model consisted of a small rectangular plenum chamber inside a fuselage shell. The bottom of the plenum chamber was removable to enable installation of different jet arrangements (fig. 3) on a common configuration. The single jet on the rectangular-plenum-chamber configuration was extended with cylindrical ducts of two different lengths. The plates were tested with various lengths of the extended jet projecting through them in order to determine the possible beneficial effects of the extension and the projection on the induced loads. Most of the data were obtained for the zero jet projection and 0.248 jet length. Additional tests were made for the following projections and lengths (shown in terms of jet diameter):

l/D	z/D
0.248	0
.910	0
.910	.5
1.410	0
1.410	.5
1.410	1.0

The model could be fitted with delta wings of various sizes or with various circular and rectangular plates, as shown in figure 4. The rectangular plenum chamber (fig. 5) was designed to fit in the scaled fuselage of the model. This requirement led to a plenum chamber which was long and rather narrow. The narrow width resulted in a small effective contraction ratio from the plenum chamber to the jet.

Inasmuch as the induced loads to be measured were expected to be only a small percentage of the total jet thrust, it was considered necessary to mount the fuselage and wings or plates of the model independently of the plenum chamber and jet assembly so that the induced loads could be measured separately from the total thrust of the jet. The arrangement used is shown in figure 5. This arrangement differs from the original plenum configuration which had different primary pressure tubes. The original tubes had larger holes which were oriented to direct the flow against the top of the plenum chamber. The fuselage consisted of a thin-wall shell fitted with a small gap around the plenum chamber and jet or jets. The induced loads on the fuselage and wings or plates were measured by a sensitive balance installed in the balance housing inside the plenum chamber as shown in figure 5. The total model forces were measured by the main balance, which was also installed in this balance chamber and attached to a sting-support system.

Air was brought into the plenum chamber through two 3/4-inch-diameter (1.91-cm) tubes that ran the length of the chamber. Each tube was drilled with 138 holes oriented as shown in figure 5 to distribute the air through the length of the chamber. The tubes extended back along the sting and were bent in a large open U-shape configuration and anchored to the support system as shown in figure 6. This method of attaching the incoming air lines provided a flexible spring connection to the balance that resulted in a very small change in the balance sensitivity. The balance was calibrated with the air lines in place and under pressure to obtain corrections to the sensitivity constants for the effects of the incoming air lines.

The model was mounted inverted as shown in figure 6 and was fitted with brackets for alternate wing positions so that high-, mid-, and low-wing configurations could be investigated.

A few of the data presented were obtained for the cylindrical-plenum-chamber configuration shown in figure 7. This apparatus consisted of a large cylindrical plenum chamber with perforated plates and screens installed to dampen the flow and fitted with a very large contraction ratio bellmouth inlet to the jet. Various size plates, as shown in figure 4, could be fitted to this configuration and supported on a flexure support system as shown in figure 7 so that only the induced loads on the plates were measured by the strain-gage unit. Both the cylindrical-plenum-chamber and the rectangular-plenum-chamber configurations were operated with a gap of 1/32 inch (0.079 cm) or less between the plate and the jet. Preliminary investigations of the cylindrical-plenum-chamber

configuration with smaller gaps, in some instances sealed with viscous damper fluid, had indicated that gaps of the order of 2 percent or less of the jet exit diameter would have a negligible effect on the data.

Tests and Procedures

Jet decay characteristics.- Jet decay characteristics were obtained by surveying the jet at various distances from the exit (with the ground board removed) with a total-pressure probe. The maximum impact pressure q_x measured at each station x from the jet exit was divided by the jet impact pressure $p_{t,p} - p$ to determine the decay parameter $\frac{q_x}{p_{t,p} - p}$. No corrections for compressibility were applied. The ground-effect tests were made by supporting a large plywood board normal to and at appropriate distances from the jets.

The loads induced on the plate are caused by the entrainment action of the surrounding air which lowers the pressures on the plate near the jet. The induced loads should therefore be a function of the amount of air entrained by the jet. The greater entrainment of surrounding air by the jets with increasing distance downstream from the exit should also cause a more rapid decay of jet impact pressure. The rate of decay of jet impact pressure with distance downstream from the exit was therefore investigated to determine whether this parameter would be a correlating factor.

Effect of plenum-chamber configuration.- The shape of the rectangular plenum chamber is quite different from the usual shape, and the possibility that the results might be affected by the effects of the plenum chamber on the flow from the jets was anticipated. Therefore, a comparison was obtained between the loads induced on a circular plate by a single jet from the rectangular plenum chamber and the loads induced on a similar plate by a single jet from the cylindrical plenum chamber. As shown in figure 8(a), the magnitudes of the loads induced on the circular plate mounted to the original rectangular plenum chamber were up to four times as large as those induced on the same plate mounted to the cylindrical plenum chamber with a clean nozzle (no flow restrictions). Surveys of the exit flow from the rectangular plenum chamber indicated a distorted impact-pressure distribution with a considerable loss at the center, as shown in figure 8(b), whereas the flow from the cylindrical plenum chamber with a clean nozzle had a perfectly flat distribution. The motion of tufts indicated that the flow from the rectangular plenum chamber was extremely rough; this extreme turbulence of the flow was assumed to be causing the higher induced loads.

In order to check this hypothesis two steps were taken: Efforts were made both to improve the quality of the flow from the rectangular plenum chamber and to produce a more turbulent flow from the cylindrical plenum chamber. For producing the more turbulent flow, a strut restriction of about 15 percent of the jet exit diameter in width was

placed across the exit on the cylindrical plenum chamber. The strut was located about 1 jet-exit diameter upstream from the exit. The cross-sectional area of the jet was less at the strut location than at the exit, but for purposes of consistency, the cross-sectional area at the exit was used as the area of the jet in the data. As can be seen in figure 8, the strut produced a very distorted exit impact-pressure distribution and increased the induced loads on the plate by almost 50 percent.

The improvements in the rectangular plenum chamber consisted of installing a fairing on the balance housing as shown in figure 5, and installing new pressure tubes which had smaller diameter holes than the original tubes. They were oriented as shown in figure 5. The original tubes had the holes oriented to direct the flow against the top of the plenum chamber where it impinged on the walls and flowed down as a sheet on the walls of the plenum chamber and balance housing. The reorientation shown in figure 5 produced a better mixing of the flow within the plenum chamber. These modifications effected an appreciable improvement in the exit impact-pressure distribution (fig. 8(b)) and an appreciable reduction in the induced loads on the plate (fig. 8(a)).

The data of figure 8 show similar induced loads for the modified rectangular plenum chamber and the cylindrical plenum chamber with the restriction in the nozzle. However, the exit impact-pressure distributions are vastly different; thus, the exit impact-pressure distribution is not a significant index of the quality of flow from the jet for predicting base losses. Additional data on other plate sizes are shown in figure 9.

RESULTS AND DISCUSSION

Jet Decay Characteristics

The jet impact pressures were measured with no plates mounted adjacent to the jet exits. Additional tests with the plates mounted gave the same decay curves. The decay curves for the cylindrical plenum chamber with the clean nozzle, the cylindrical plenum chamber with the restriction in the nozzle, and the modified rectangular plenum chamber are shown in figure 10. As can be seen, the modified rectangular plenum chamber and the cylindrical plenum chamber with the nozzle restriction have similar plate-induced load characteristics and similar decay characteristics. They both indicate significantly more rapid decay than the cylindrical plenum chamber with the clean nozzle. The decay curves for various pressure ratios for some of the jet configurations used in this investigation are shown in figure 11.

Pressure Distributions

A general flow of air at very low speeds in the direction of the exiting jet was created when the jet was operating during the tests of both plenum-chamber configurations.

In order to separate the direct effect of the jet-inducing suction pressures on the exit side of the plate from the effect of the flow normal to the plate, the cylindrical-plenum-chamber configuration with the large circular plate $\left(S/A_j = 69.5\right)$ was installed in a wall between two rooms to prevent the general flow past the model. Pressure distributions and forces were measured on the circular plate installed in the wall and on the plate in free air (finite plate). The results are presented in figures 12 and 13.

Although the measured induced loads (fig. 13) for the two installations are almost the same in magnitude, there appears to be no fundamental reason for this similarity, and it is probably a coincidence for the particular plate size used.

The results presented in figure 12 show that the pressure coefficients obtained with the plate in free air are more negative near the edge of the plate and less negative near the jet than those obtained with the plate installed in the wall. The reason for the reduction in magnitude of the pressure coefficients for the plate in free air is not understood. The more negative pressure coefficients near the edge of the plate are believed to be caused by the flow around the edge of the plate. Thus it is evident that the flow normal to the plate has a significant effect on the static-pressure distribution.

Comparison with Theory

The measured pressure distributions have been compared with the theory of reference 1 in figure 12. The measured pressures show a reduction in the magnitude of the suction pressure coefficients with increased jet pressure ratio. The theory does not account for the effects of pressure ratio, and because it assumes incompressible flow, it should be compared with the lowest pressure-ratio data measured. As can be seen in figure 12(b), the theory predicts the shape of the pressure curve for the wall installation but underestimates the magnitude of the measured pressures. Since the theory is for an infinite plate, it would not be expected to predict the increase in pressure near the edge of the finite plate (fig. 12(a)).

A theoretical prediction of the jet-induced load on the plate can be obtained by integrating the pressure distribution calculated from reference 1. The integration produces a theoretical variation of the induced loads as a function of the square root of the ratio of plate area to jet-exit area. The result is very nearly a straight line for the size of plates covered in the investigation for $\sqrt{S/A_j} > 2.0$. (See fig. 10.) It is interesting to note that the measured data are also fairly linear. However, the theoretical loads in figures 10 and 13 are lower than the measured loads on the plate because of the underprediction of the pressures.

Effect of Jet Length and Jet Projection

The effect of jet length on induced loads for the single round jet on the modified rectangular plenum chamber with rectangular-planform plates and with a jet projection of zero is presented in figure 14. Summary plots for the effect of jet length and projection are presented in figures 15 to 18. As can be seen in figures 14 and 15, extending the jet caused a slight reduction in the induced loads for the case of zero projection (that is, the plate surface coincident with the jet exit). A further reduction of induced loads was obtained by projecting the jet through the circular plate distances of 1/2 jet-exit diameter and 1 jet-exit diameter (figs. 16 and 17). This reduction is due to the increased distance between the plate and the free surface of the jet which is entraining air. A summary plot showing the effect of jet projection is presented in figure 18.

Effect of Planform Shape

In order to determine the effect of planform shape on the induced load, four plate shapes were installed on the cylindrical plenum chamber. The four shapes were circular, square, rectangular (Length/Width = 1.52), and triangular (equilateral). In all cases the ratio of plate area to jet-exit area was 69.5 and the center of the jet was located at the centroid of the plate. The results in figure 19 show no consistent effect of planform shape on the induced loads.

Effect of Single- and Multiple-Jet Configurations

Low-wing configurations.- The basic data for the jet configurations shown in figure 3 are presented in figures 20 to 23 and summarized in figure 24. The basic data are for the single-jet, the four-jet, the eight-jet, and the four-slot rectangular slotted-jet configurations; for all configurations, as the wing size is increased (all wings in low position) the induced loads similarly increase. The multiple-jet configurations produce much higher induced loads (3 to 4 percent of the thrust) than the single-jet configuration (about 1 percent). (See figure 24(a).) As shown by the decay curves (fig. 24 (b)), these higher induced loads are caused by the entrainment action which occurs closer to the surface of the plate for the multiple-jet configurations than for the single-jet configuration.

The apparent rapid decay for the four- and eight-jet configurations is due to the fact that the decay curves of figure 24(b) are presented in terms of the equivalent diameter of a single jet whose area equals the total areas of the multiple jets (4 sq in. or 25.8 sq cm). As shown in figure 25, the decay rates for the individual jets of the four- and eight-jet configurations based on their individual diameters are very nearly the same as the rate for the single-jet configuration. However, it is the decay rate based on the equivalent diameter of a multiple-jet configuration that is important in determining induced loads, because it is this decay curve that indicates the proximity of the mixing zone to the plate.

Effect of wing height.- The effects of wing height on the single-jet, four-jet, and four-slot rectangular-jet configurations are presented in figures 26 to 28 and summarized in figure 29. There is a decrease in induced loads as the wings are moved farther from the plane of the emitting jet stream. The induced load of the single-jet configuration is approximately one-half that of the four-jet and about one-third that of the slotted-jet configuration. (See fig. 29.) The reduction in induced load as the wings are raised to a higher position (fig. 29) is due to the greater distance between the wing surface and the jet which is entraining the surrounding flow.

Prediction of Induced Loads

The preceding discussion has indicated the close relationship between the rate of decay of the jet and the loads induced on the plate. Both of these parameters are functions of the amount of air drawn into the jet and the proximity of the entrainment to the plate. An attempt was made to find a parameter expressing these properties of the jet (entrainment rate and proximity to the plate) that would correlate with the induced plate loads. It was reasoned that the plate loads should be proportional to the maximum rate of change of impact pressure and inversely proportional to the distance between the plate and the point at which this maximum rate of change occurs. As shown in figure 30 the plate loads are, in fact, a function of the square root of the maximum rate of change of jet impact pressure decay with the distance from the plate at which this maximum rate of change occurs. Within the accuracy of the present investigation, and within the range of plate sizes investigated, the plate loads can be given by the following empirical expression:

$$\frac{\Delta L}{T} = -0.009 \sqrt{\frac{S}{A_j}} \sqrt{-\left[\frac{\partial\left(\frac{q_x}{p_{t,p} - p}\right)}{\partial\left(\frac{x}{D_e}\right)}\right]_{max} \left(\frac{x}{D_e}\right)_i}$$

This correlation is based on data which were obtained at small scale from cold jets at a critical pressure ratio. At present there are no data available on hot jets to permit a comparison. The data show a small decrease in induced load with increasing pressure ratio, but this decrease is within the accuracy of the correlation.

Several additional approaches were tried in attempting to correlate these data. One method, which gave similar results, was based on the area above the decay curve. The data showed that this area increased as the magnitude of the induced plate load increased. The area between the decay curve and $\frac{q_x}{p_{t,p} - p} = 1$ and between $x/D_e = 0$ and $x/D_e = 10$ was used in place of the square root of the maximum rate of change of jet impact pressure decay divided by the distance from the plate at which this maximum rate of change occurred.

Ground Effects

The ground effects that can be encountered by a jet VTOL configuration hovering within ground effect were investigated by supporting a large sheet of plywood at appropriate distances from the models. The results are presented in figures 31 to 35. Figure 31 presents the effect of height above the ground on the induced loads for the single-jet cylindrical-plenum-chamber configuration with circular planform plates of several sizes at four plenum pressures. Figures 32, 33, and 34 present similar data for the delta-wing airplane configuration with the rectangular plenum chamber. In figure 32 the data are for a single jet; in figure 33 the data are for the four-jet configurations; and in figure 34 the data are for the eight-jet configuration. All the models on which ground effects were investigated were low-wing configurations. In general, as expected from reference 4, the suction force was primarily a function of the ratio of planform area to jet area. The pressure-ratio effects that were noted within ground effect appeared to be of the same magnitude as those measured out of ground effect (fig. 34). The four-jet configuration (fig. 33) exhibited a significant reduction in the suction force very close to the ground; this reduction is attributed to the positive pressure buildup between the jets. The same effect should be encountered with the eight-jet configurations but was not measured because the tests were terminated at too high a height above the ground board.

In preliminary tests, two ground-board sizes were used with the single-jet configuration. Figure 35 shows that no significant differences in the data resulted from changing the size of the ground board. The data presented in figures 31 to 34 are from tests in which the larger ground board was used.

CONCLUDING REMARKS

A small-scale investigation of the loads induced on a flat plate by a single jet or combinations of multiple jets issuing normal to the plate (representing a jet-VTOL aircraft hovering out of ground effect) has indicated that induced loads less than 1 percent of the thrust for the single jet and as high as 3 or 4 percent of the thrust for the multiple-jet configurations were encountered. Induced loads increased with wing size and the number of jets, but could be reduced by increasing the distance between the jet exits and the wing surfaces either by increasing wing height or by increasing jet projection distance. Changes in plate planform shape had no consistent effect on the induced loads. The jet-induced loads were found to be a function of the square root of the ratio of plate area to jet-exit area. The induced loads were also very strongly influenced by the rate at which the jet entrained the surrounding air and by the distance between the area of maximum entrainment and the plate. The plate loads were found to be proportional to the square root of the maximum rate of change of impact pressure decay in the jet with distance

downstream from the jet and inversely proportional to the square root of the nondimensional distance from the plate at which this maximum occurred. An empirical expression for calculating the jet-induced loads has been presented.

Langley Research Center,
National Aeronautics and Space Administration,
Langley Station, Hampton, Va., August 27, 1965.

REFERENCES

1. Wygnanski, I.: The Flow Induced by Two-Dimensional and Axisymmetric Turbulent Jets Issuing Normally to an Infinite Plane Surface. Rept. No. 63-12 (DRB Grant No. 9551-12), Mech. Eng. Res. Lab., McGill Univ., Dec. 1963.

2. Otis, James H., Jr.: Induced Interference Effects on a Four-Jet VTOL Configuration With Various Wing Planforms in the Transition Speed Range. NASA TN D-1400, 1962.

3. Mechtly, E. A.: The International System of Units - Physical Constants and Conversion Factors. NASA SP-7012, 1964.

4. Spreemann, Kenneth P.; and Sherman, Irving R.: Effects of Ground Proximity on the Thrust of a Simple Downward-Directed Jet Beneath a Flat Surface. NACA TN 4407, 1958.

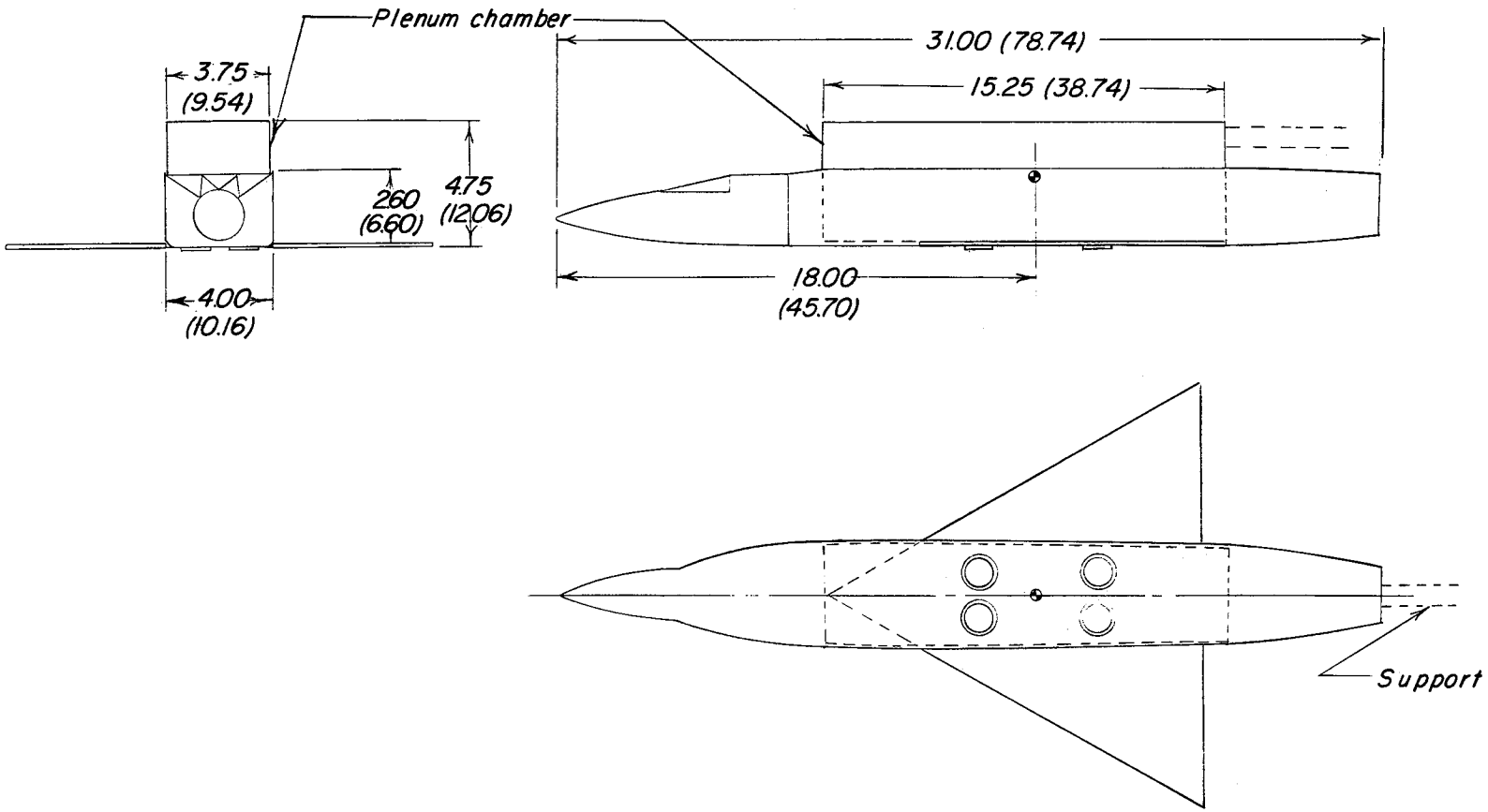

Figure 1.- General arrangement of rectangular-plenum-chamber model. All dimensions are in inches with centimeters given in parentheses.

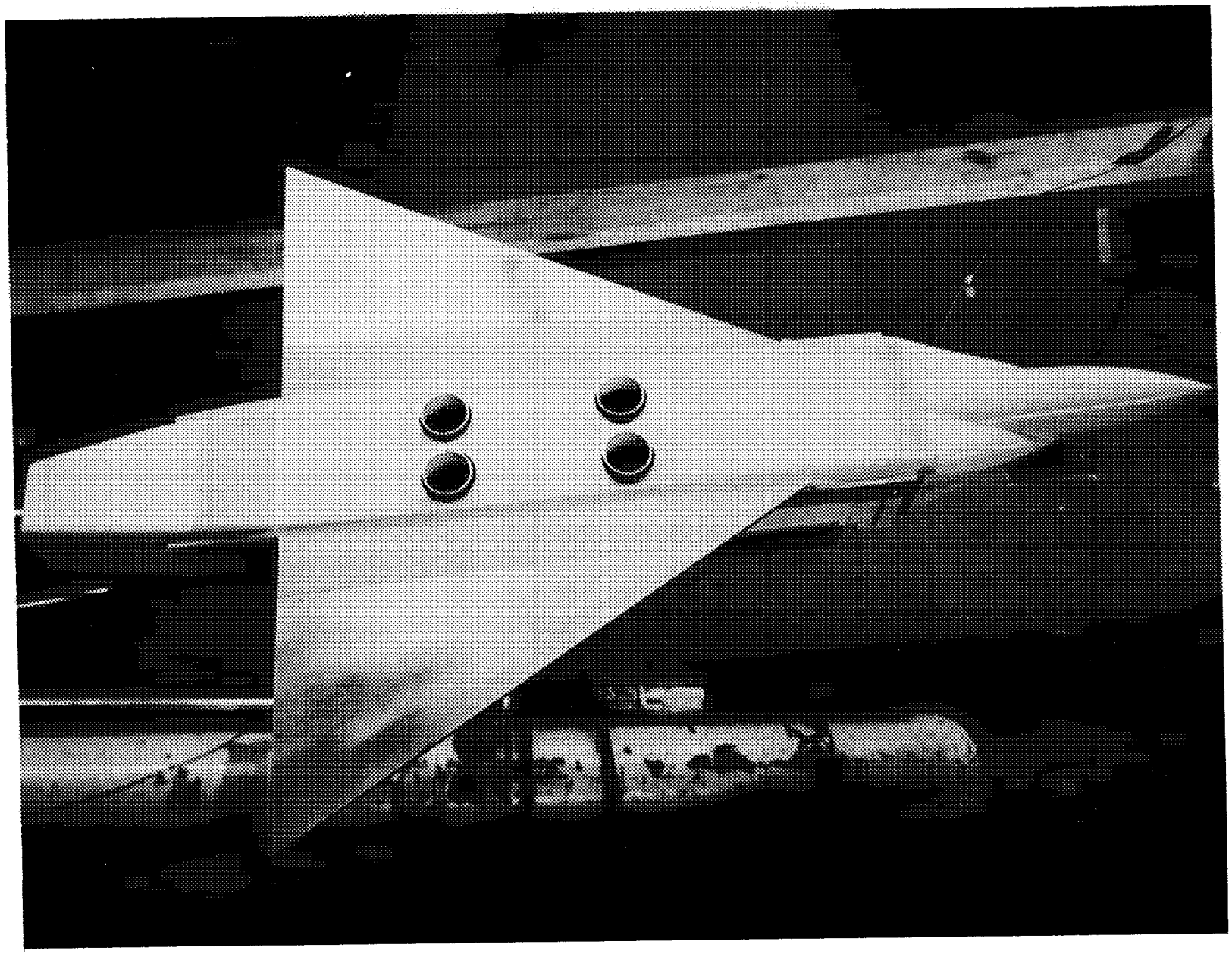

Figure 2.- Photograph of rectangular-plenum-chamber model.

L-64-9764

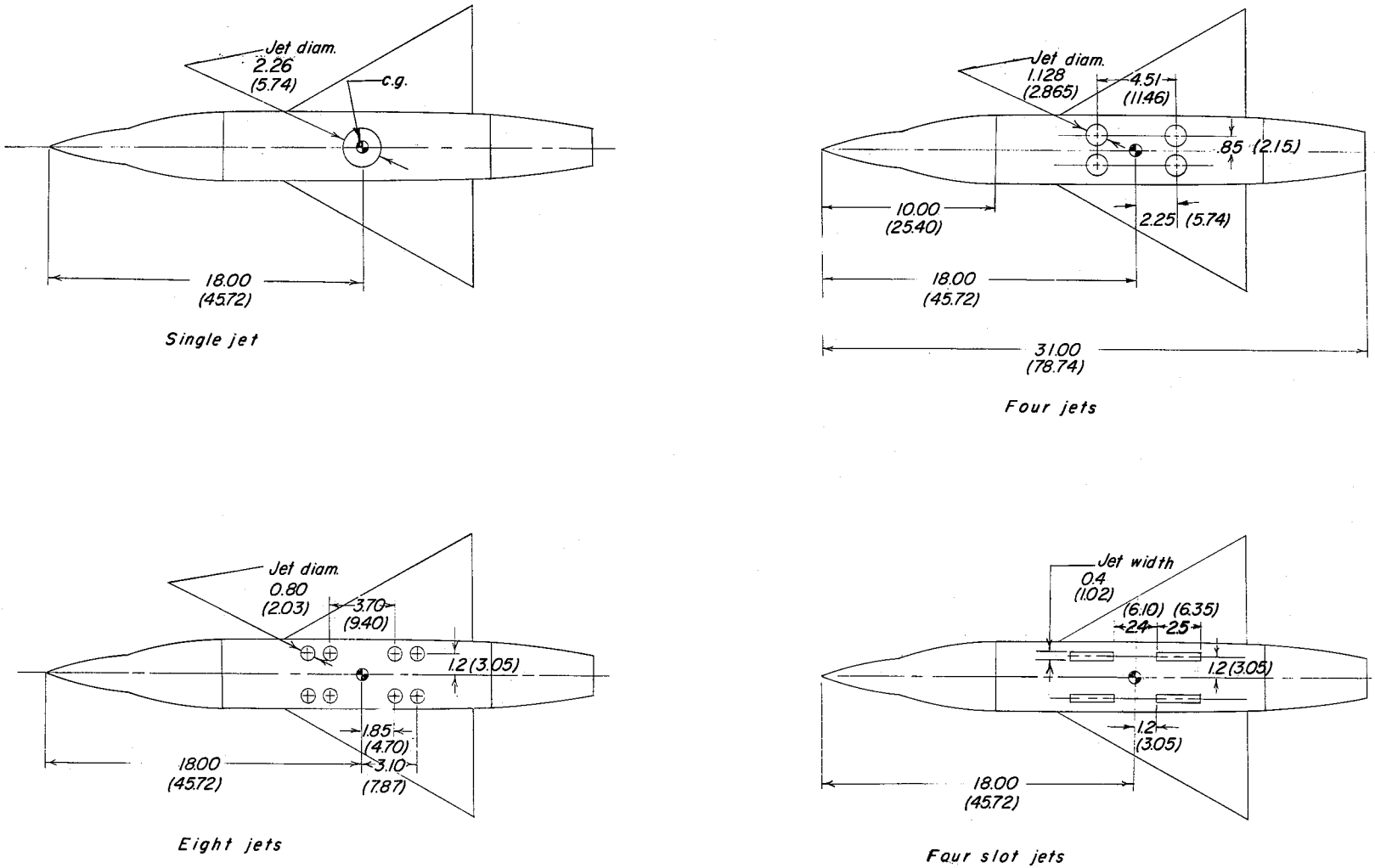

Figure 3.- Geometry of four jet configurations investigated (total jet-exit area for each configuration is equal). All dimensions are in inches with centimeters given in parentheses.

Circular	
R	S/Aj
9.4 (23.90)	69.5

Triangular		
c_r	b/2	S/Aj
12.40 (31.50)	7.17 (18.21)	34.5
14.08 (35.76)	8.13 (20.65)	39.0
16.66 (42.32)	9.62 (24.43)	49.0

Rectangular		
c_r	b/2	S/Aj
19.00 (48.26)	4.00 (10.16)	38.0
19.00 (48.26)	6.00 (15.24)	57.0
19.00 (48.26)	8.00 (20.32)	76.0
19.00 (48.26)	10.00 (25.40)	95.0

Circular	
R	S/Aj
3.16 (8.03)	10.0
4.47 (11.35)	20.0
5.48 (13.92)	30.0
8.35 (21.21)	69.5

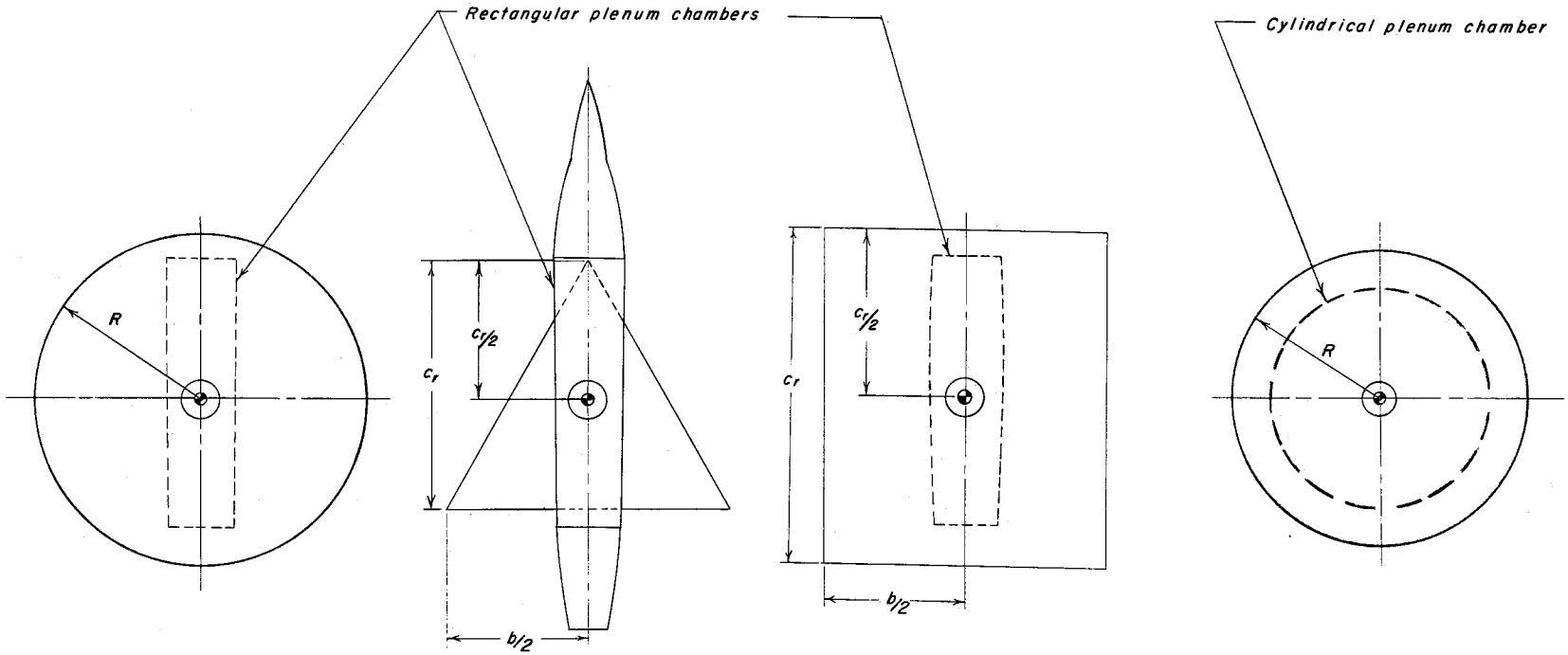

Figure 4.- Size and shape of flat plates used in investigation. All dimensions are in inches with centimeters given in parentheses; plates are 1/8 inch (0.32 cm) thick.

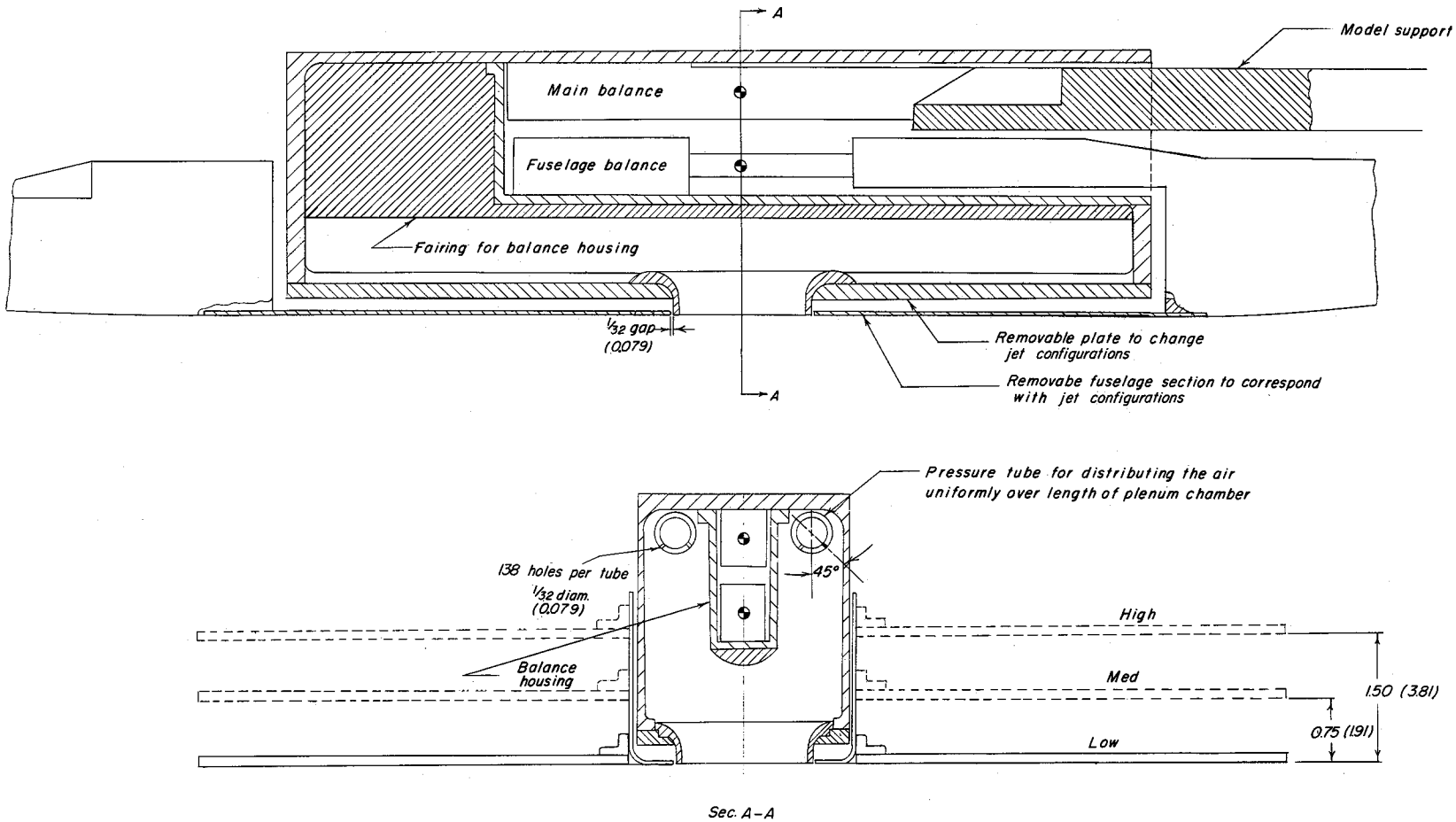

Figure 5.- Drawing of internal plenum chamber, fuselage, adjustable wings, and balance system employed in investigation. All dimensions are in inches with centimeters given in parentheses.

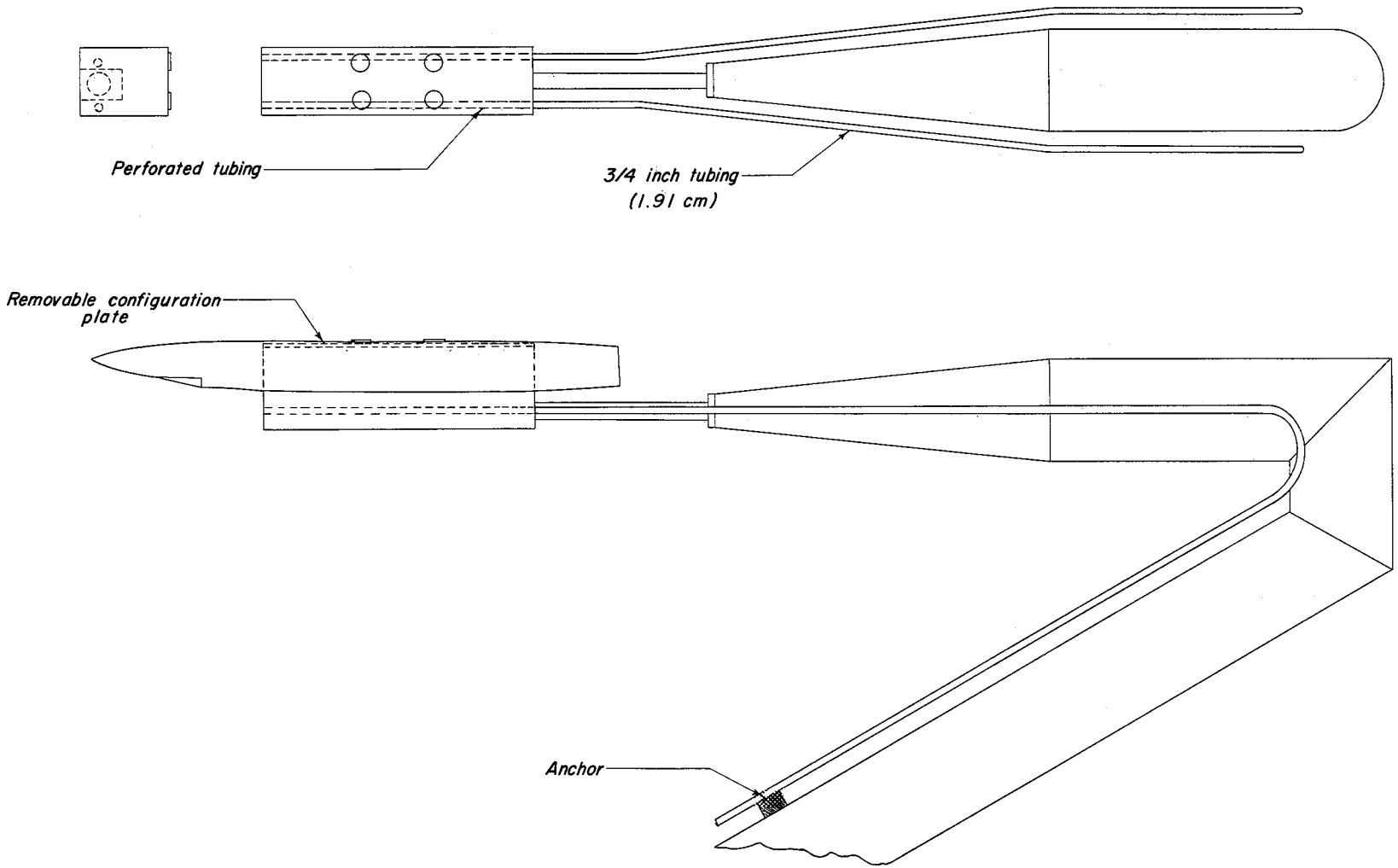

Figure 6.- Sketch showing sting mount of inverted model and tubing for getting air to model.

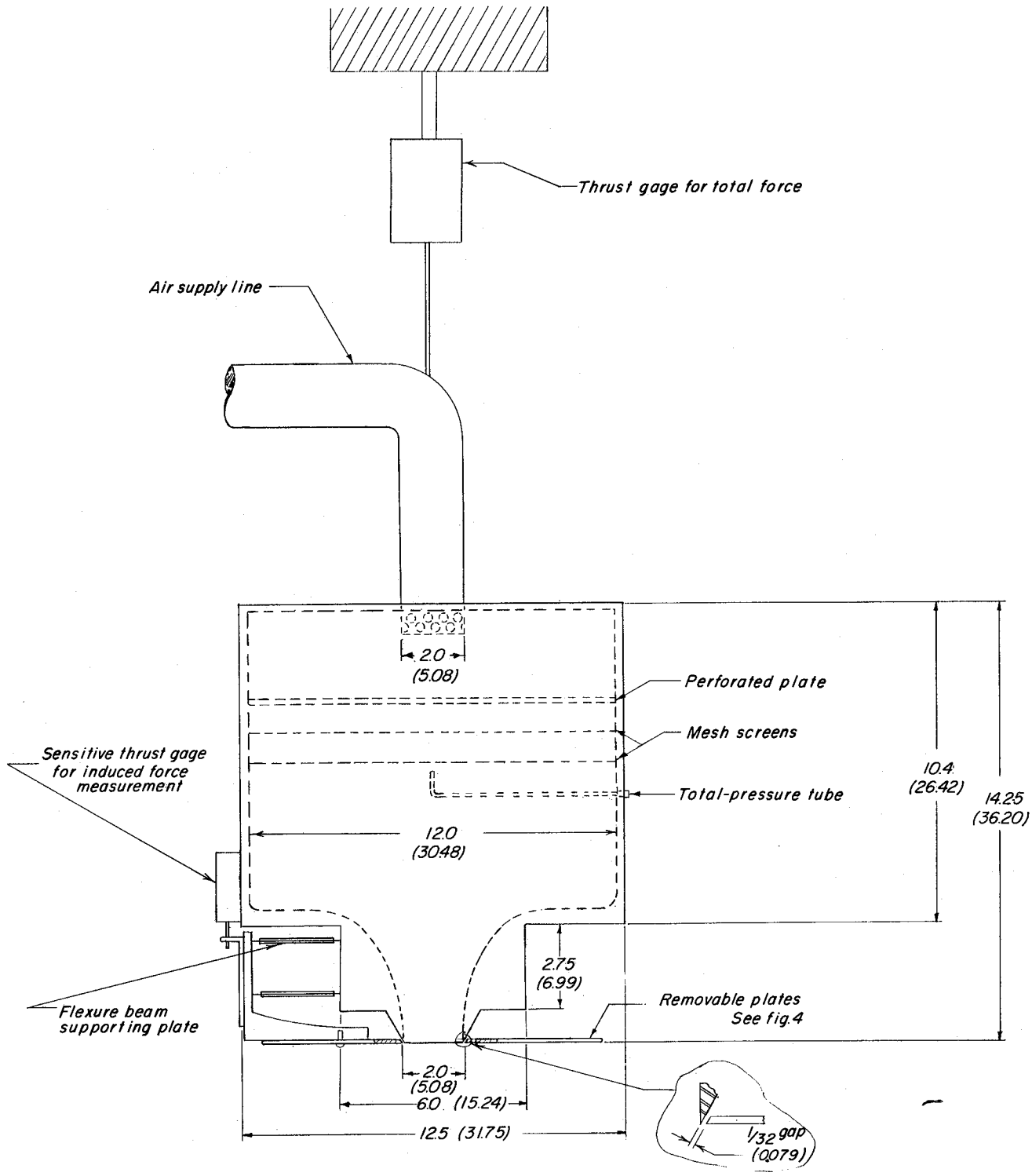

Figure 7.- Sketch showing cylindrical-plenum-chamber configuration with thrust gages. All dimensions are in inches with centimeters given in parentheses.

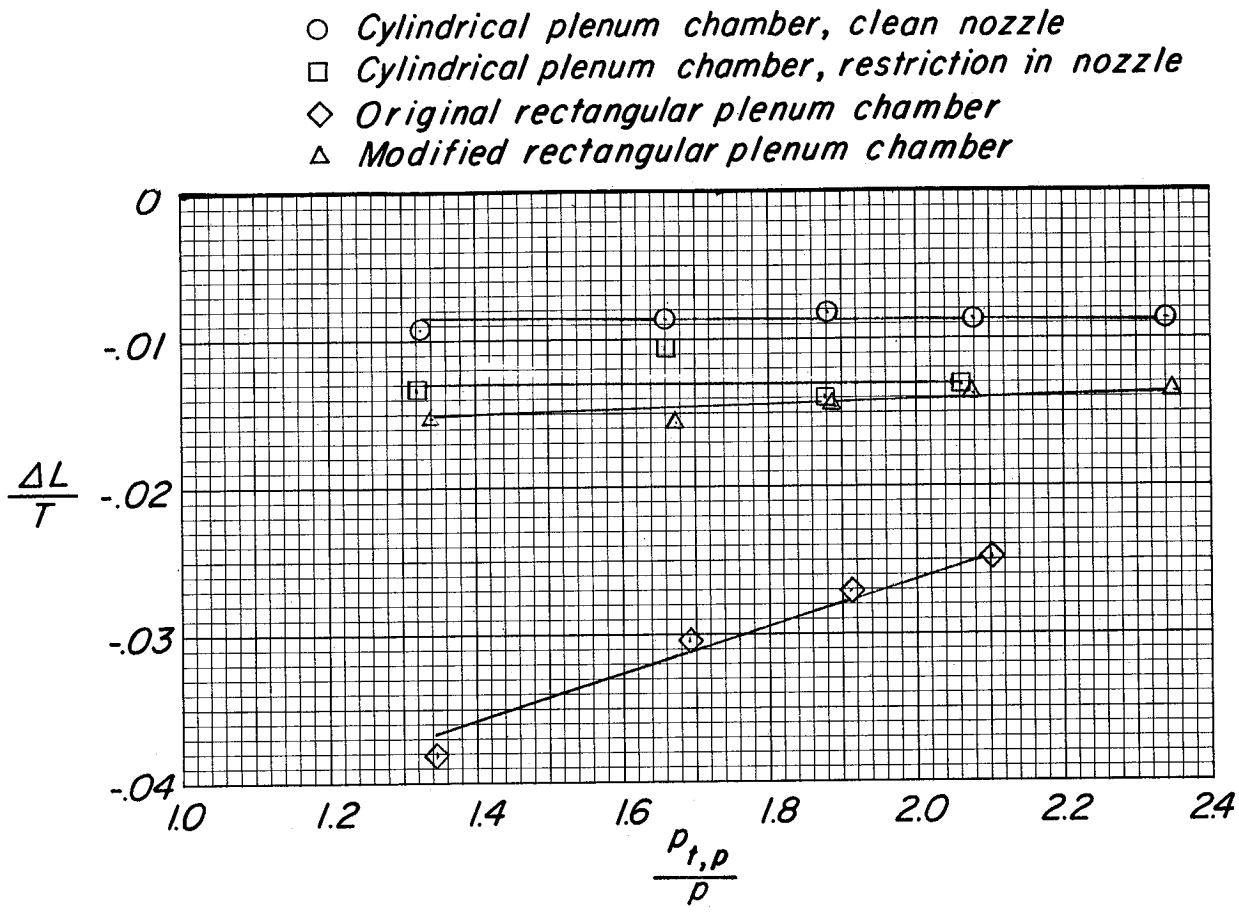

(a) Induced loads.

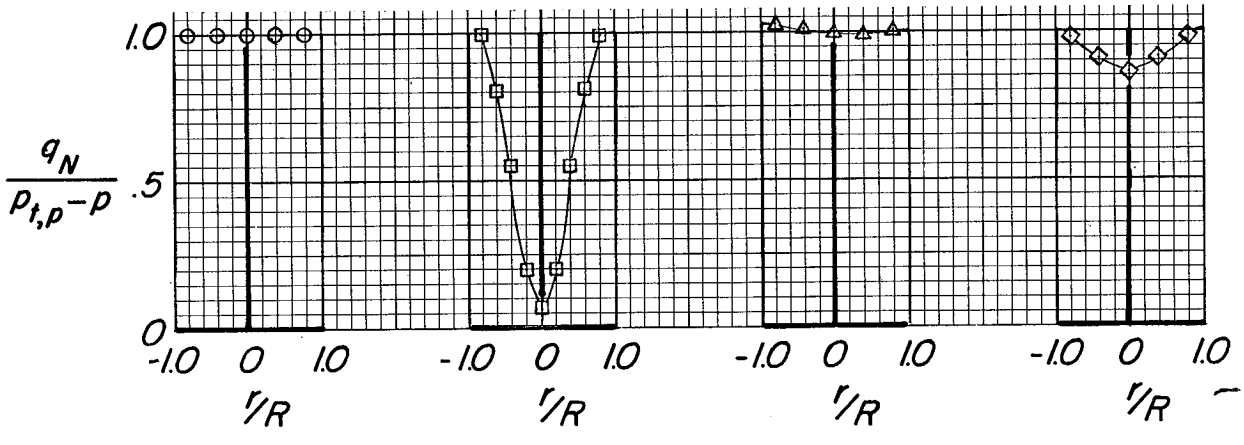

(b) Exit impact-pressure distribution. $\frac{p_{t,p}}{p} = 1.89$.

Figure 8.- Induced loads and exit impact-pressure distributions for several single-jet configurations. $S/A_j = 69.5$. (Circular planforms.)

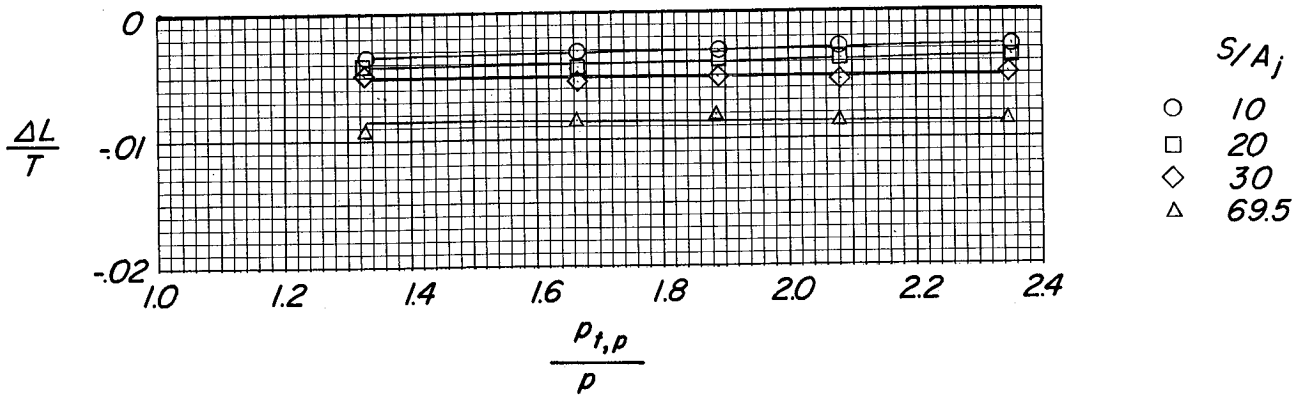

(a) Cylindrical plenum chamber with clean nozzle.

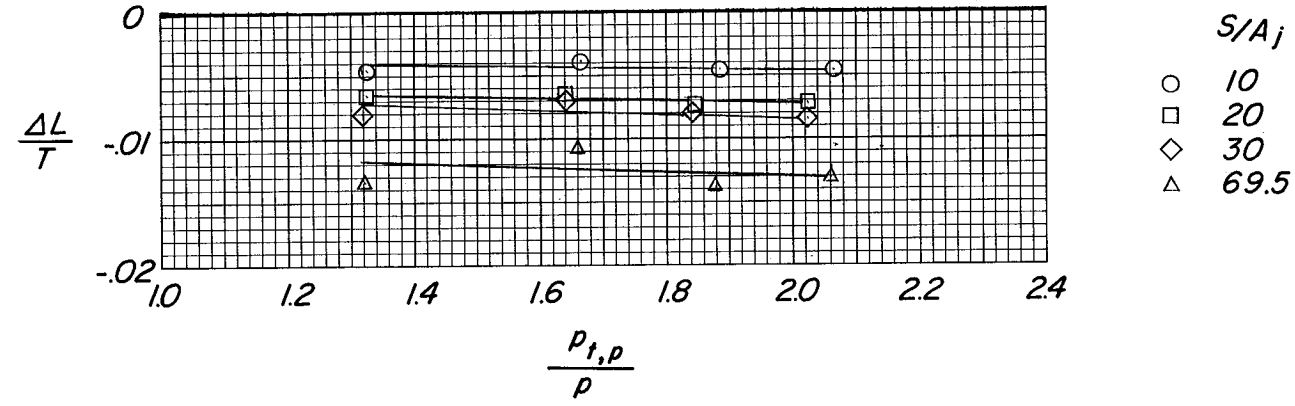

(b) Cylindrical plenum chamber with restriction in nozzle.

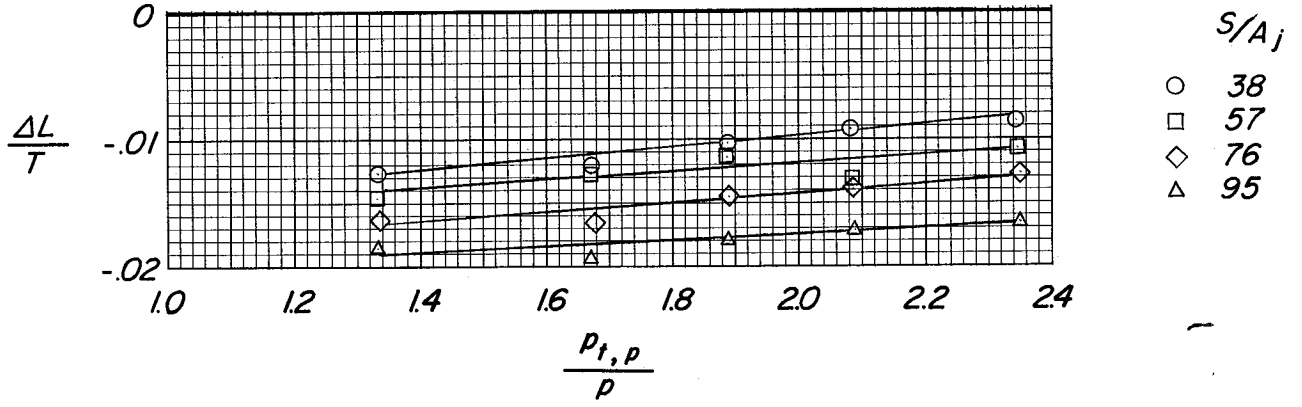

(c) Modified rectangular plenum chamber.

Figure 9.- Effect of plenum chamber and jet configuration on loads induced on a circular-planform plate for a single jet.

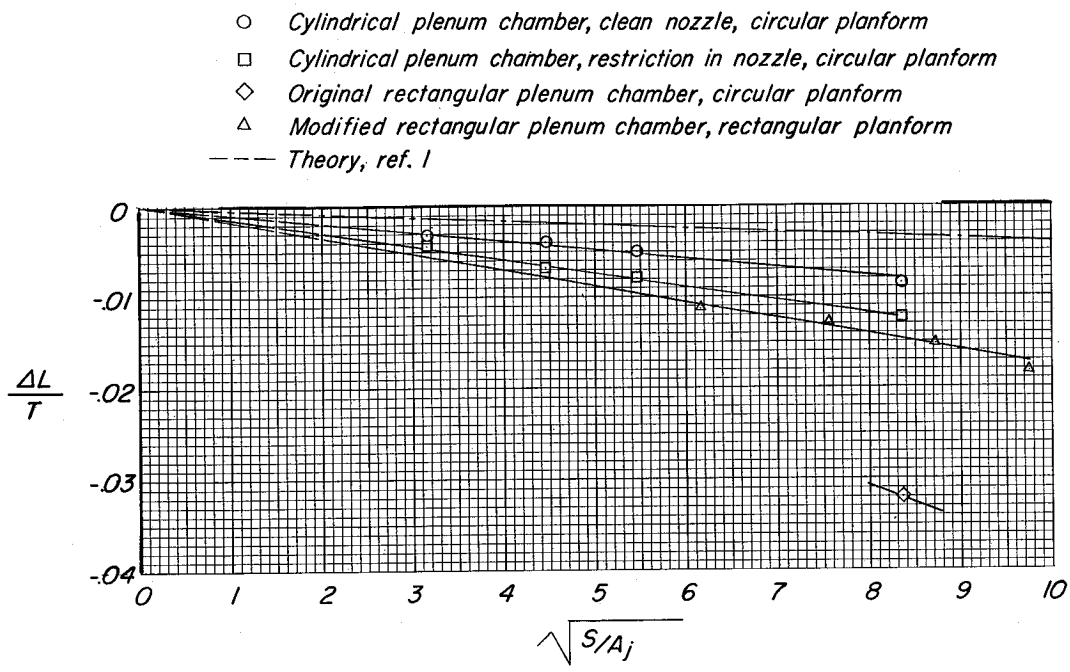

(a) Induced loads.

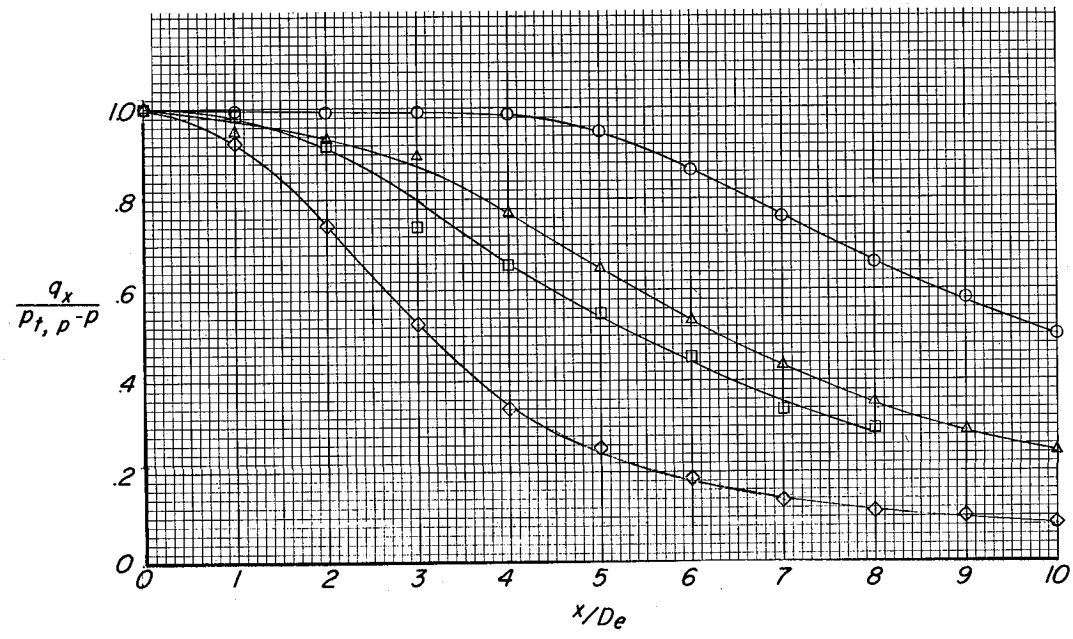

(b) Jet decay.

Figure 10.- Effect of plenum chamber and nozzle configuration on loads induced on several plate shapes and on jet impact-pressure decay $\frac{p_{t,p}}{p} = 1.64$.

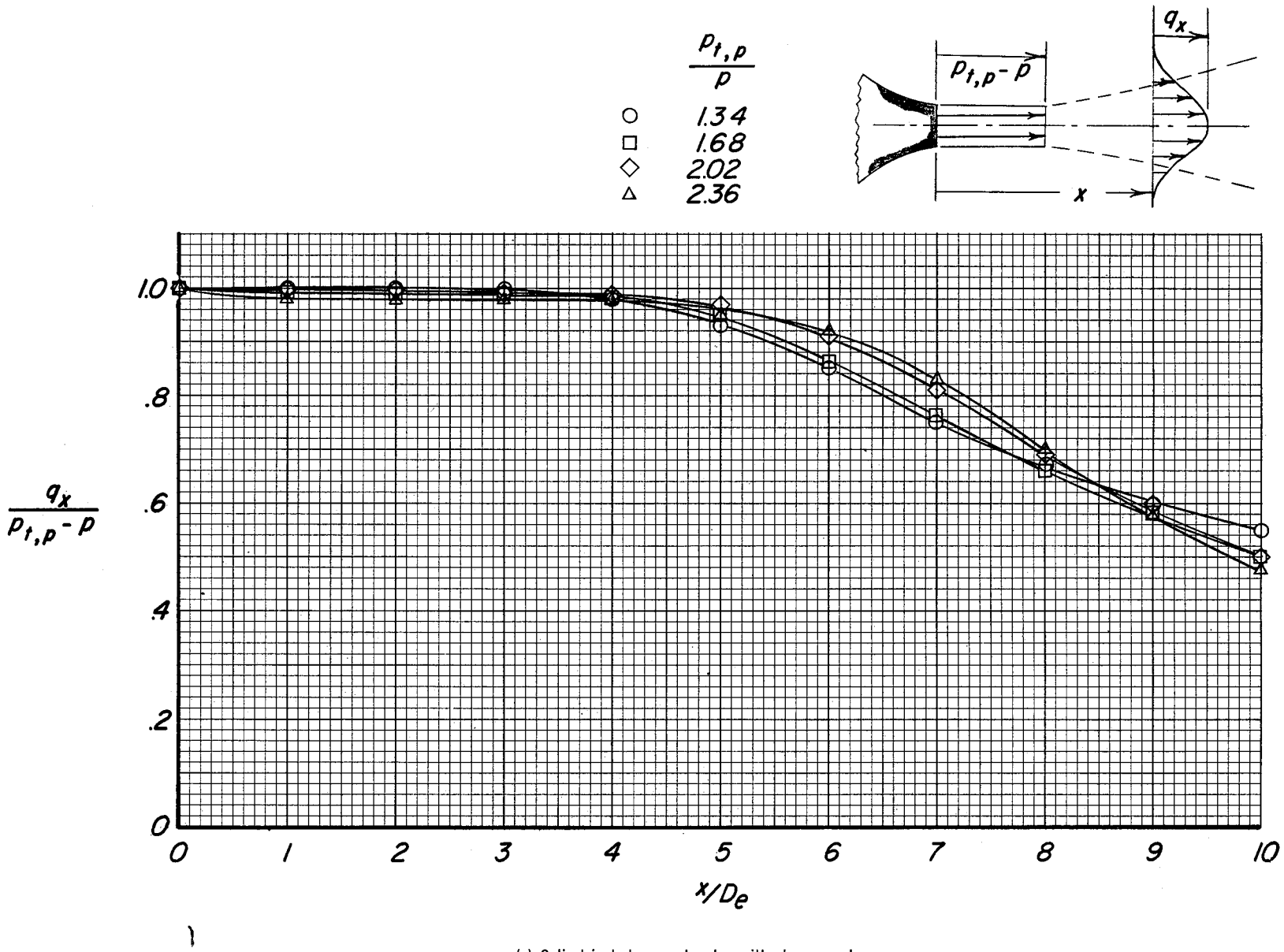

(a) Cylindrical plenum chamber with clean nozzle.

Figure 11.- Effect of pressure ratio on impact-pressure decay.

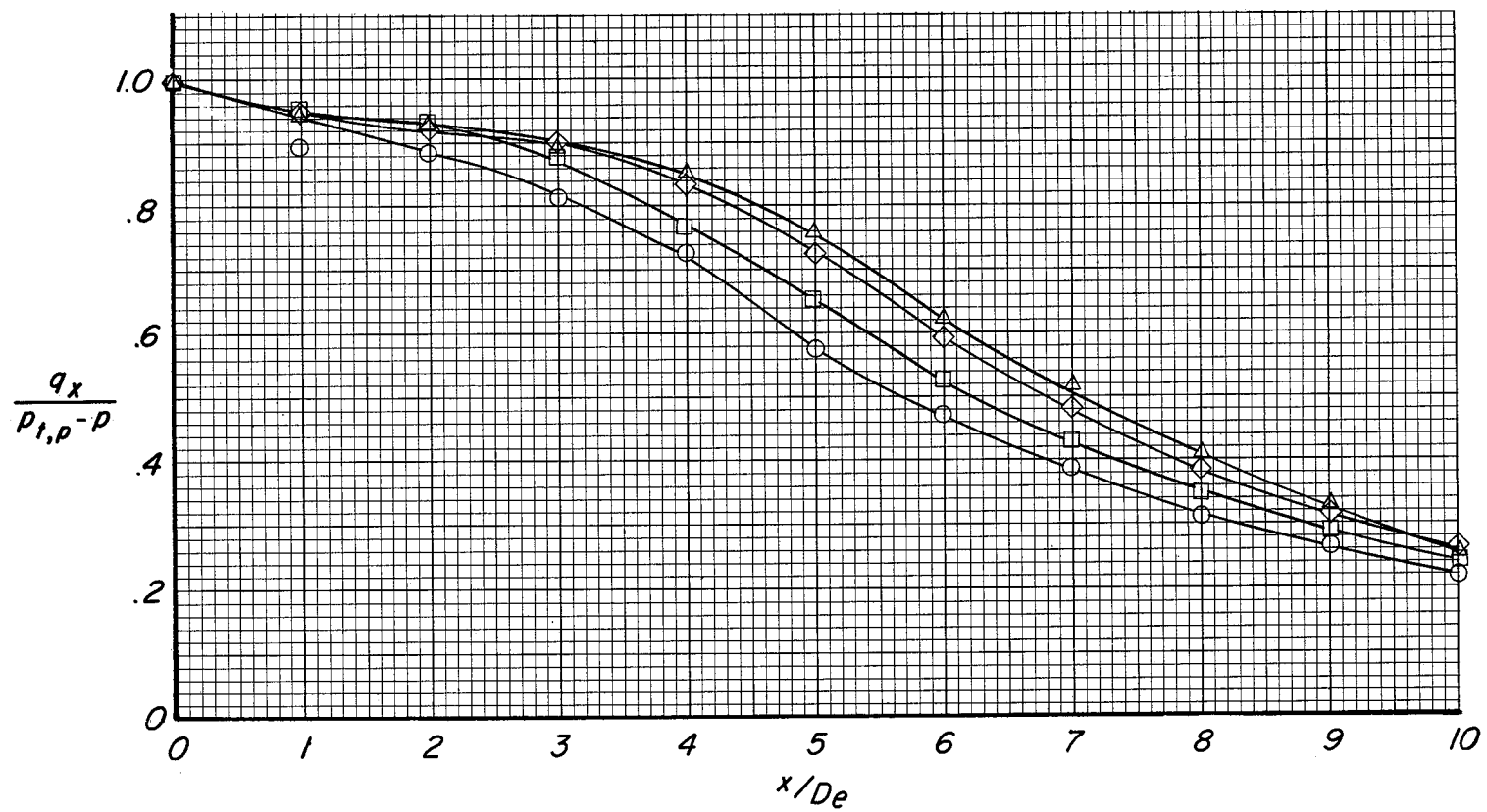

(b) Modified rectangular plenum chamber with single round jet. l/D_e = 0.248.

Figure 11.- Continued.

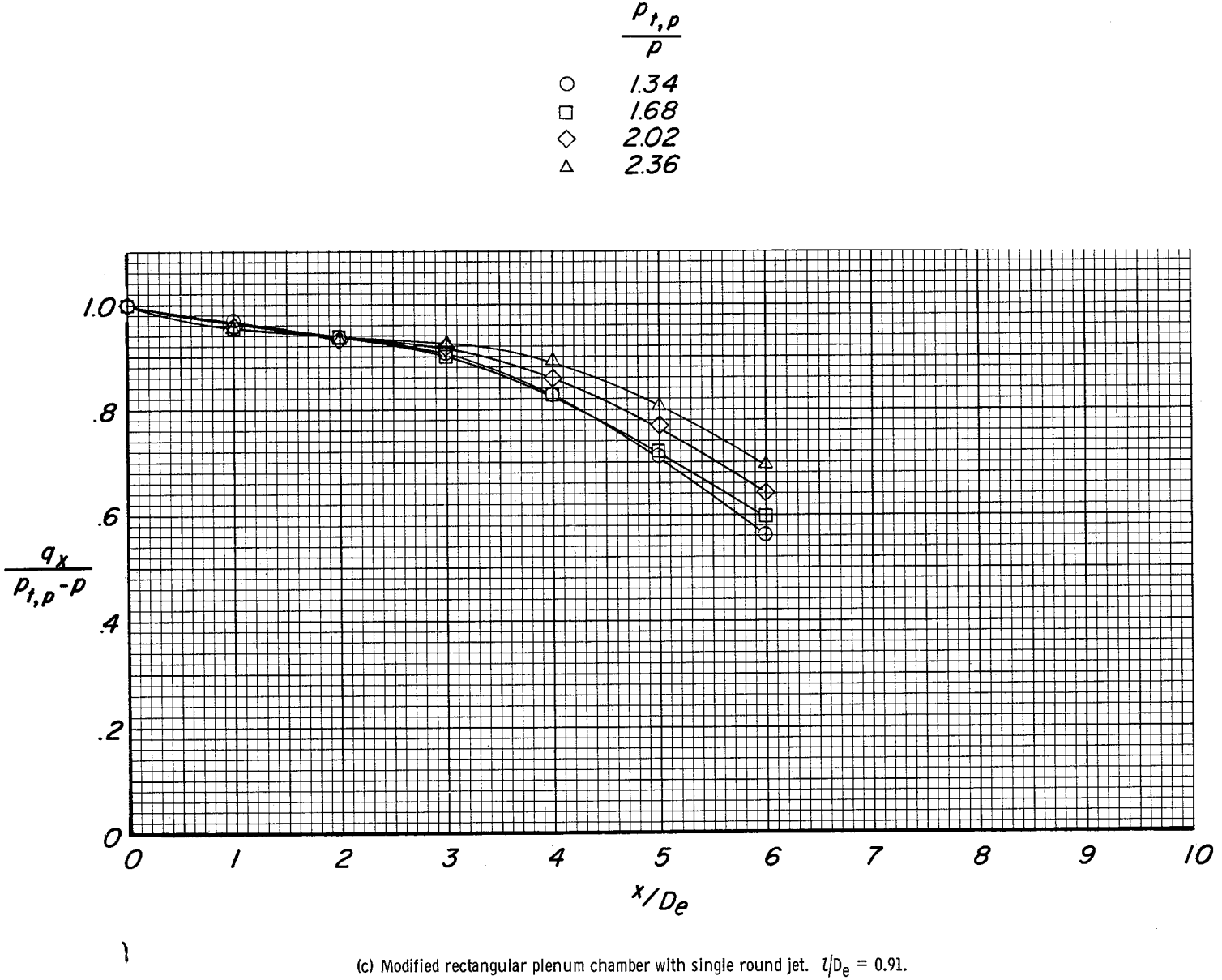

(c) Modified rectangular plenum chamber with single round jet. $\ell/D_e = 0.91$.

Figure 11.- Continued.

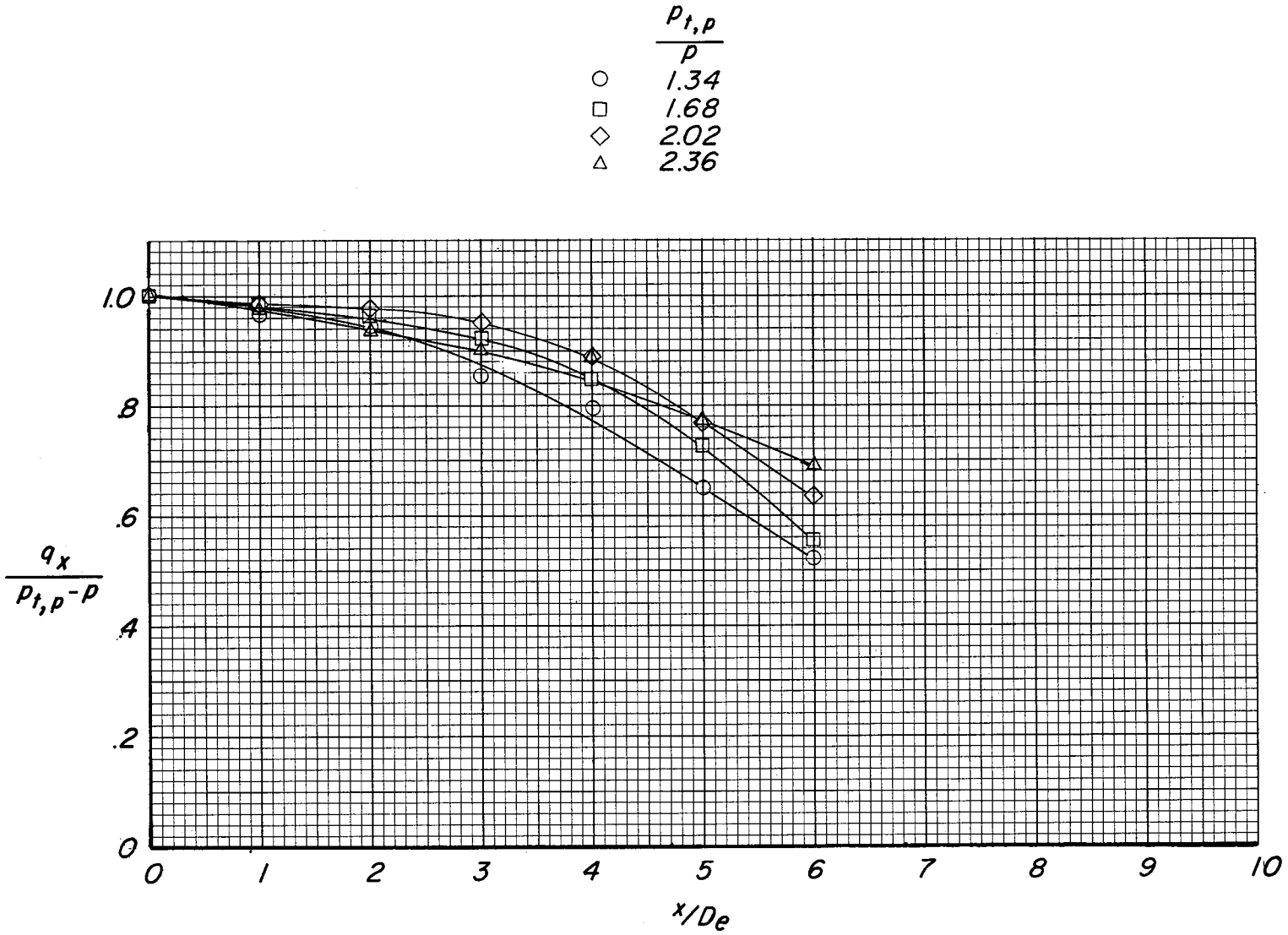

(d) Modified rectangular plenum chamber with single round jet. l/D_e = 1.41.

Figure 11.- Continued.

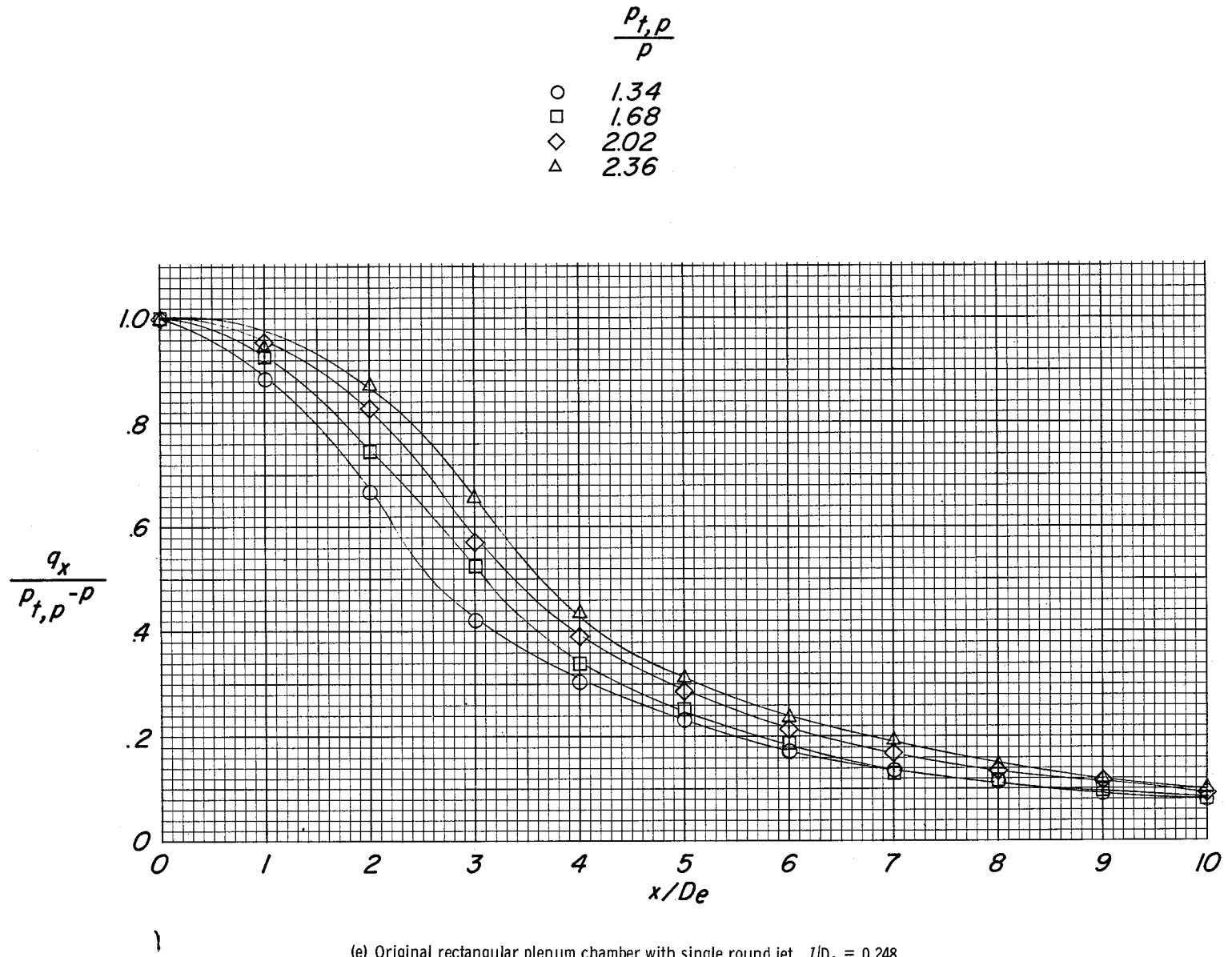

(e) Original rectangular plenum chamber with single round jet. l/D_e = 0.248.

Figure 11.- Continued.

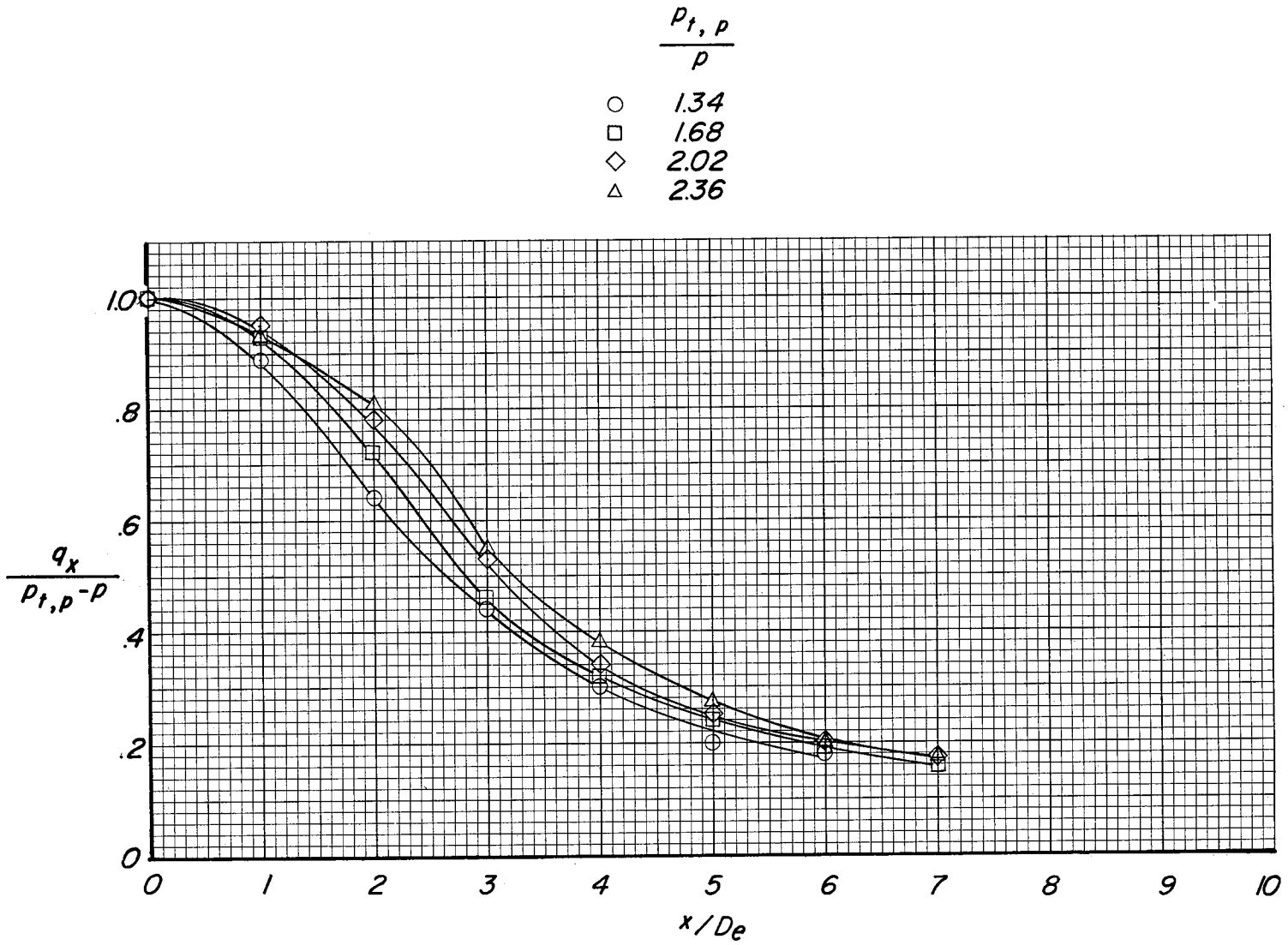

(f) Modified rectangular plenum chamber with four jets.

Figure 11.- Concluded.

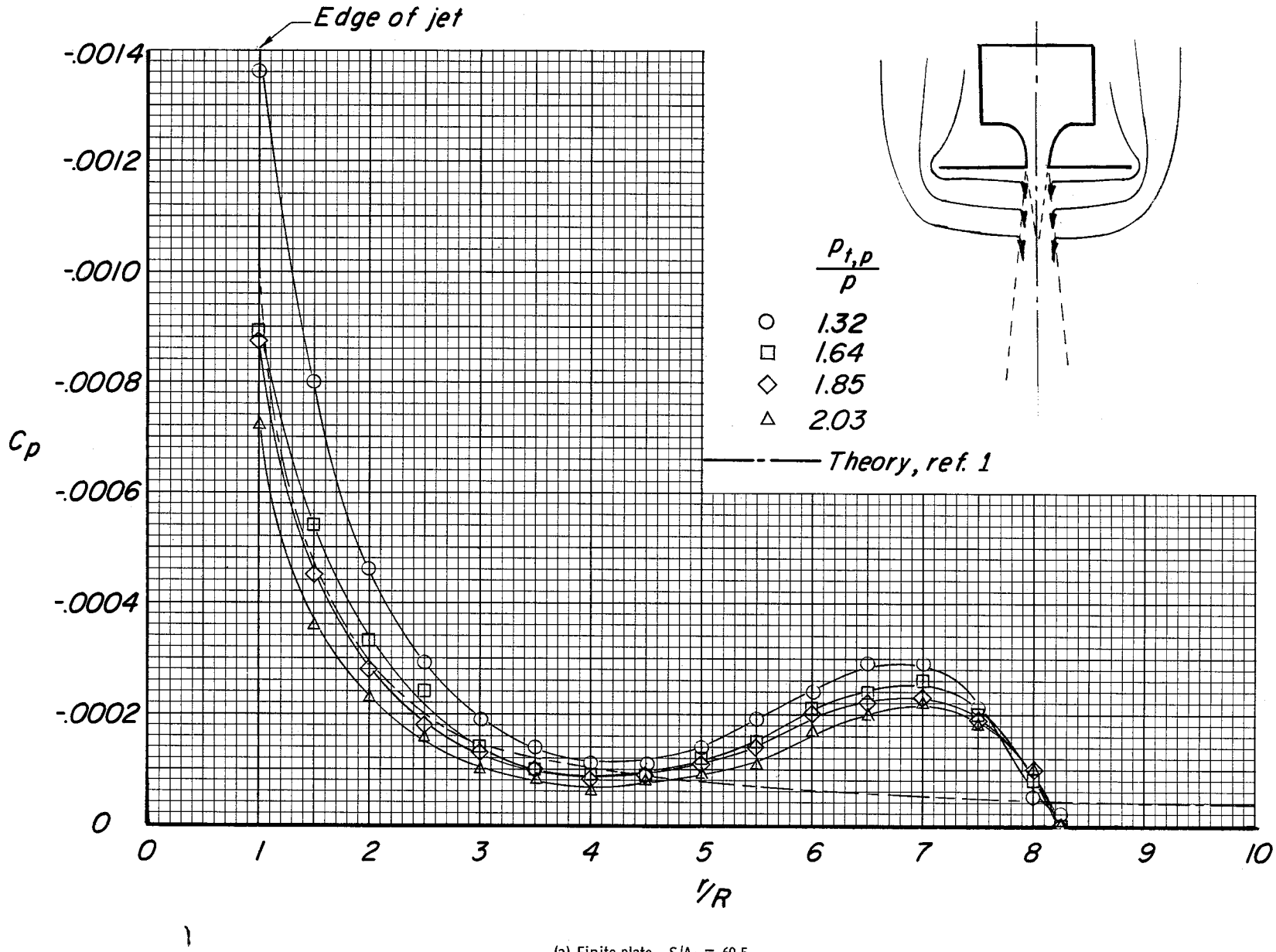

(a) Finite plate. $S/A_j = 69.5$.

Figure 12.- Radial distribution of pressure induced by jet on circular-planform plates.

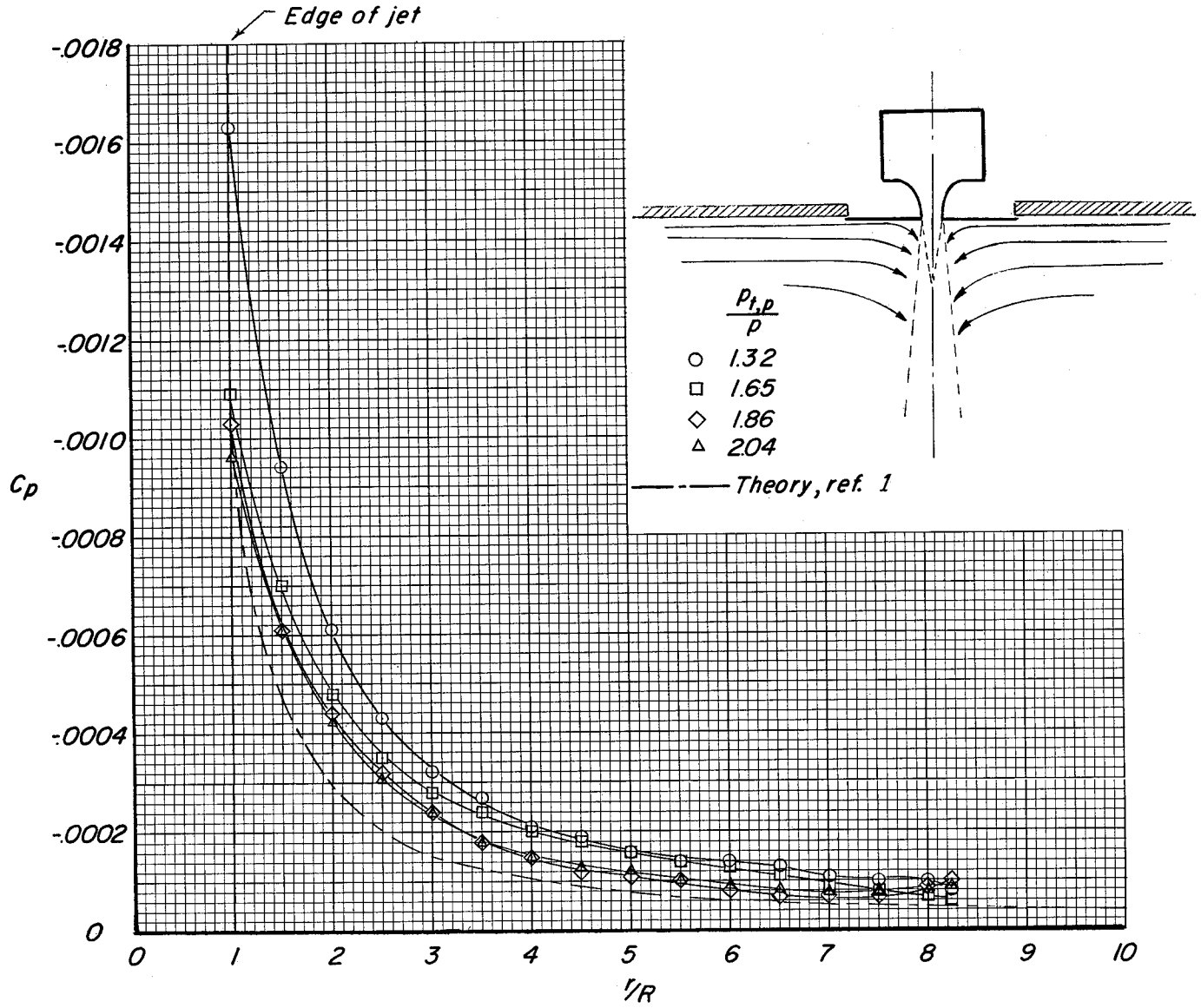

(b) Plate installed in wall.

Figure 12.- Concluded.

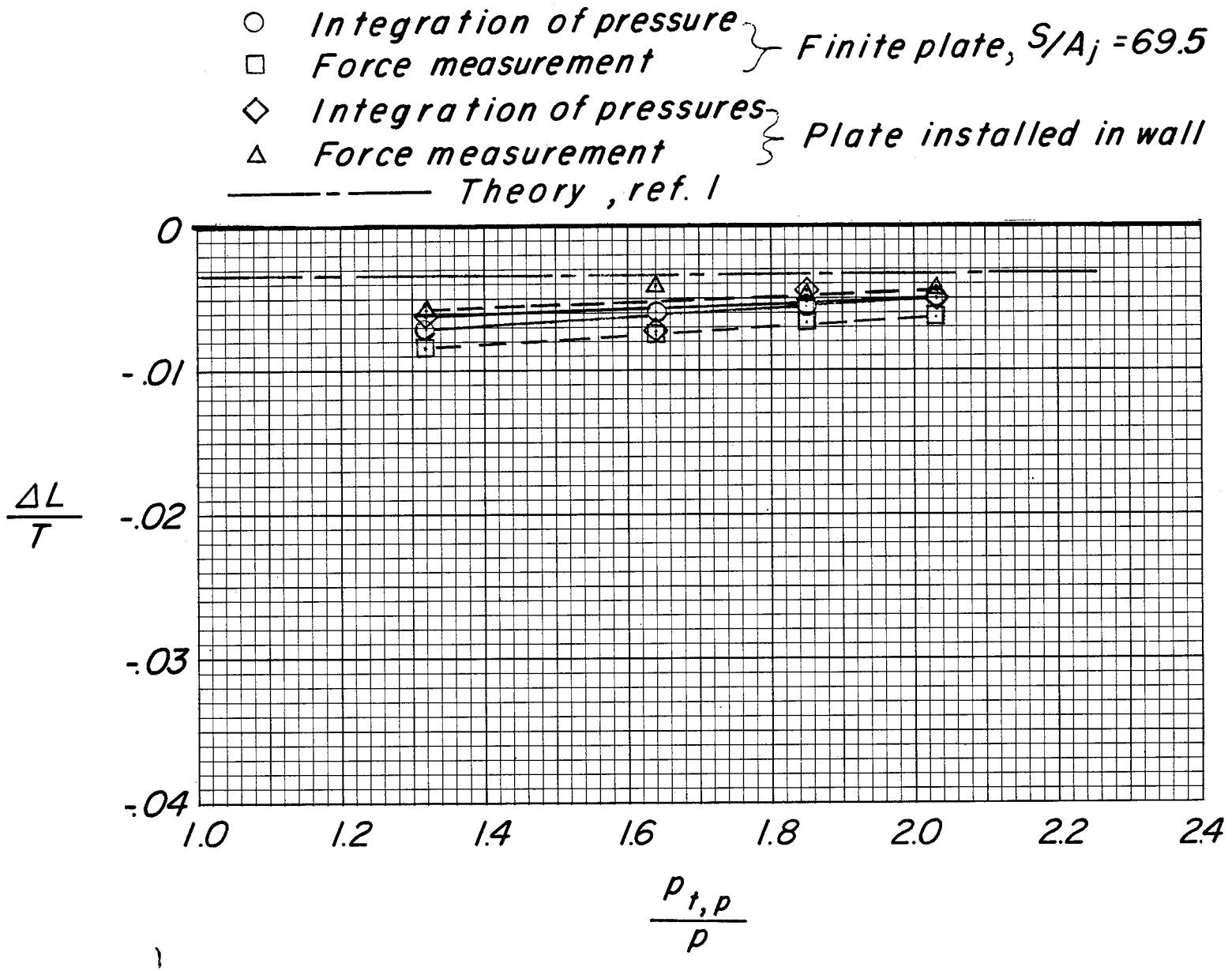

Figure 13.- Comparison of induced force on circular-planform plates determined by integration of measured pressures with that determined by direct force measurement.

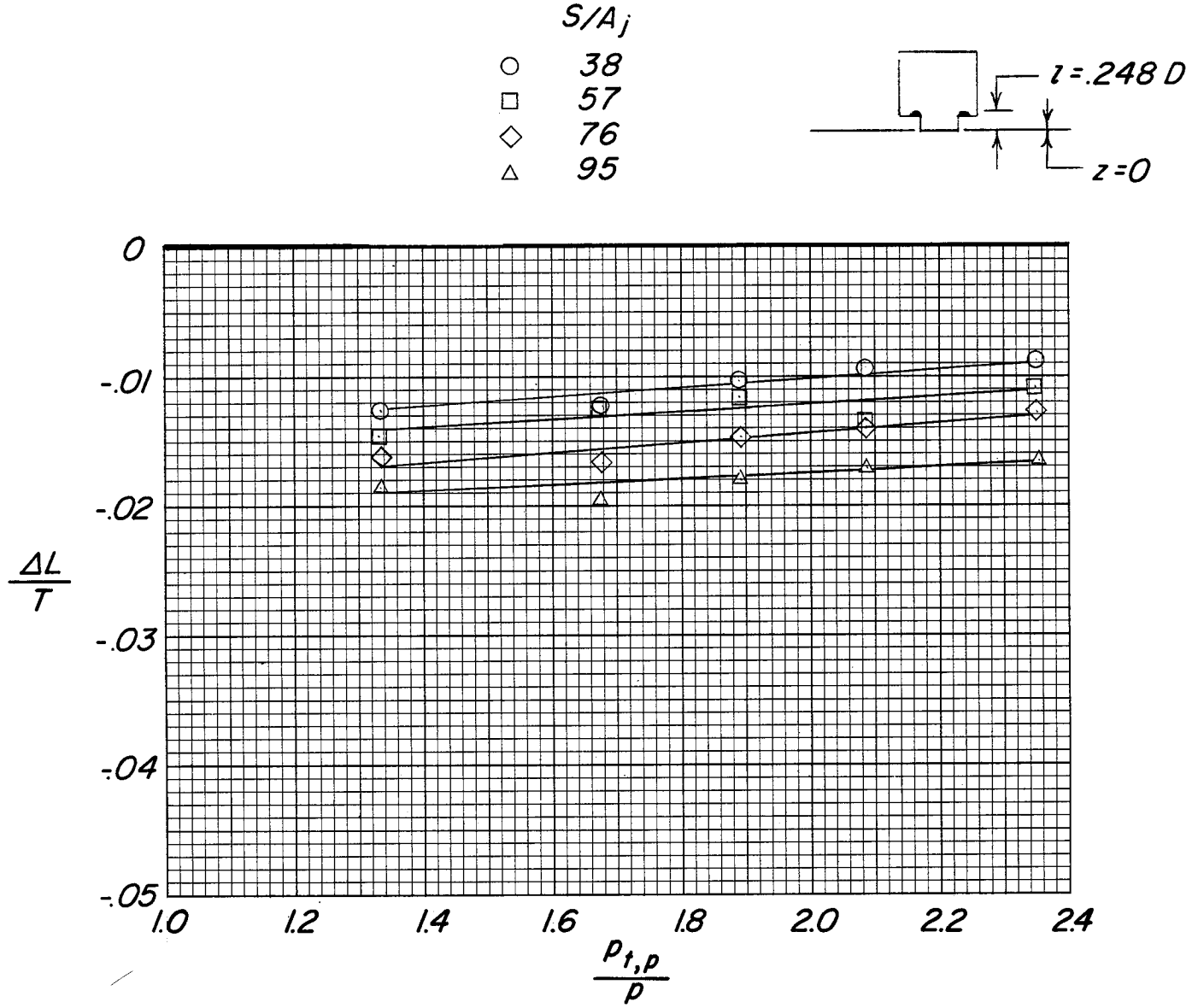

(a) $l/D = 0.248$.

Figure 14.- Effect of jet length on induced loads. Single round jet on modified rectangular plenum chamber with rectangular-planform plates. $z/D = 0$.

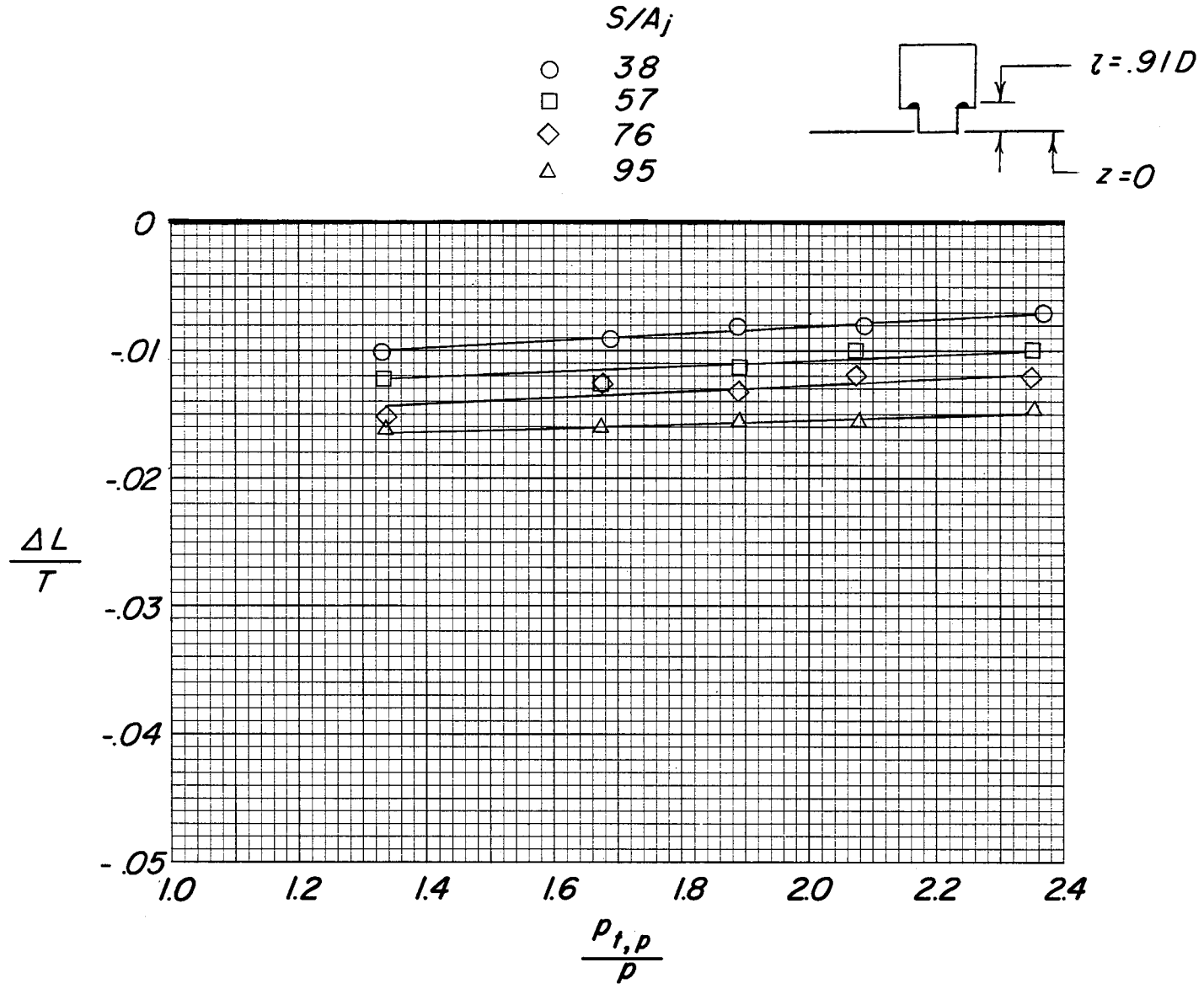

(b) $\ell/D = 0.91$.

Figure 14.- Continued.

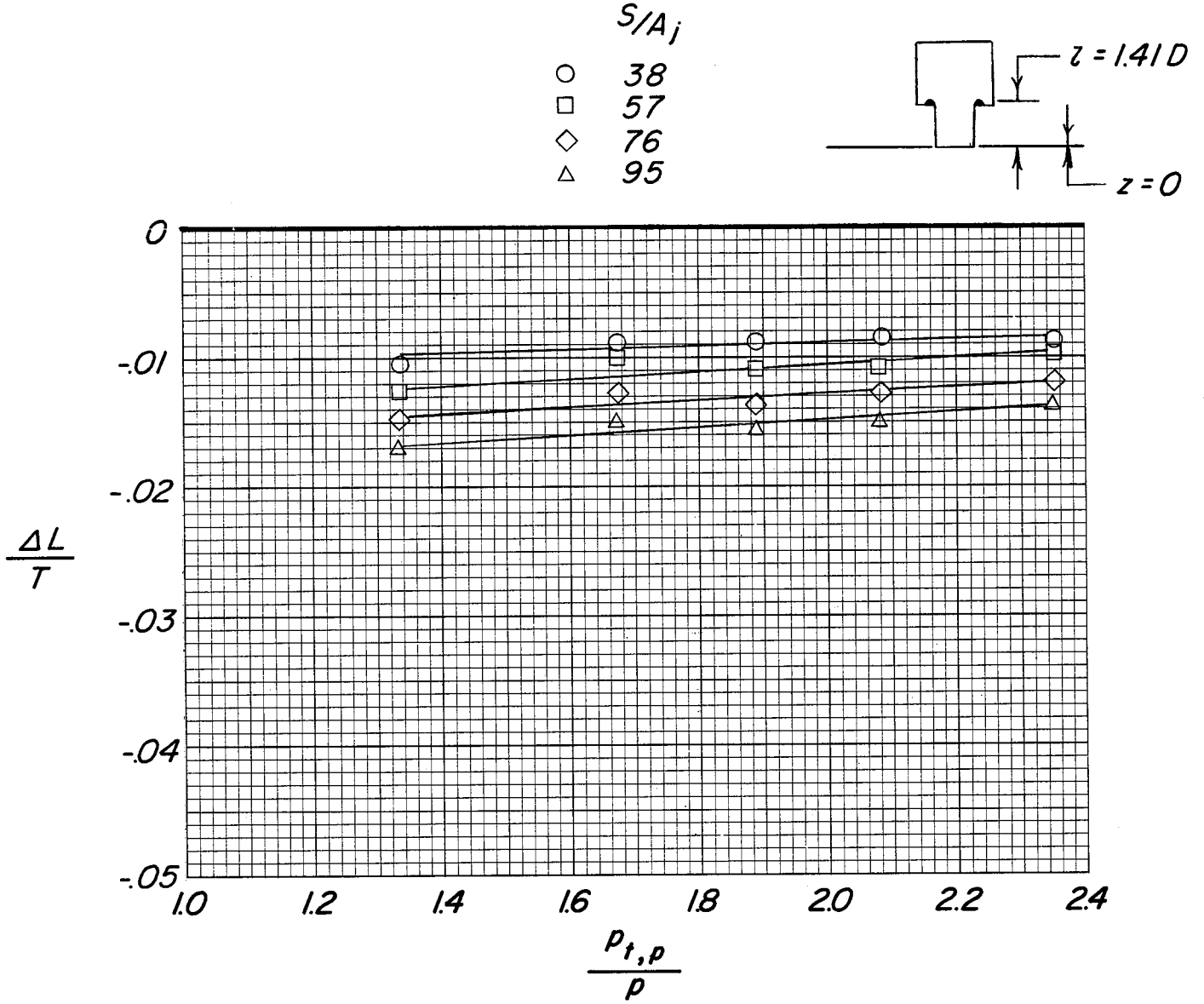

(c) l/D = 1.41.

Figure 14.- Concluded.

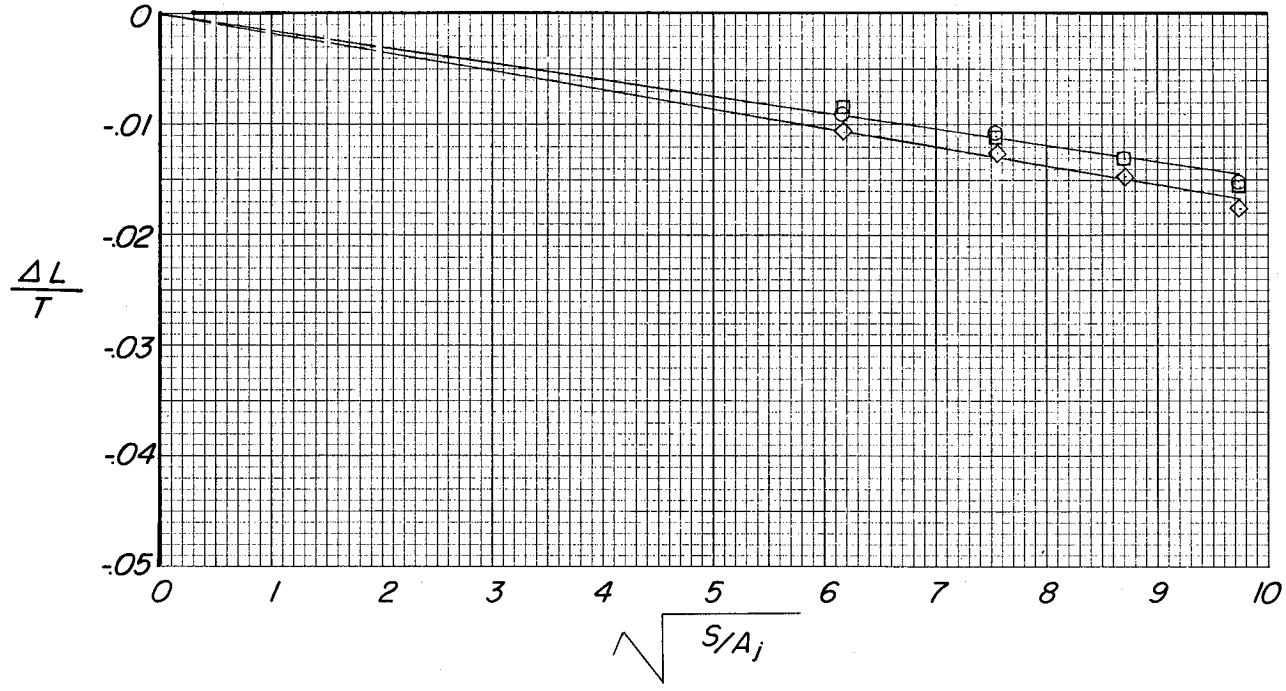

(a) Induced load on plate.

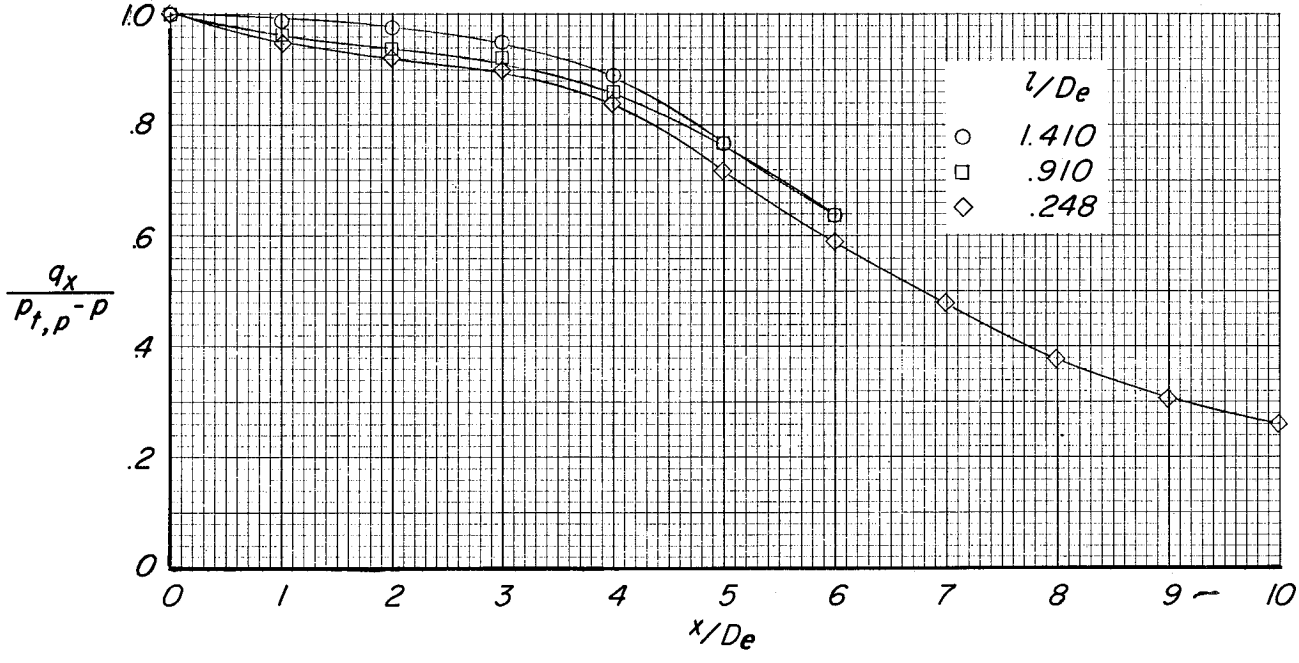

(b) Impact-pressure decay.

Figure 15.- Effect of jet length on induced loads and impact-pressure decay. $\frac{p_{t,p}}{p} = 1.89$; $z/D_e = 0$; rectangular-planform plates.

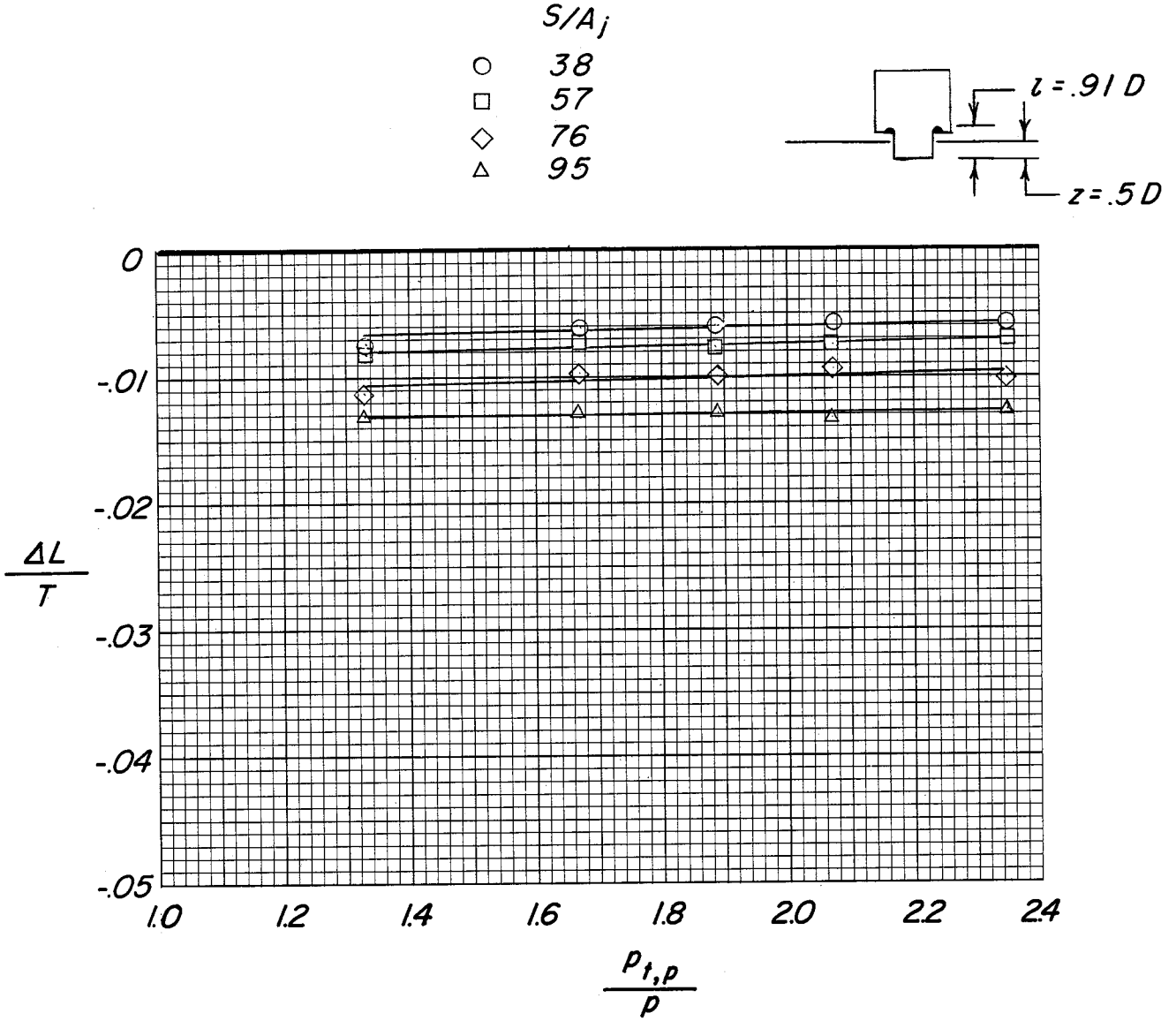

(a) $\ell/D = 0.91$; $z/D = 0.5$.

Figure 16.- Effects of jet projection and length on induced loads. Single round jet on modified rectangular plenum chamber with rectangular-planform plates.

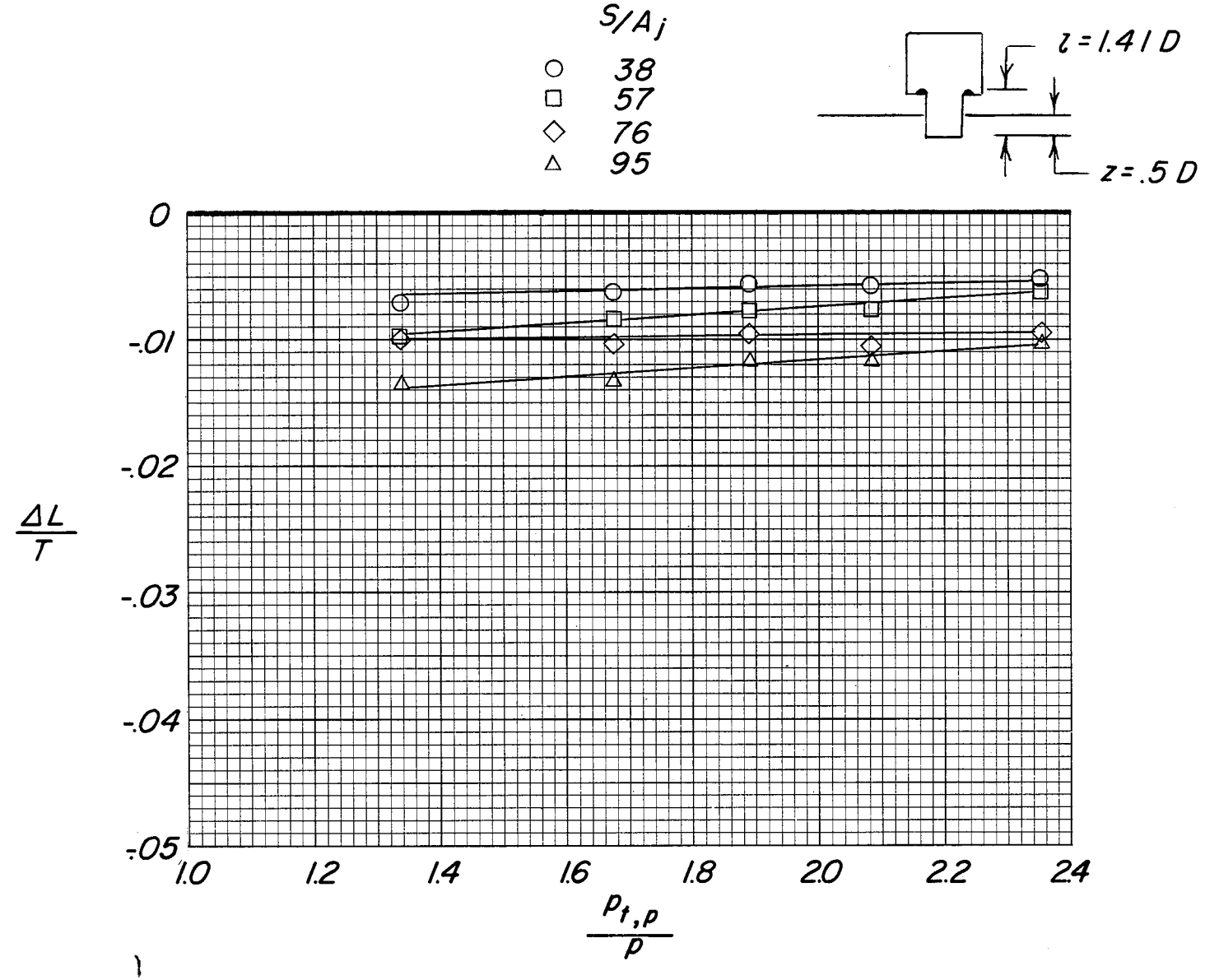

(b) $\ell/D = 1.41$; $z/D = 0.5$.

Figure 16.- Continued.

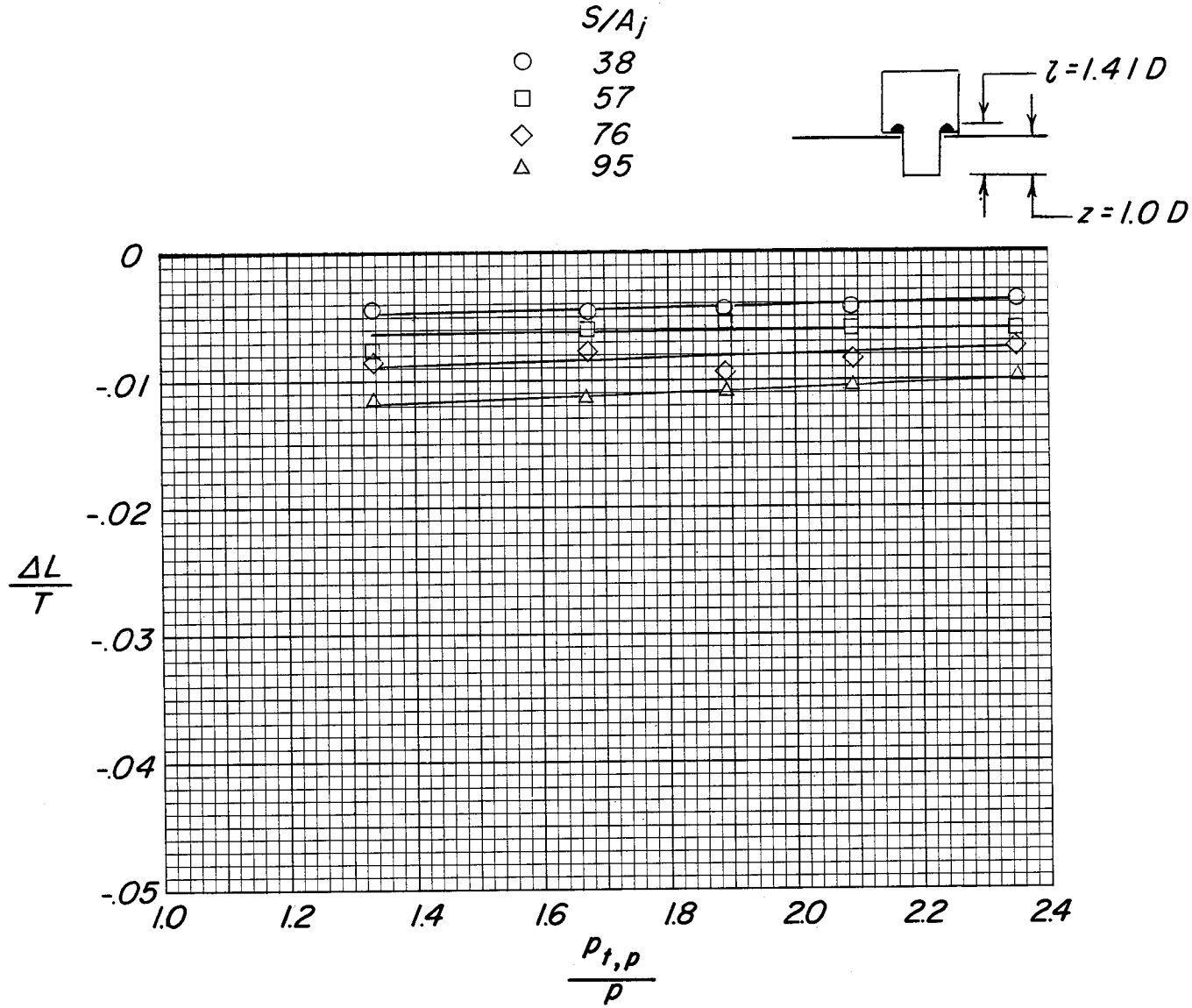

(c) $\ell/D = 1.41$; $z/D = 1.0$.

Figure 16.- Concluded.

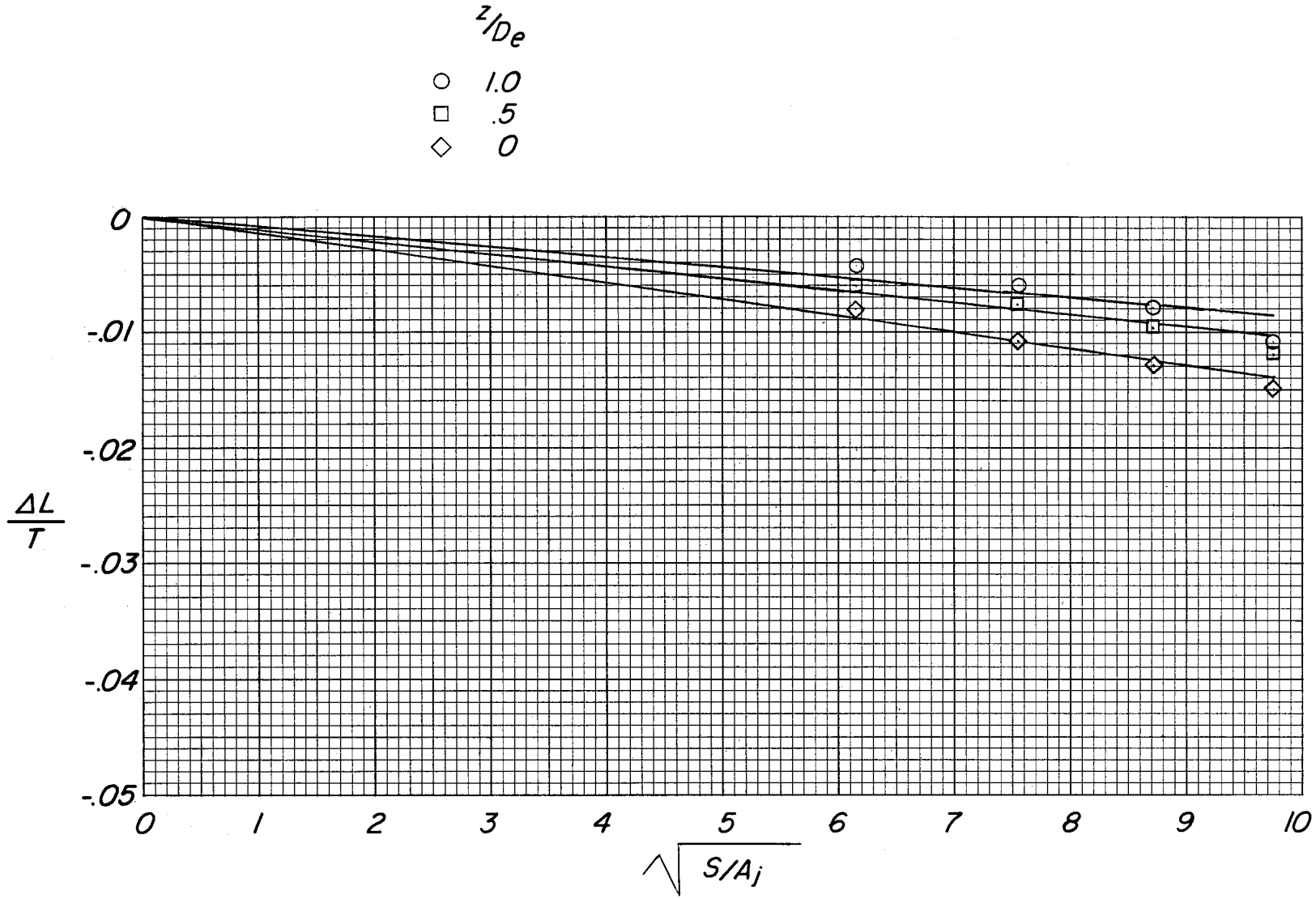

Figure 17.- Effect of jet projection on induced load for long jet. $\ell/D_e = 1.41$; $\frac{p_{t,p}}{p} = 1.89$; rectangular-planform plates.

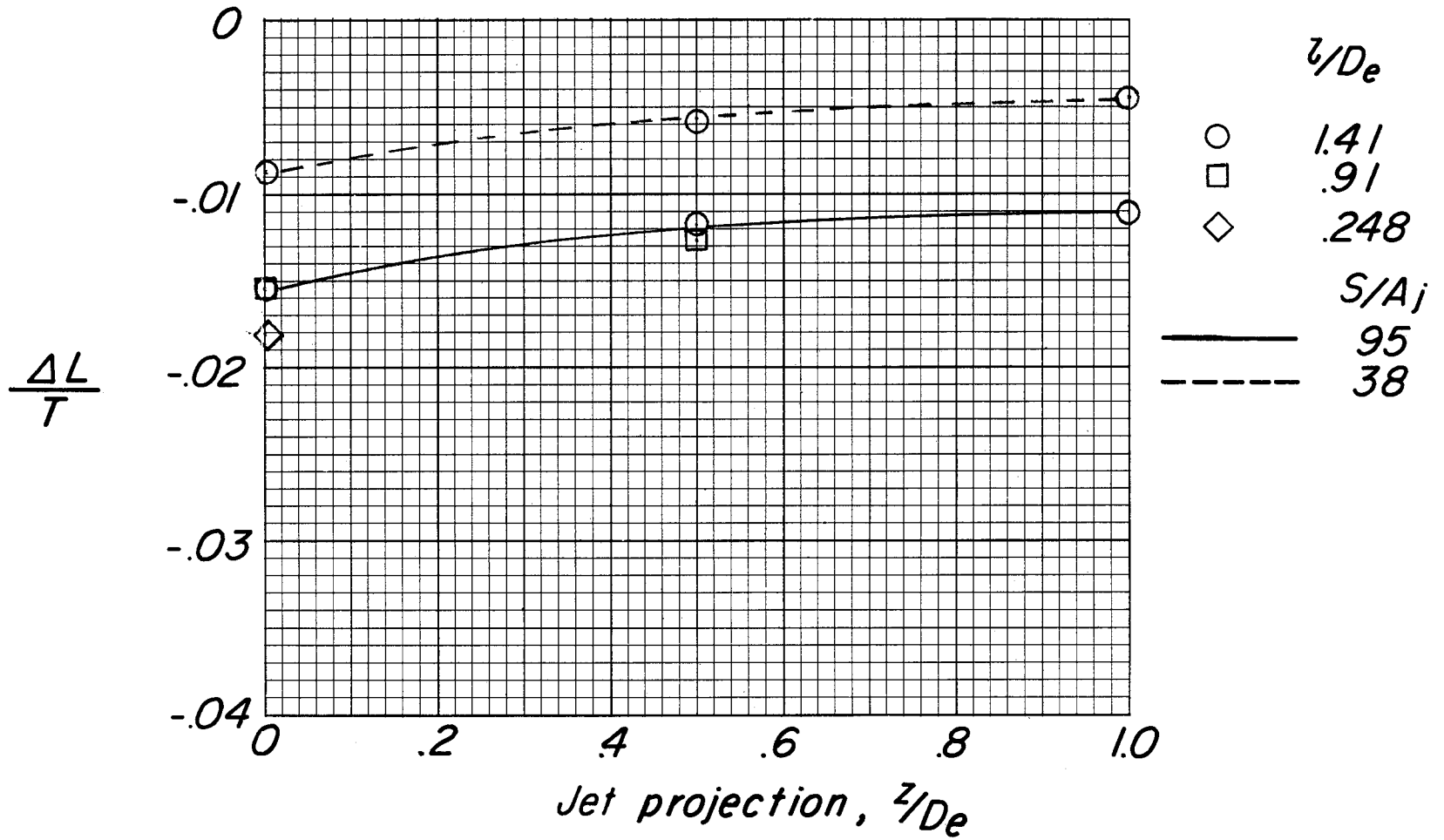

Figure 18.- Variation of induced load on circular plate with jet projection. $\frac{p_t,p}{p} = 1.89$.

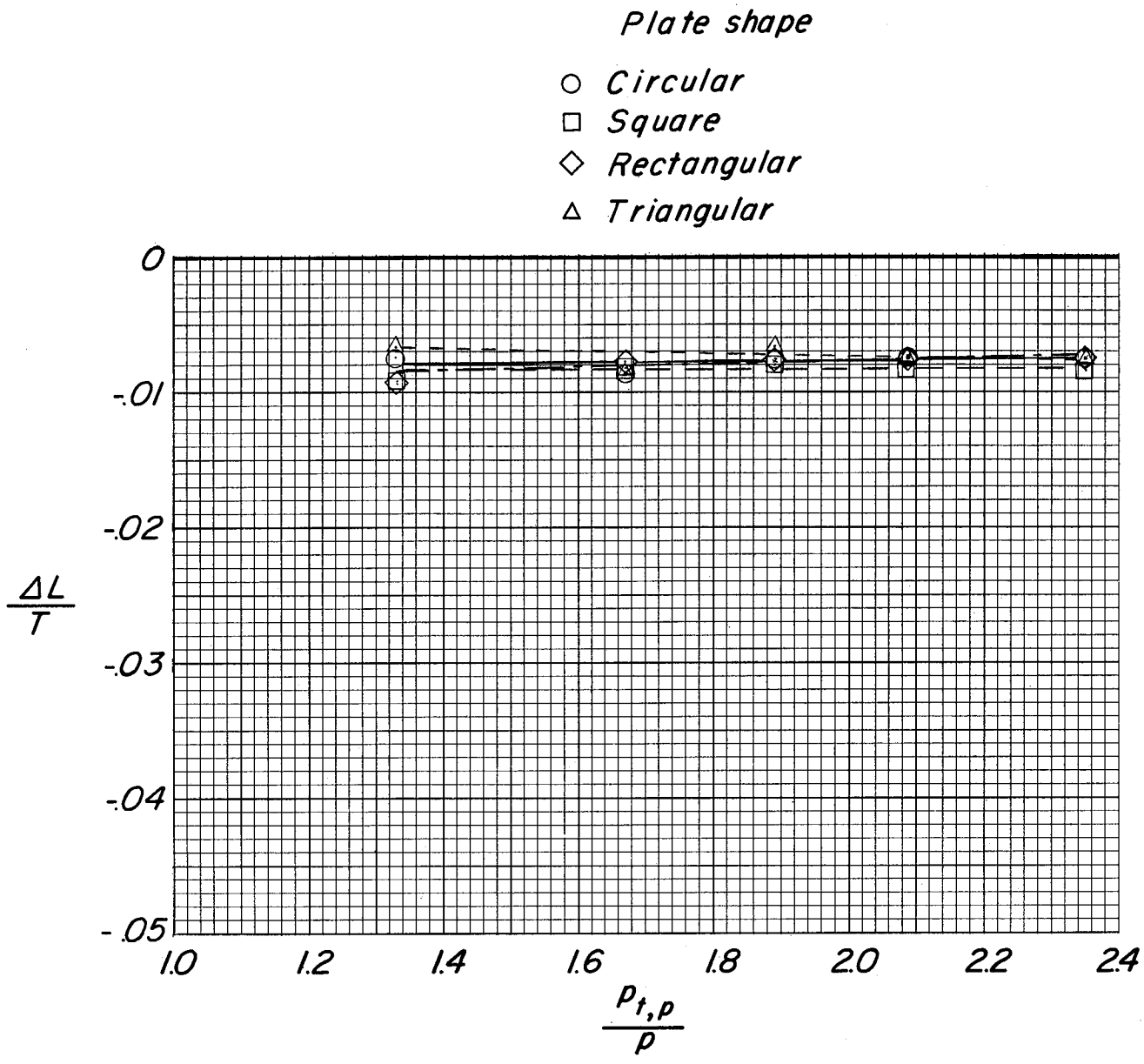

Figure 19.- Effect of planform shape on thrust losses. Cylindrical plenum chamber; $S/A_j = 69.5$.

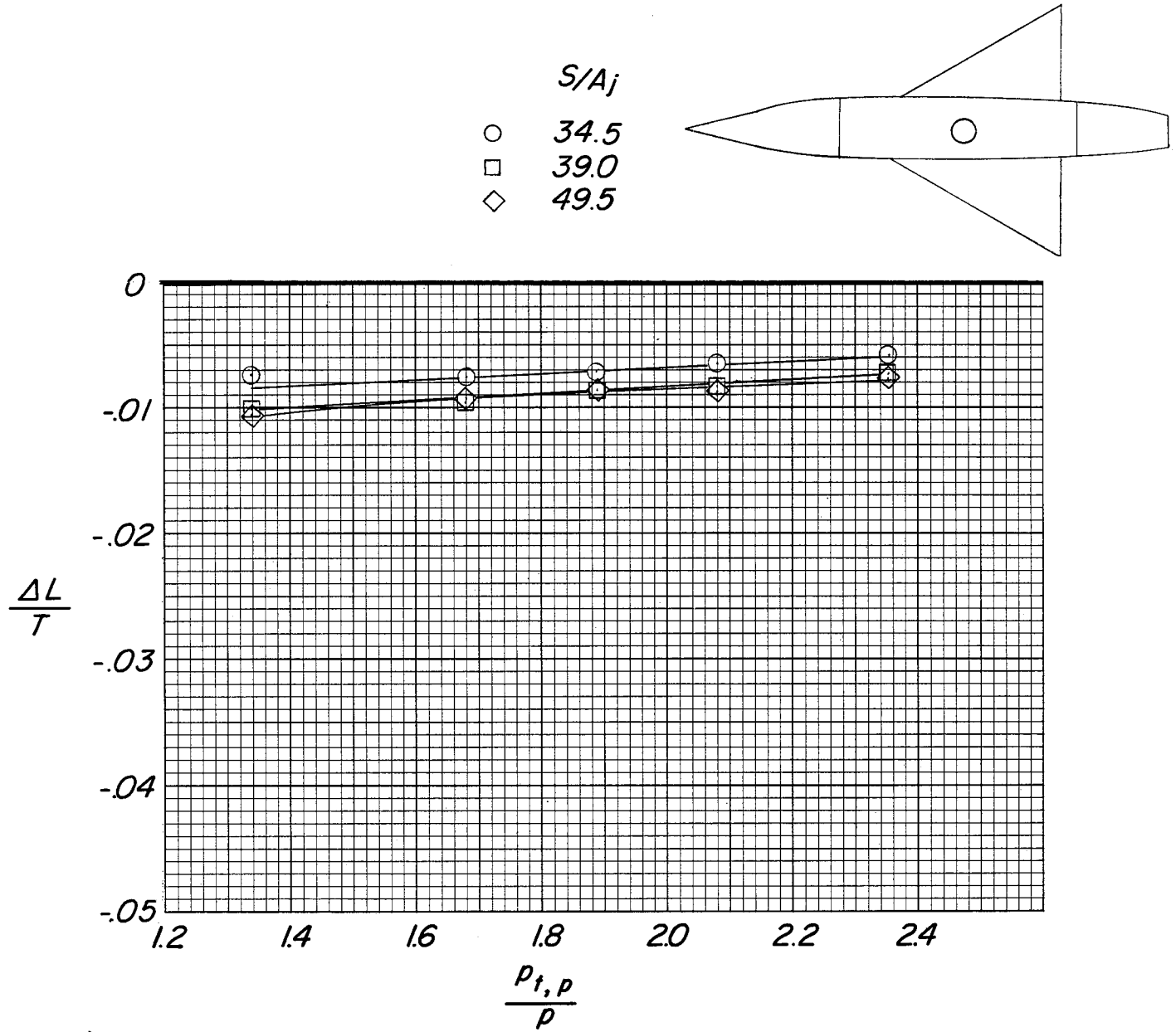

Figure 20.- Effect of wing size on induced loads for single jet on rectangular plenum chamber with delta wings in low-wing position.

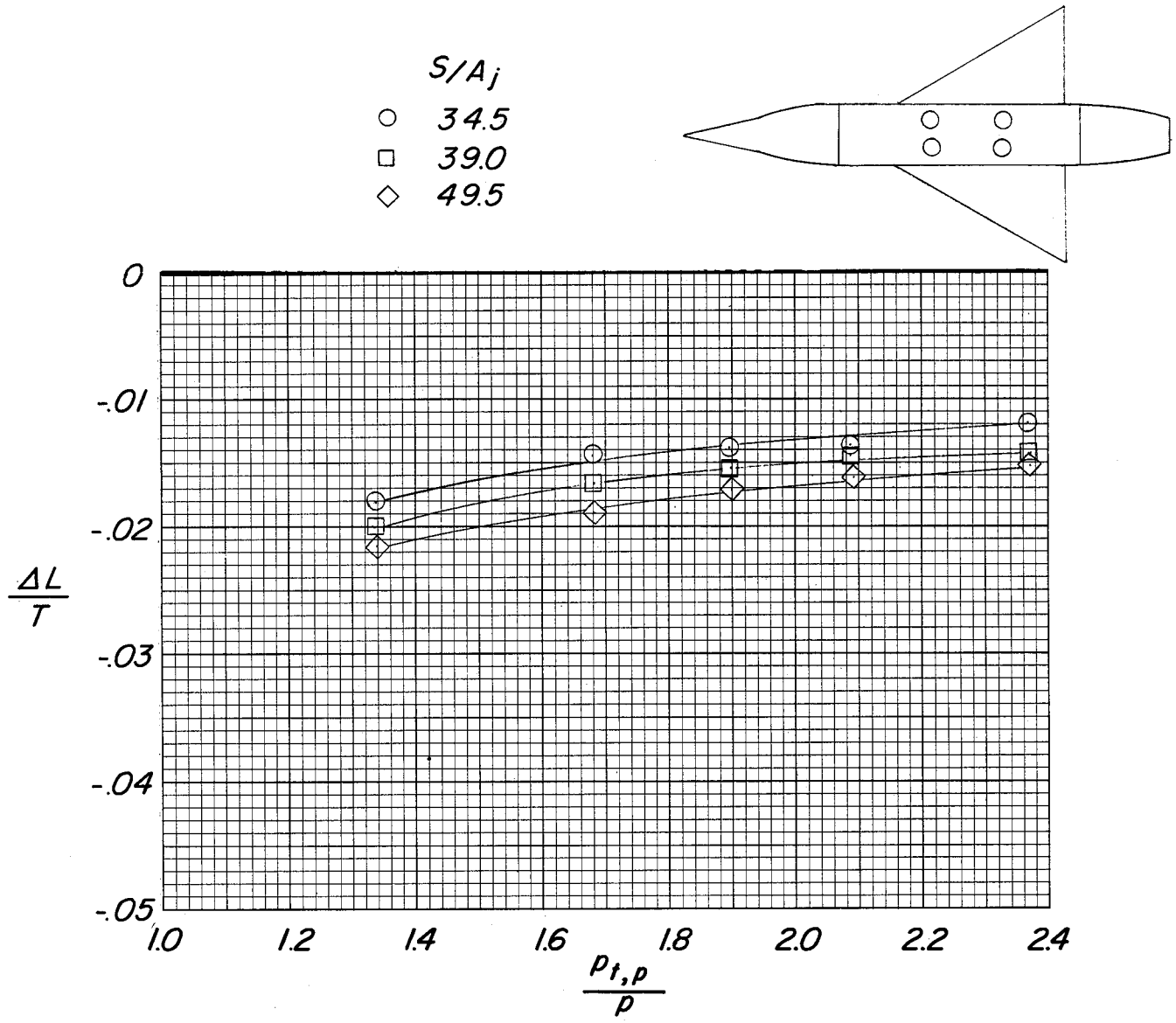

(a) Delta wings.

Figure 21.- Effect of wing size and planform on induced loads for four jets on rectangular plenum chamber. Low-wing position.

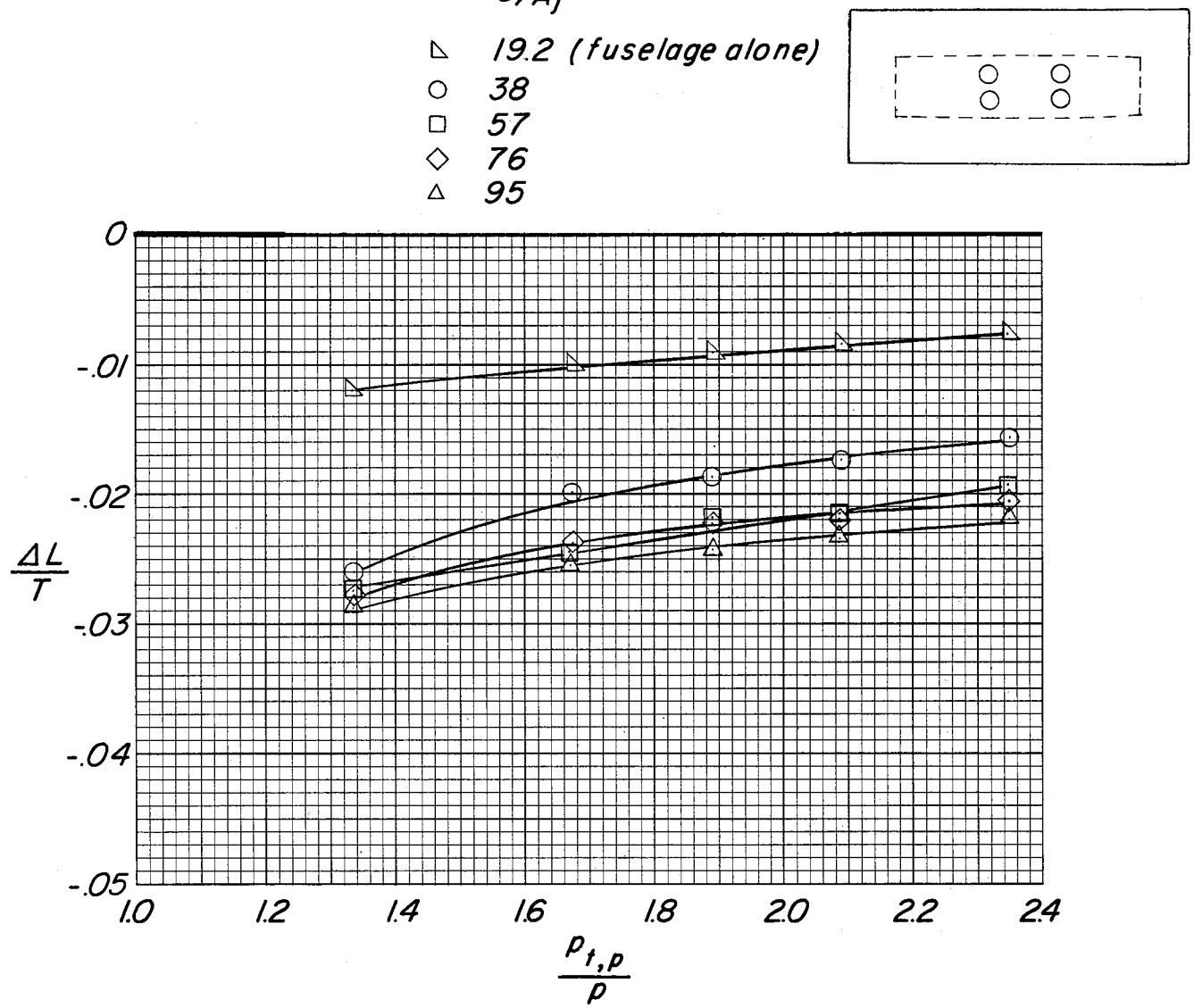

(b) Rectangular plates.

Figure 21.- Concluded.

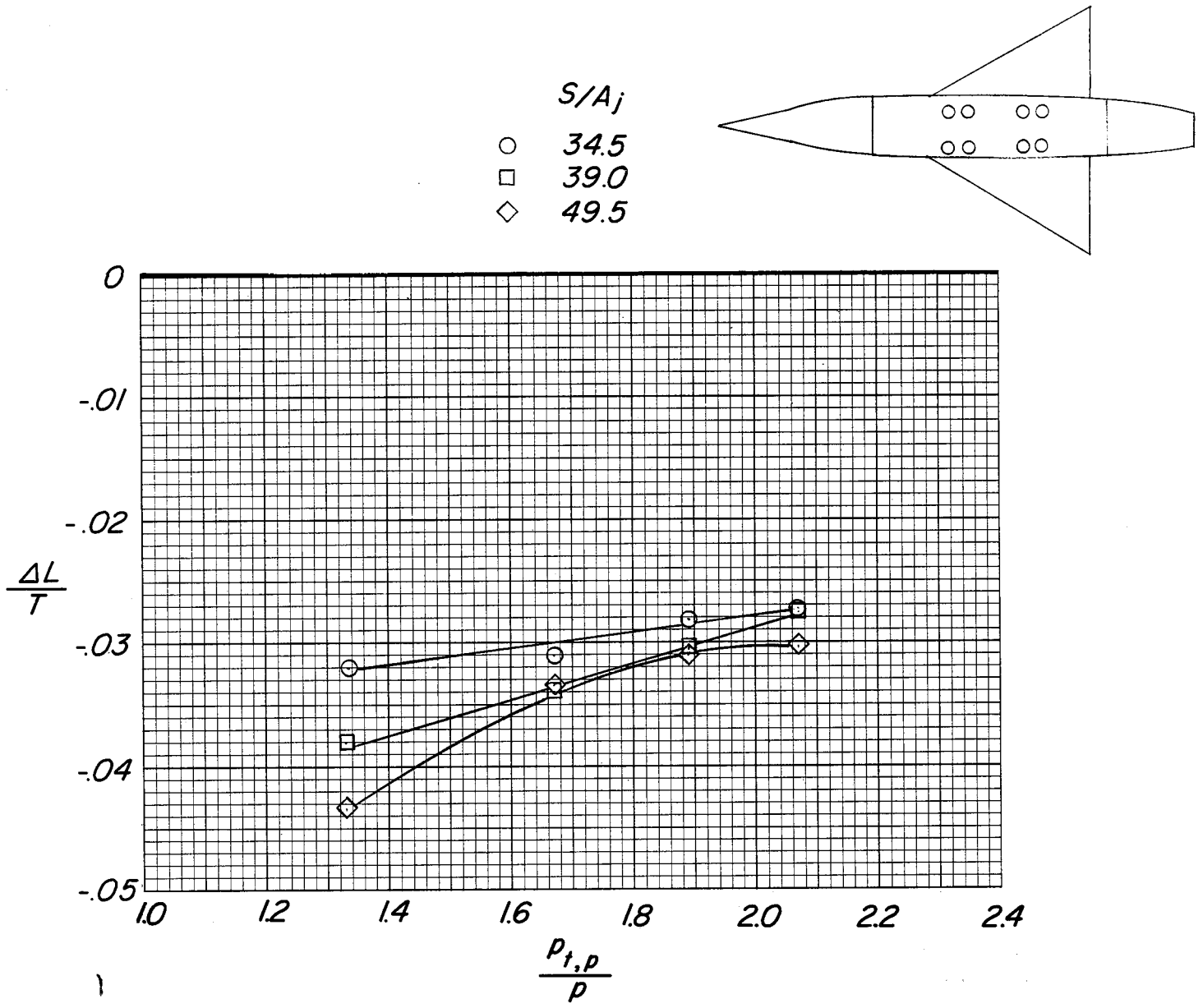

Figure 22.- Effect of wing size on induced loads for eight jets on rectangular plenum chamber. Low-wing position.

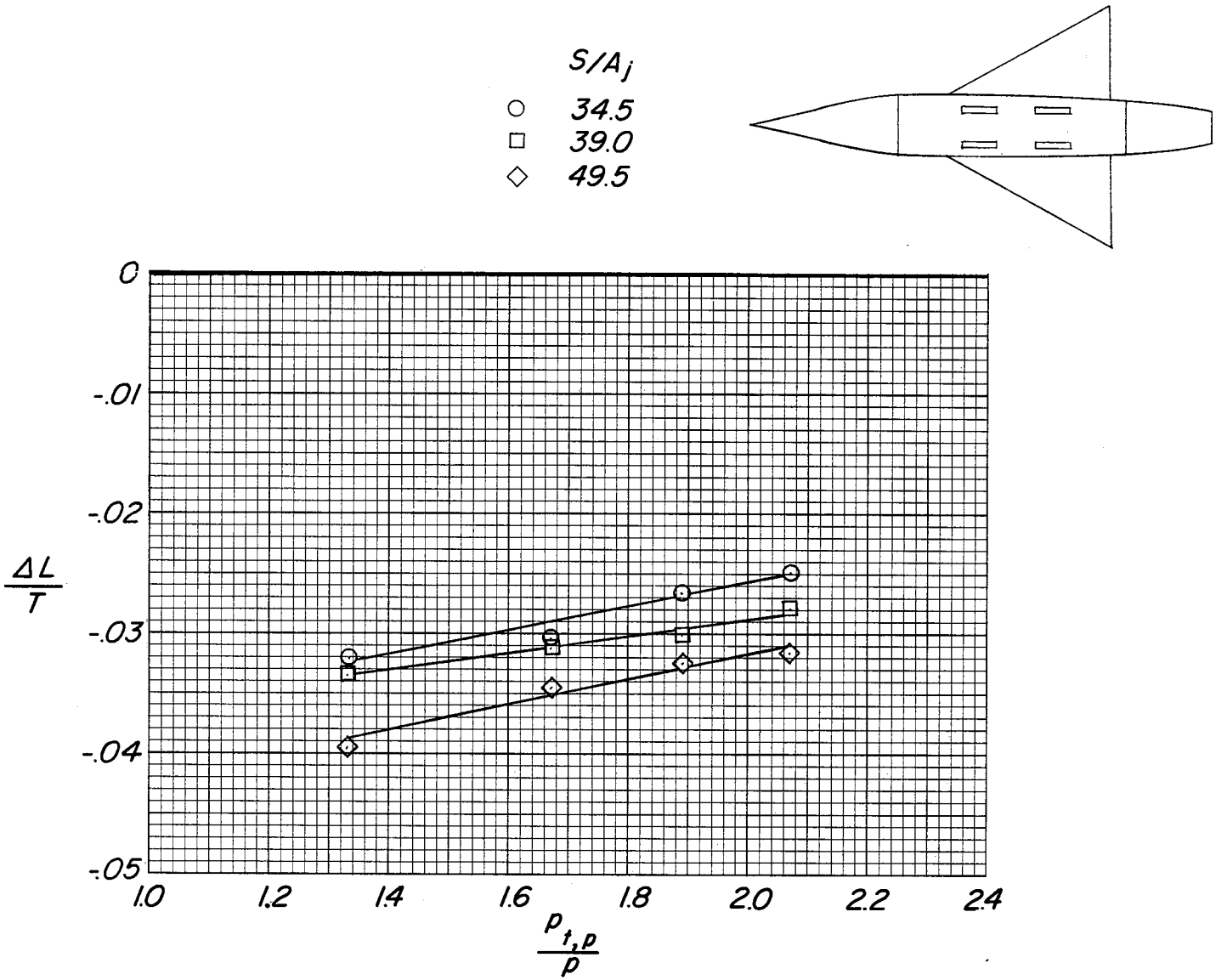

(a) Delta wings.

Figure 23.- Effect of planform size on induced loads for four-slot configuration. Low-wing position.

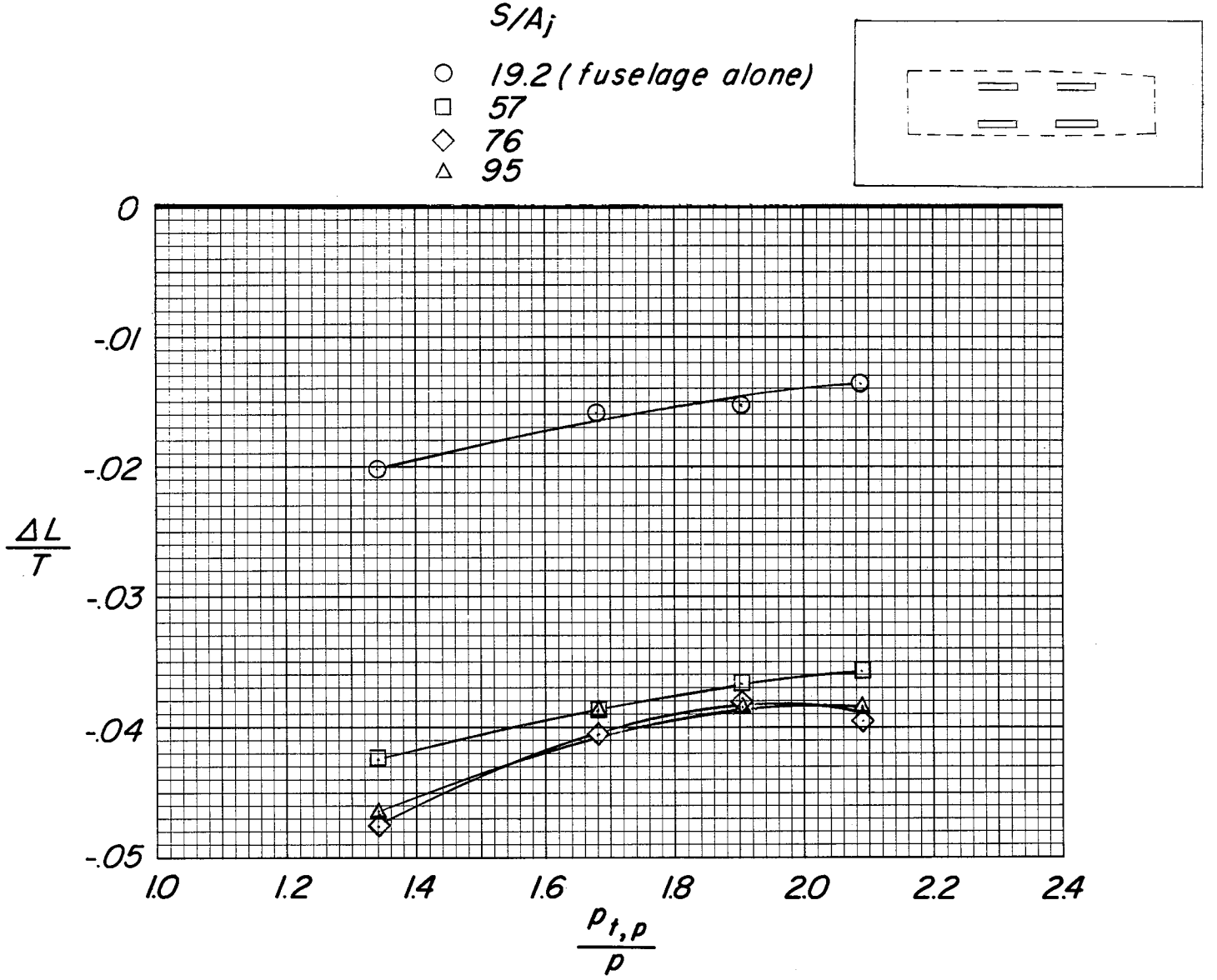

(b) Rectangular plates.

Figure 23.- Concluded.

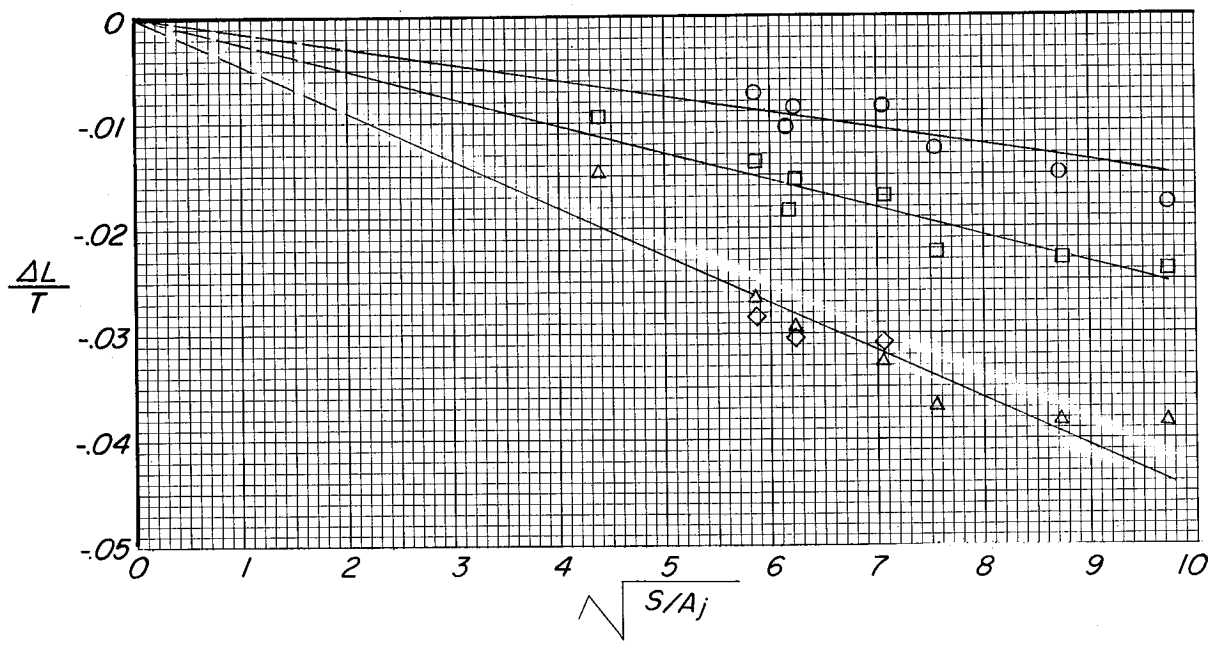

(a) Induced load.

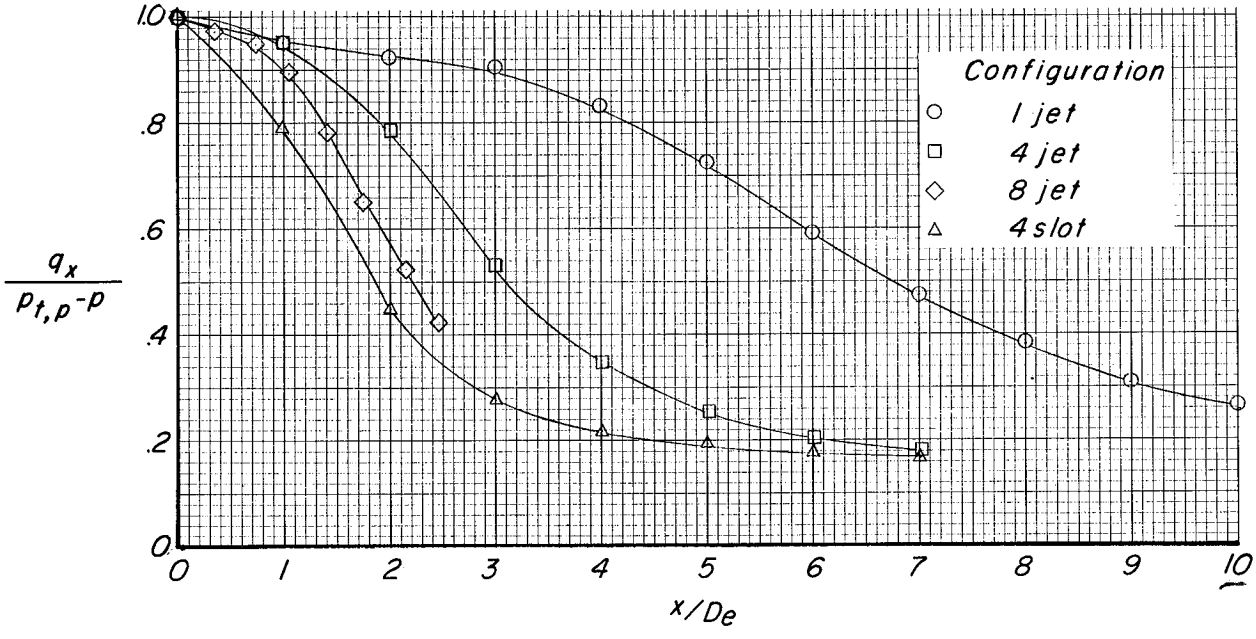

(b) Impact-pressure decay.

Figure 24.- Induced load on several planform plates and impact-pressure decay for single-jet and multiple-jet configurations. $\frac{p_{t,p}}{p} = 1.89$.

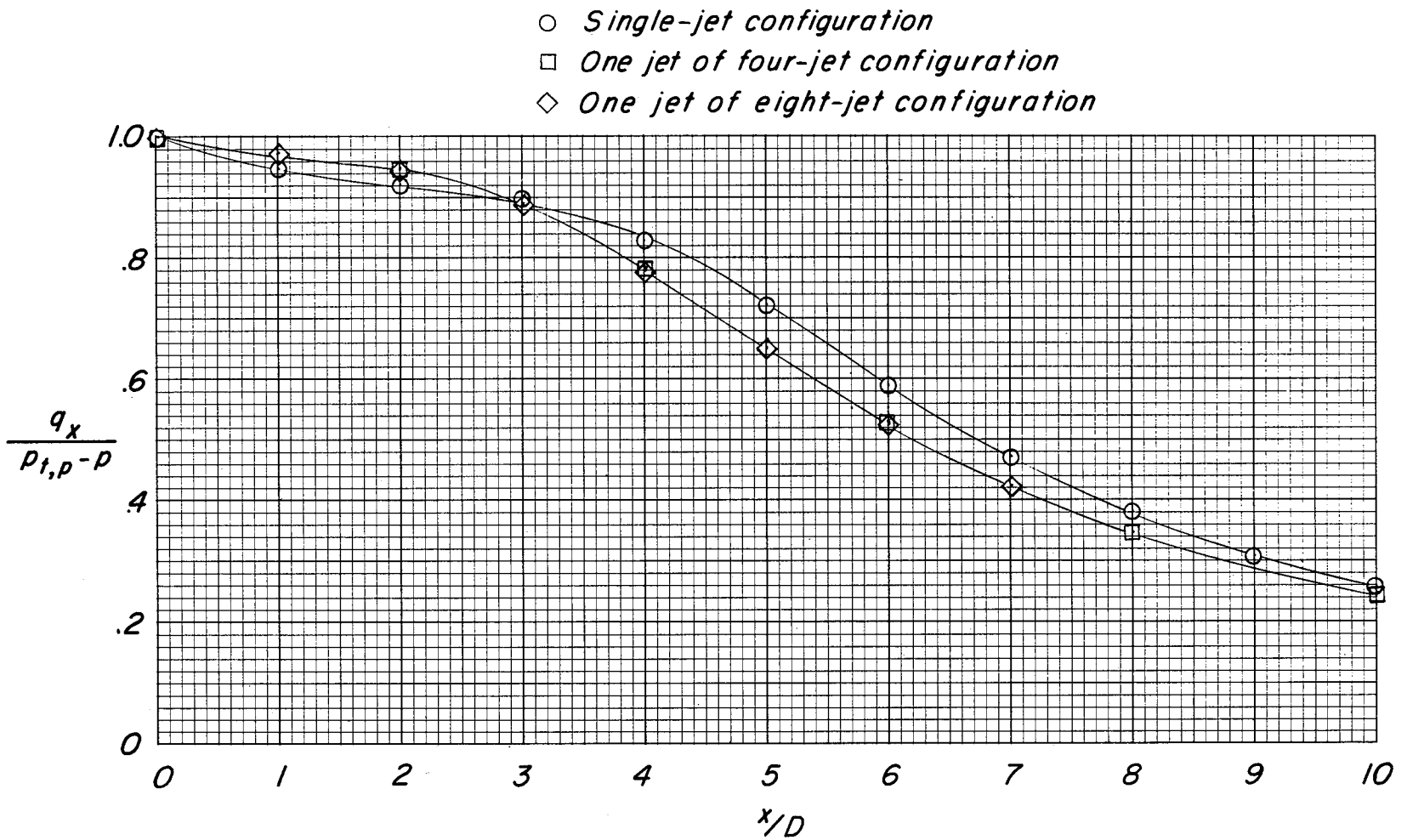

Figure 25.- Comparison of decay curves based on actual jet diameter. $\frac{p_{t,p}}{p} = 1.89$.

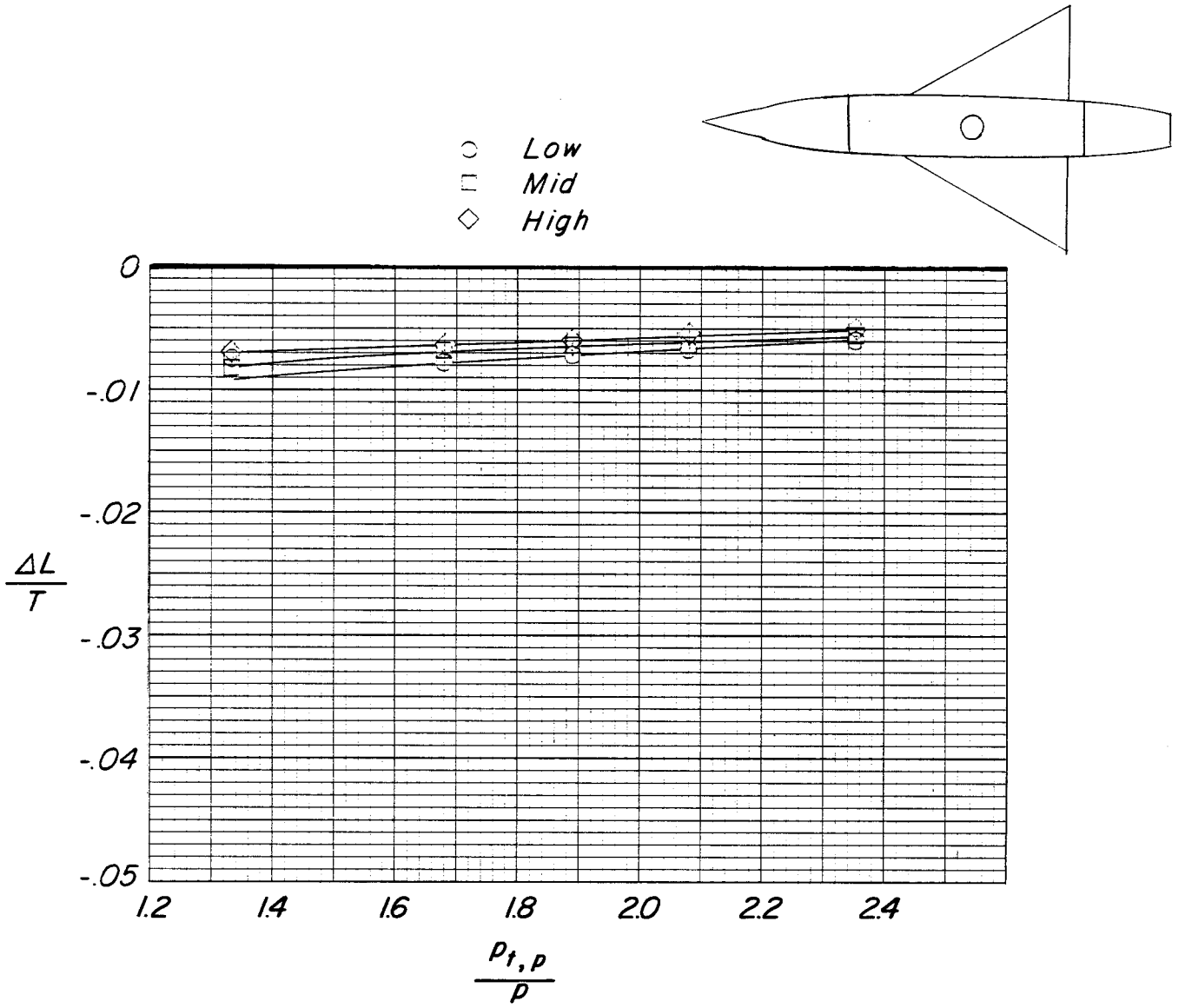

(a) $S/A_j = 34.5$.

Figure 26.- Effect of wing height for single jet on rectangular plenum chamber.

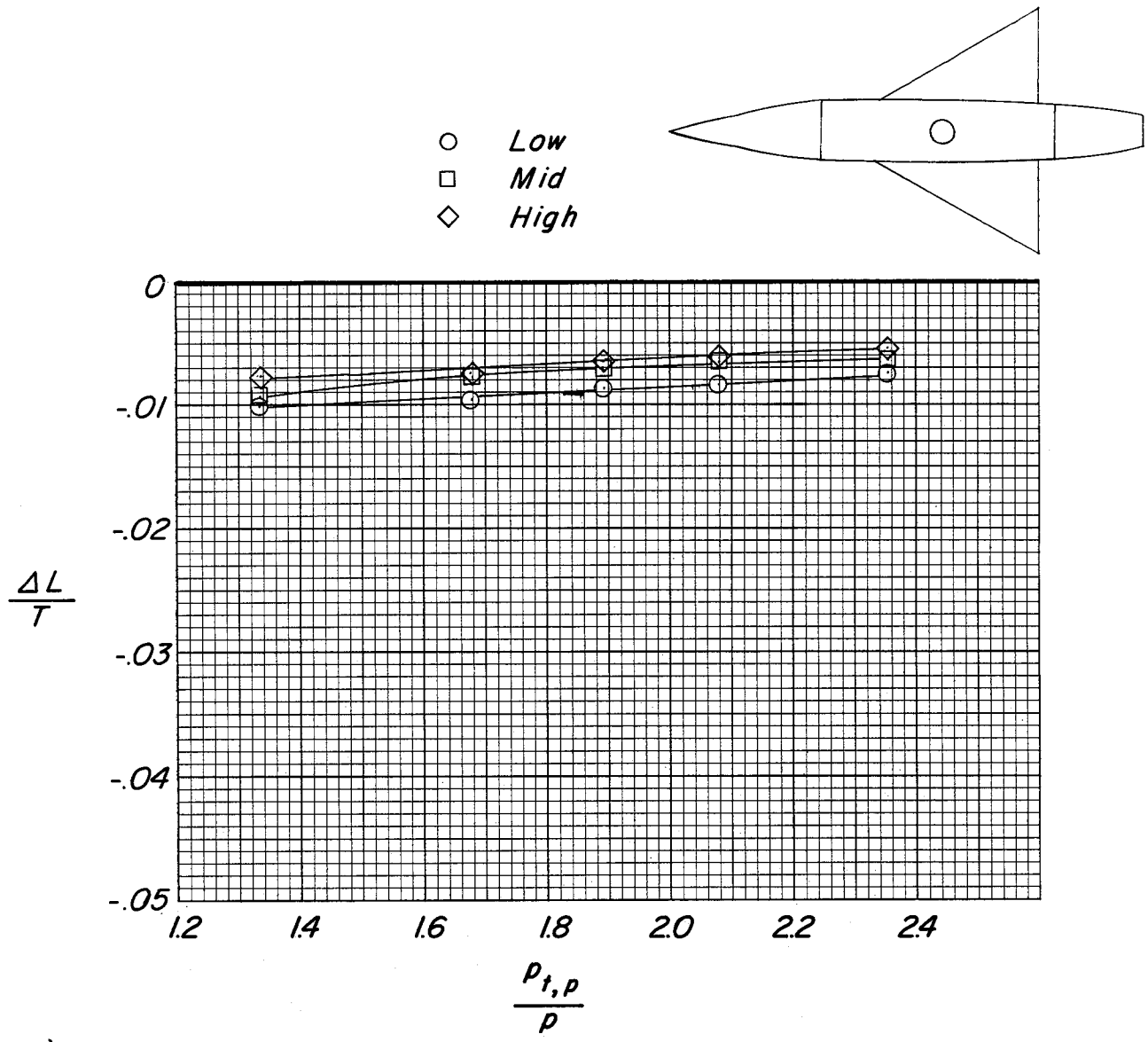

(b) $S/A_j = 39.$

Figure 26.- Continued.

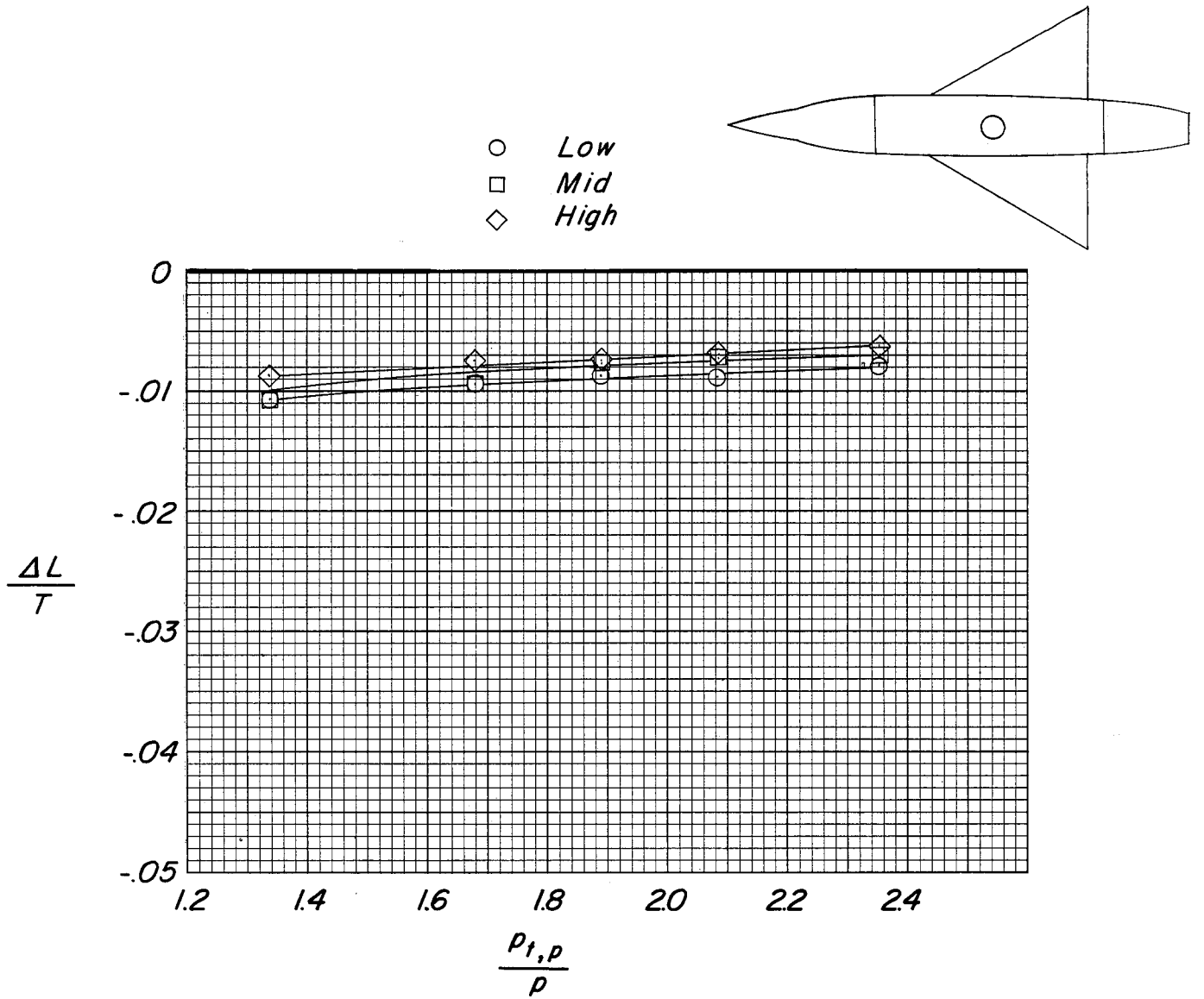

(c) $S/A_j = 49.5$.

Figure 26.- Concluded.

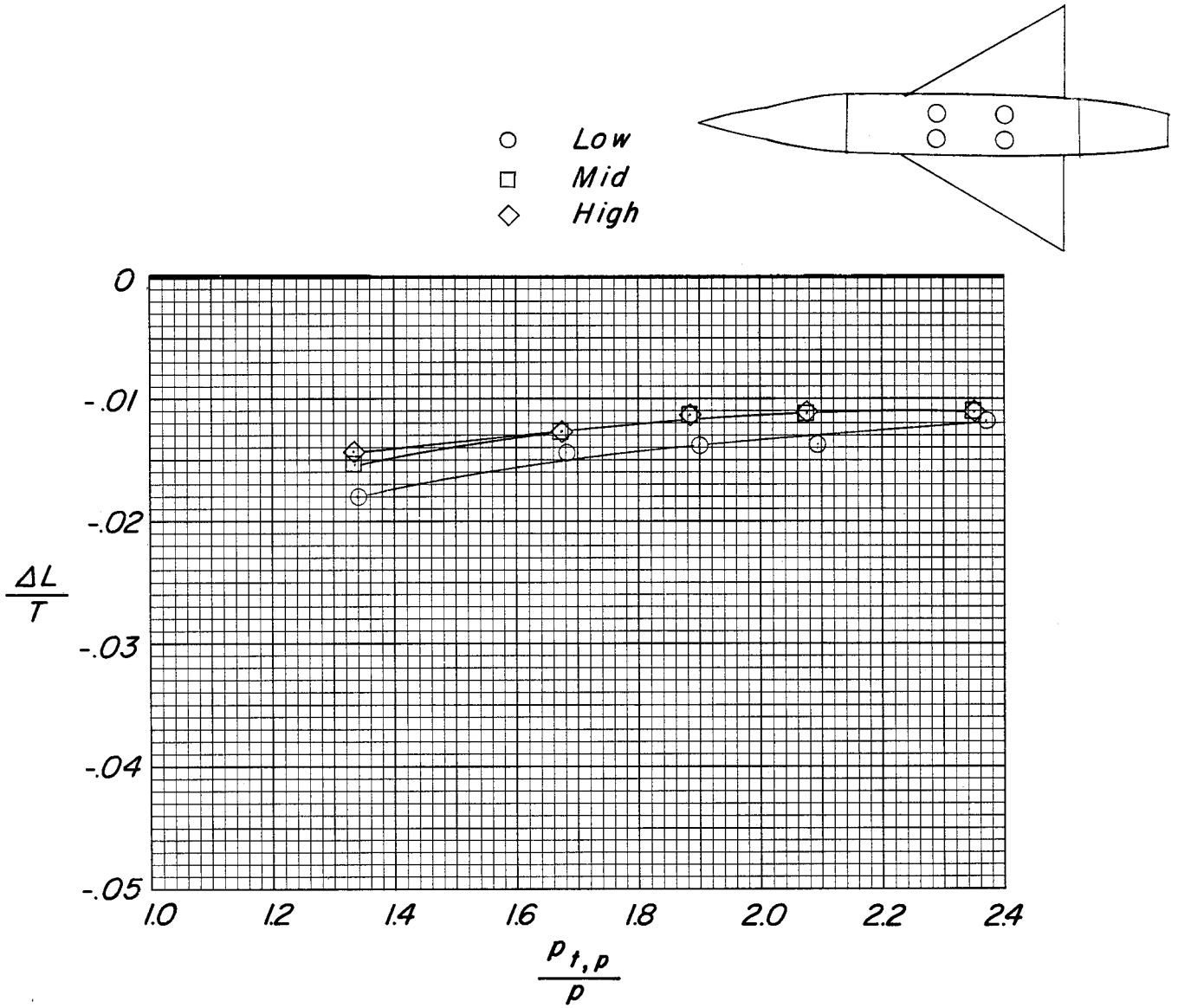

(a) $S/A_j = 34.5$.

Figure 27.- Effect of wing height for four-jet configuration on rectangular plenum chamber.

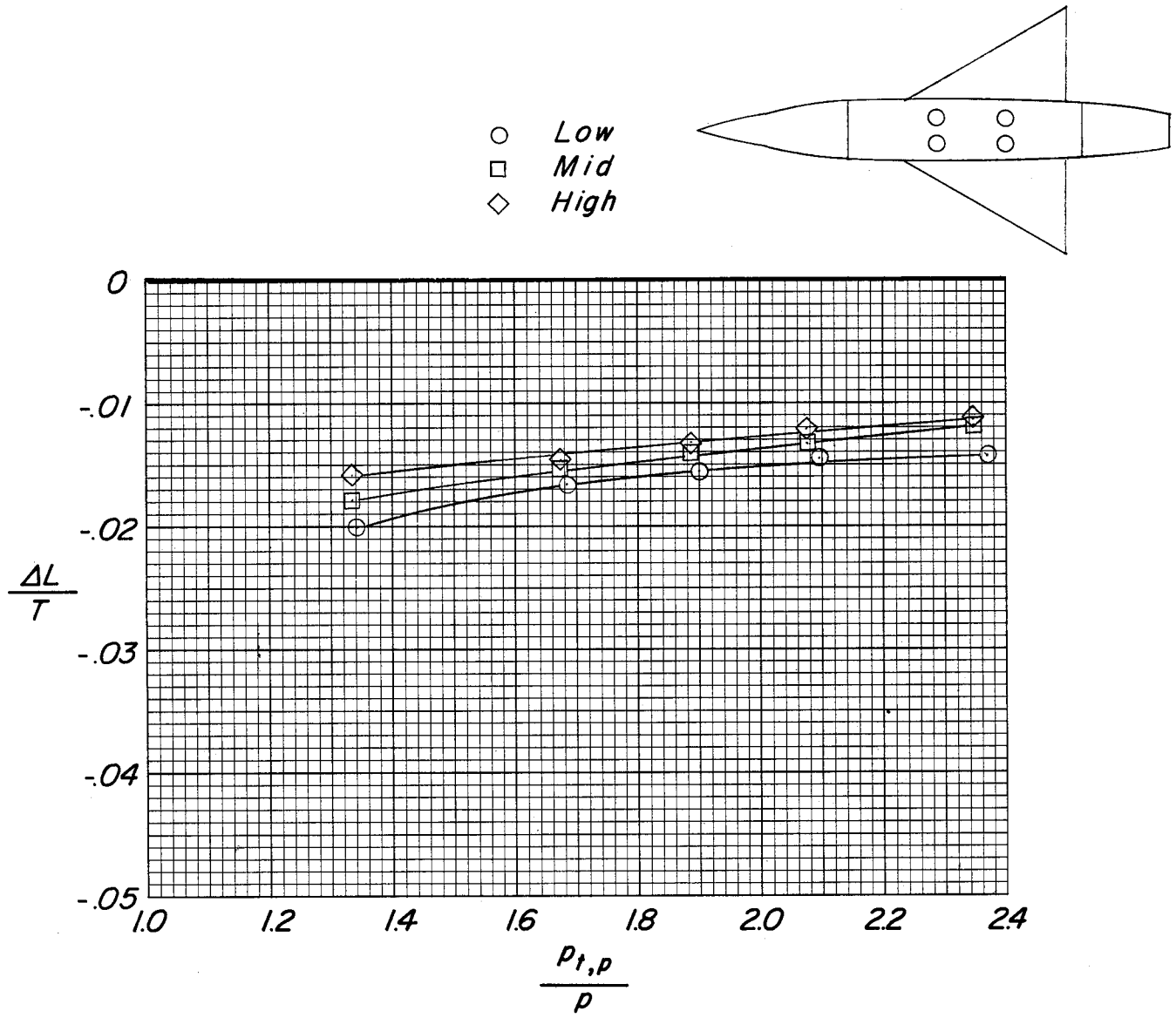

(b) $S/A_j = 39.$

Figure 27.- Continued.

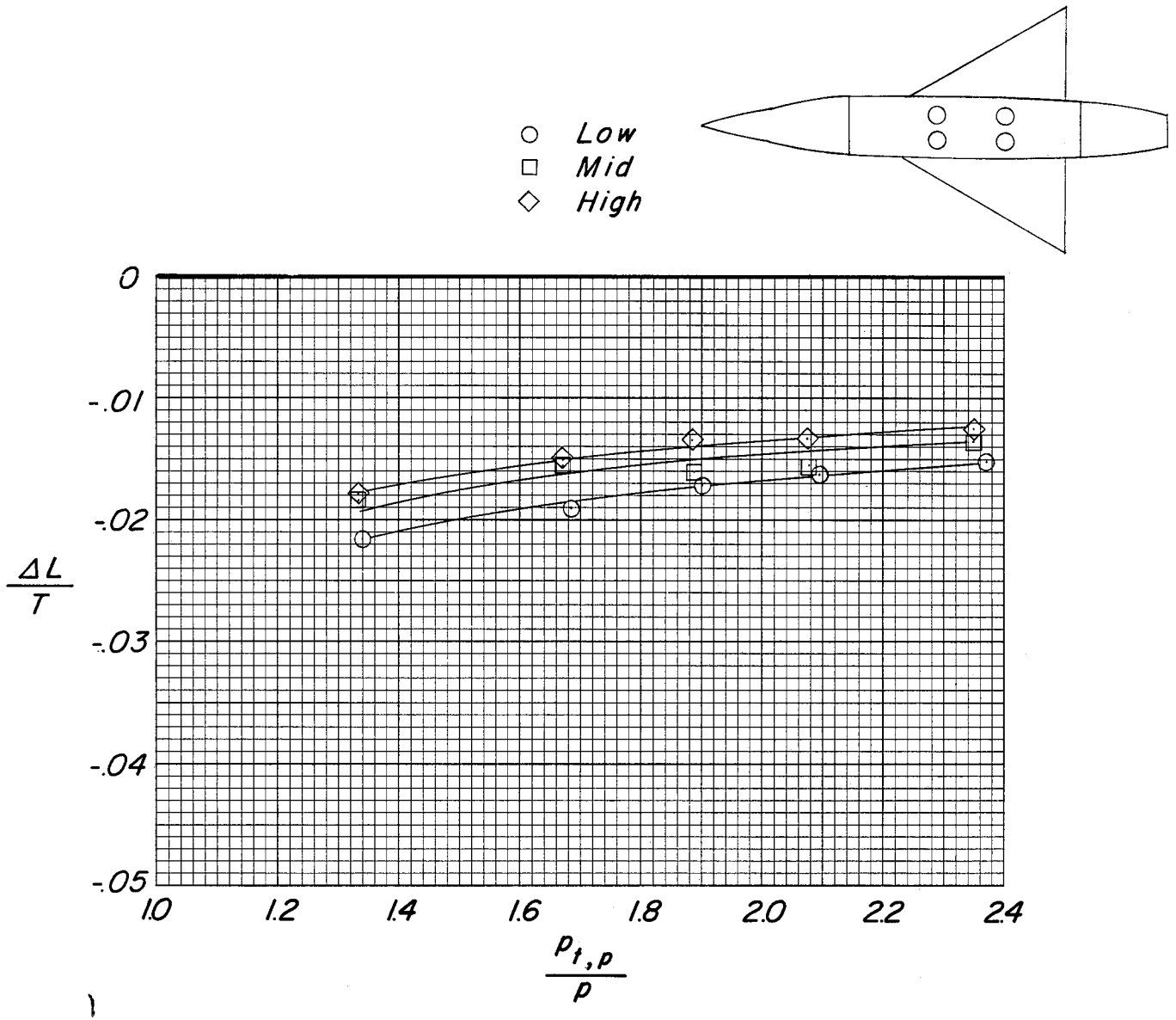

(c) $S/A_j = 49.5$.

Figure 27.- Concluded.

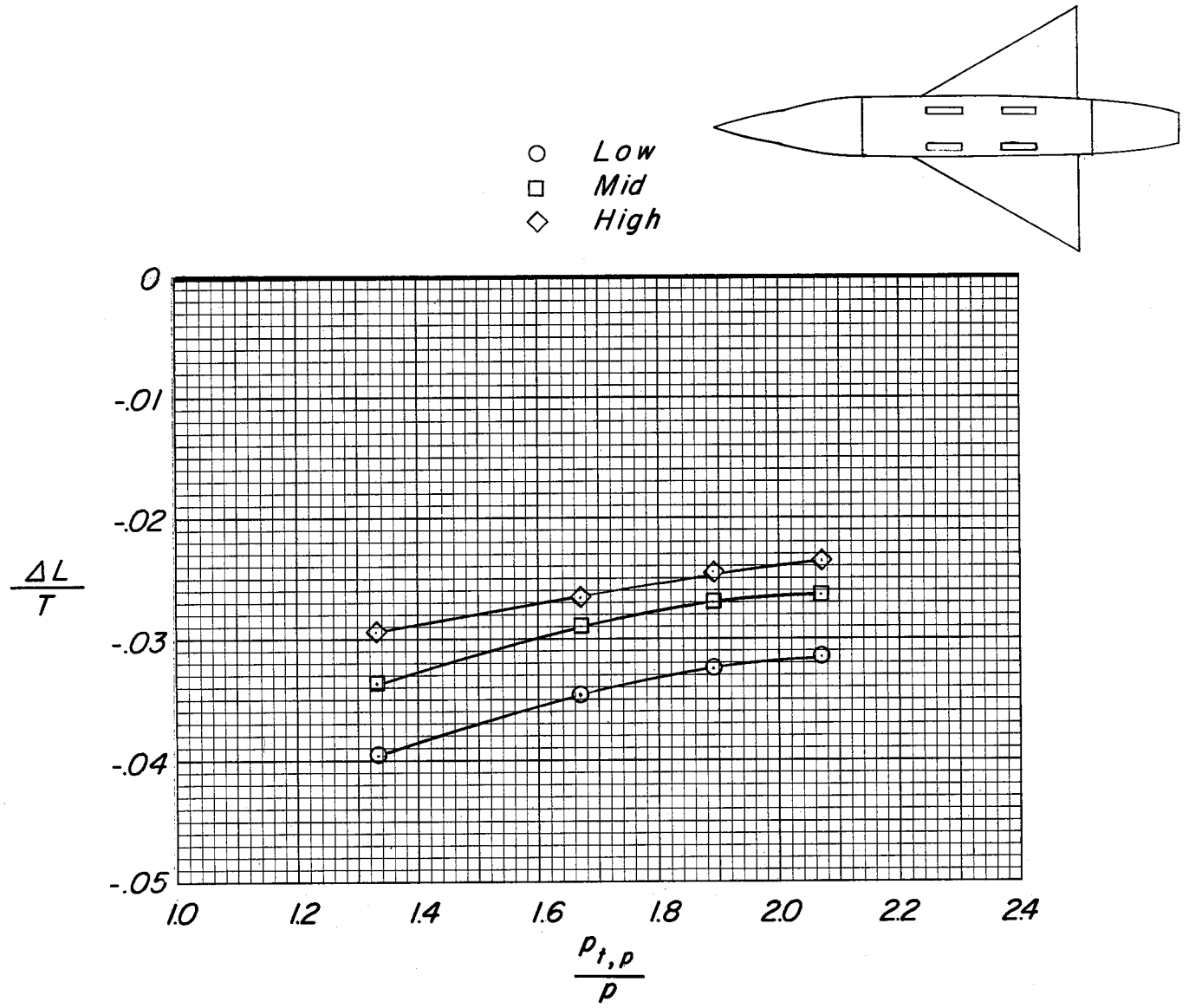

Figure 28.- Effect of wing height for slot-jet configuration on rectangular plenum chamber. $S/A_j = 49.5$.

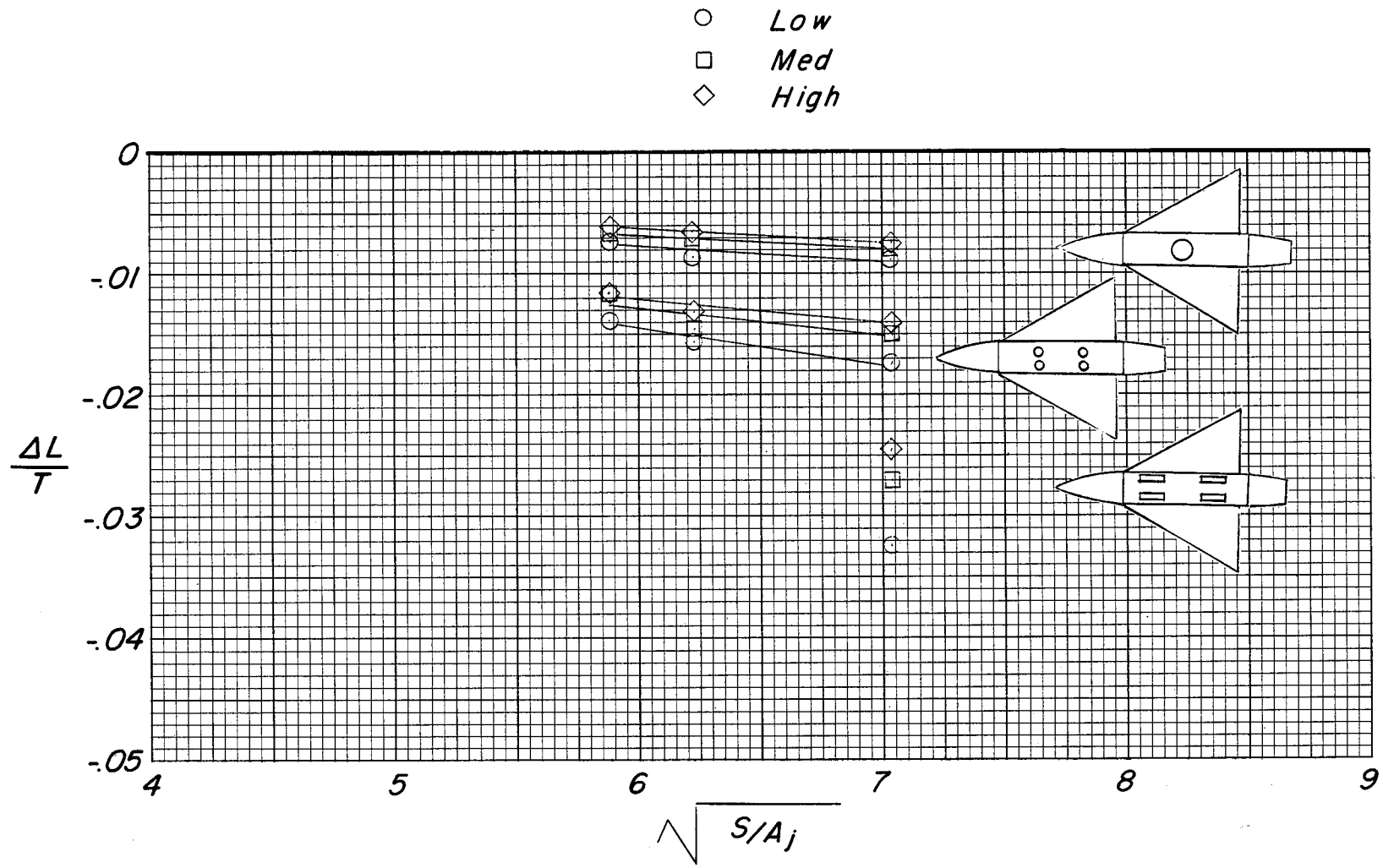

Figure 29.- Comparison of effect of wing height for single-jet, four-round-jet, and four-slot-jet configurations. $\frac{p_{t,p}}{p} = 1.89$.

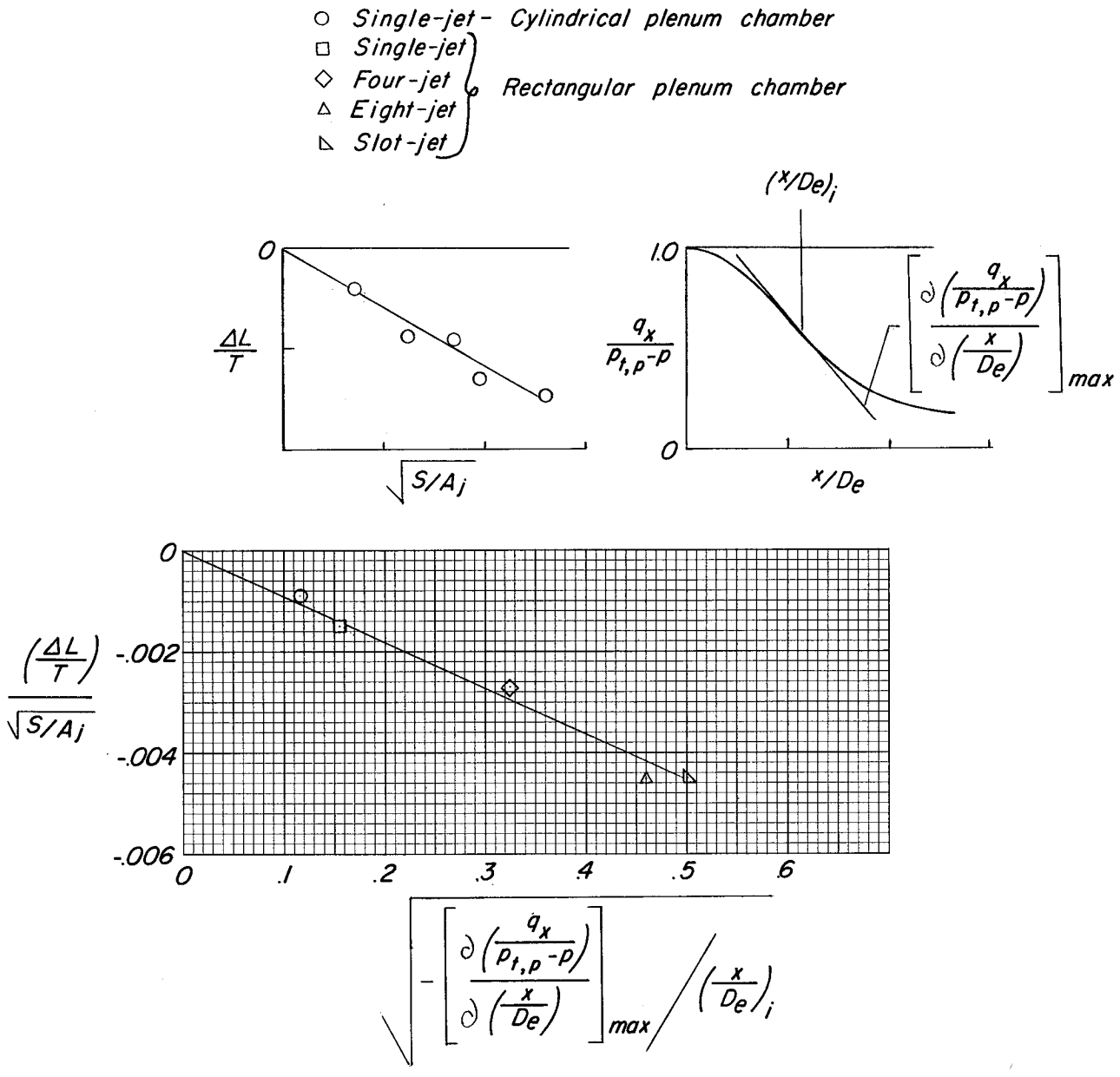

Figure 30.- Correlation of induced loads with jet decay parameter.

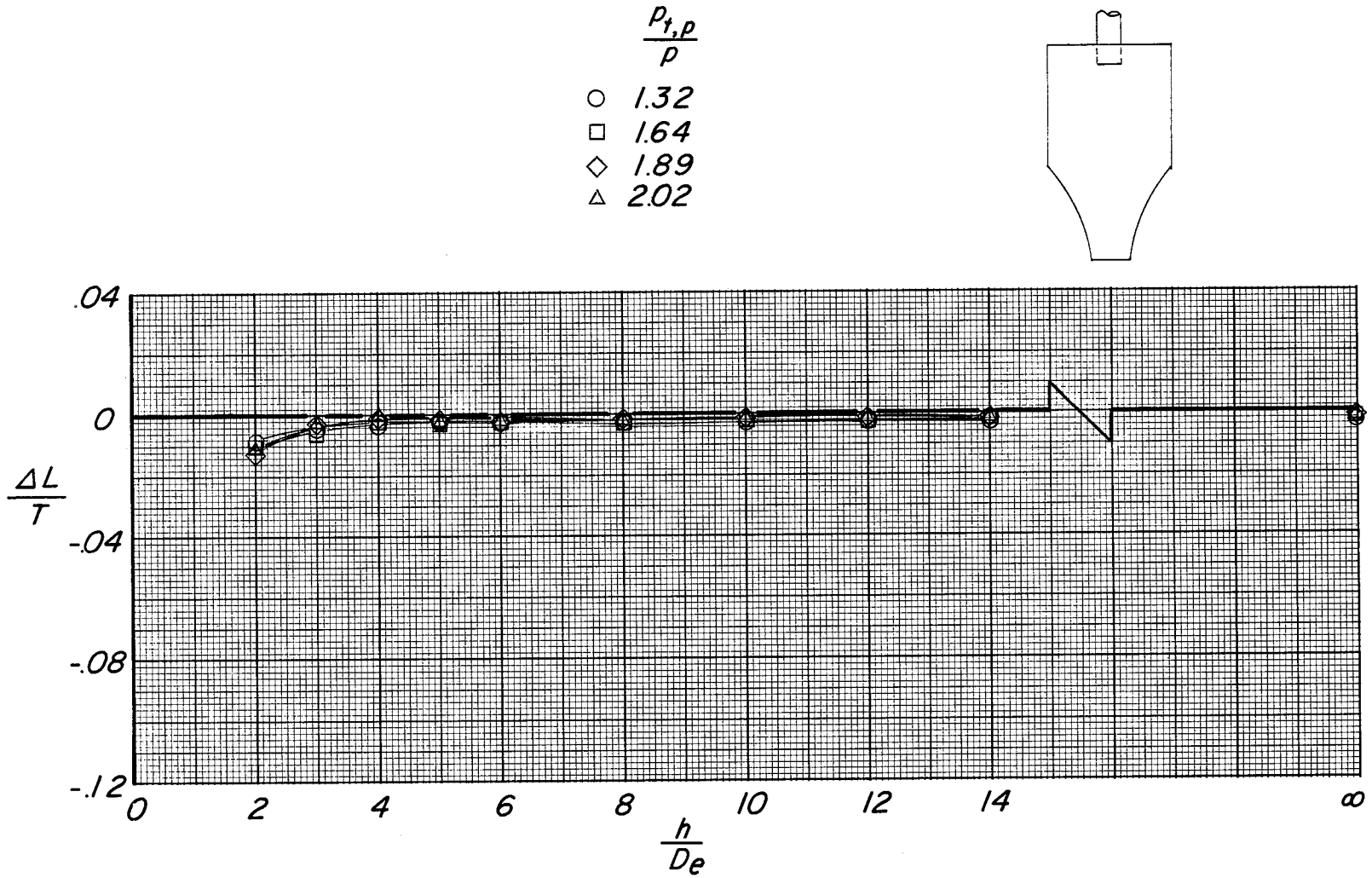

(a) $S/A_j = 10.$

Figure 31.- Effect of height above ground on $\frac{\Delta L}{T}$ as $\frac{p_{t,p}}{p}$ increases on cylindrical plenum chamber with circular-planform plates.

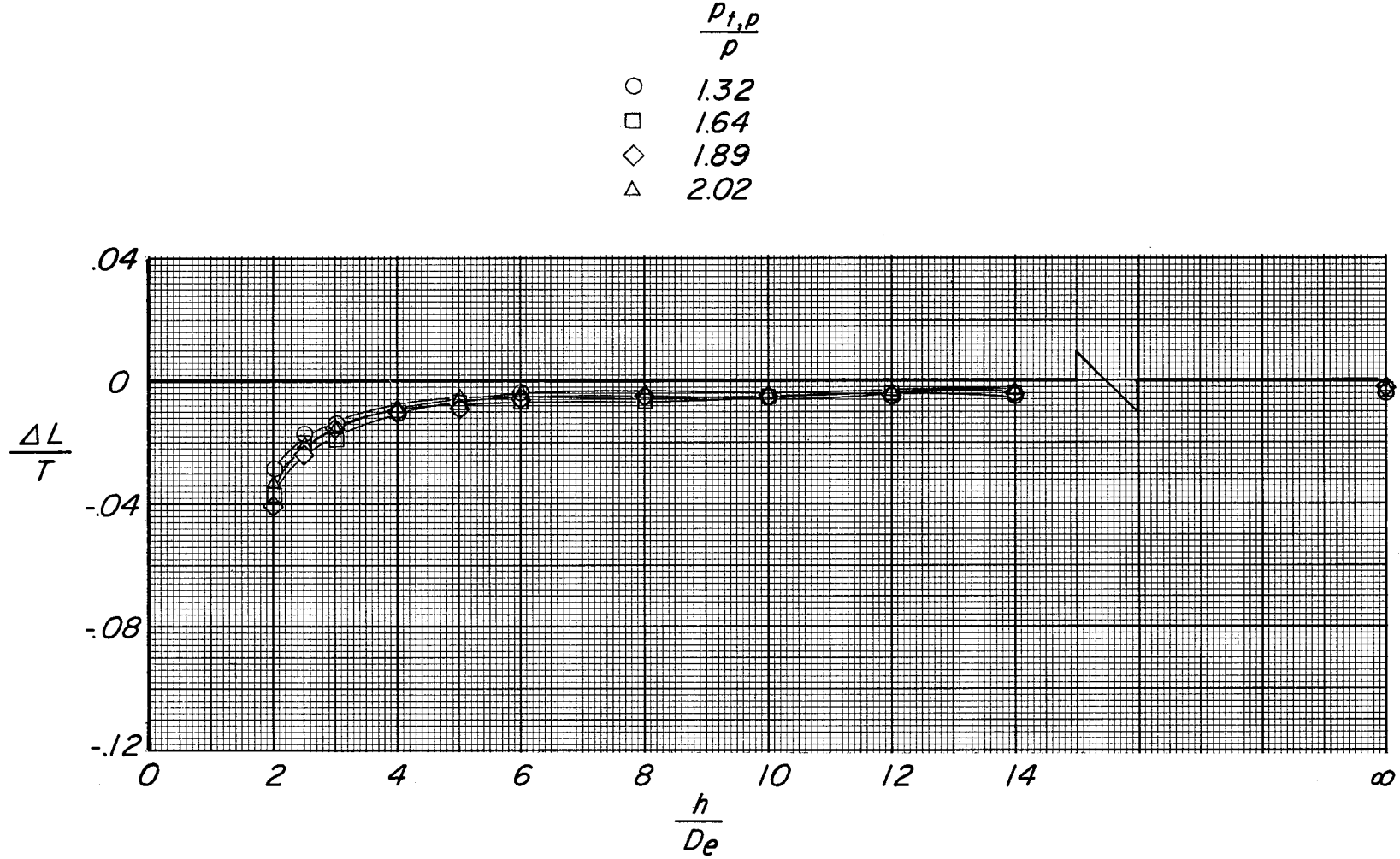

(b) $S/A_j = 20.$

Figure 31.- Continued.

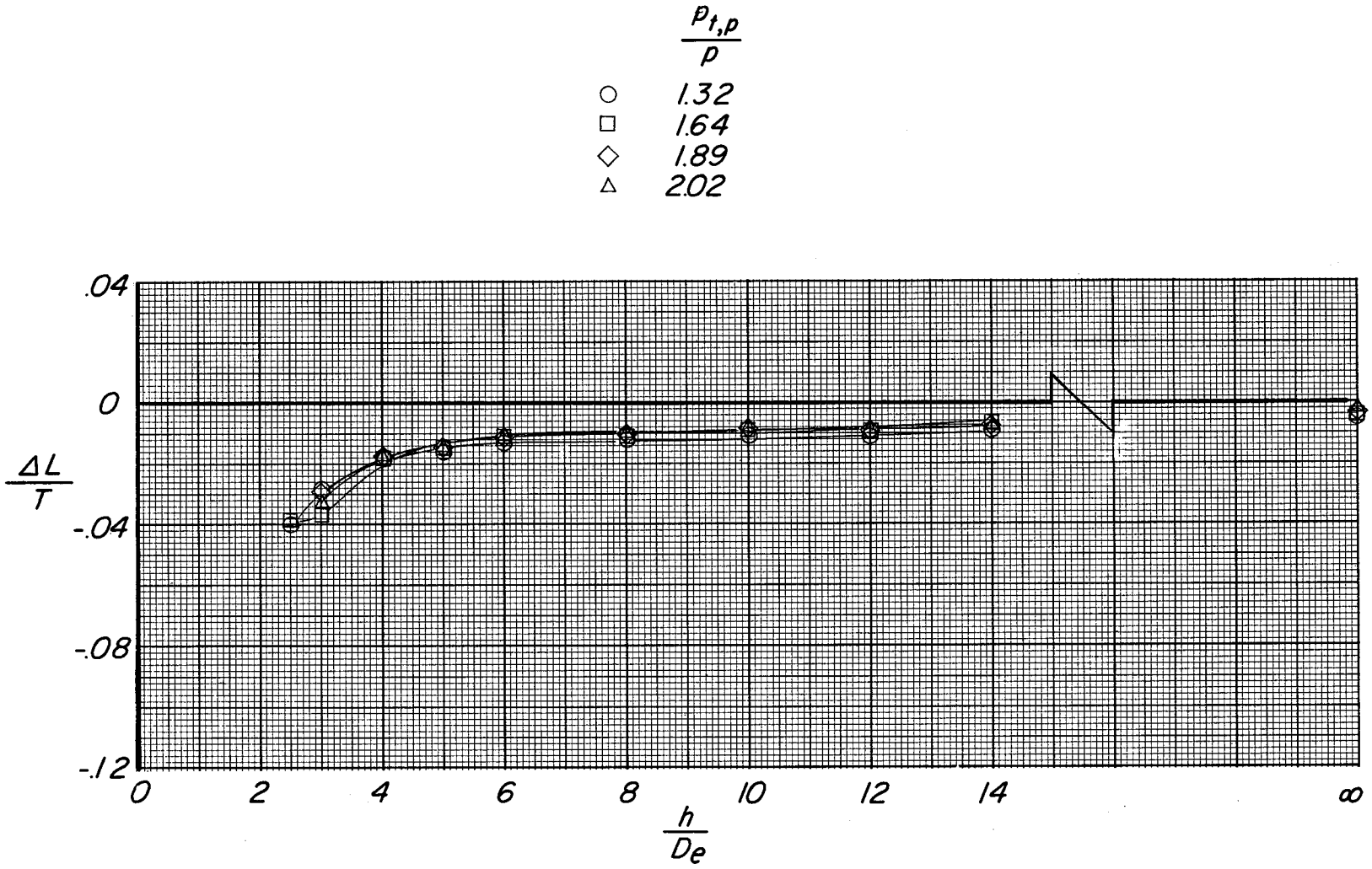

(c) $S/A_j = 30.$

Figure 31.- Continued.

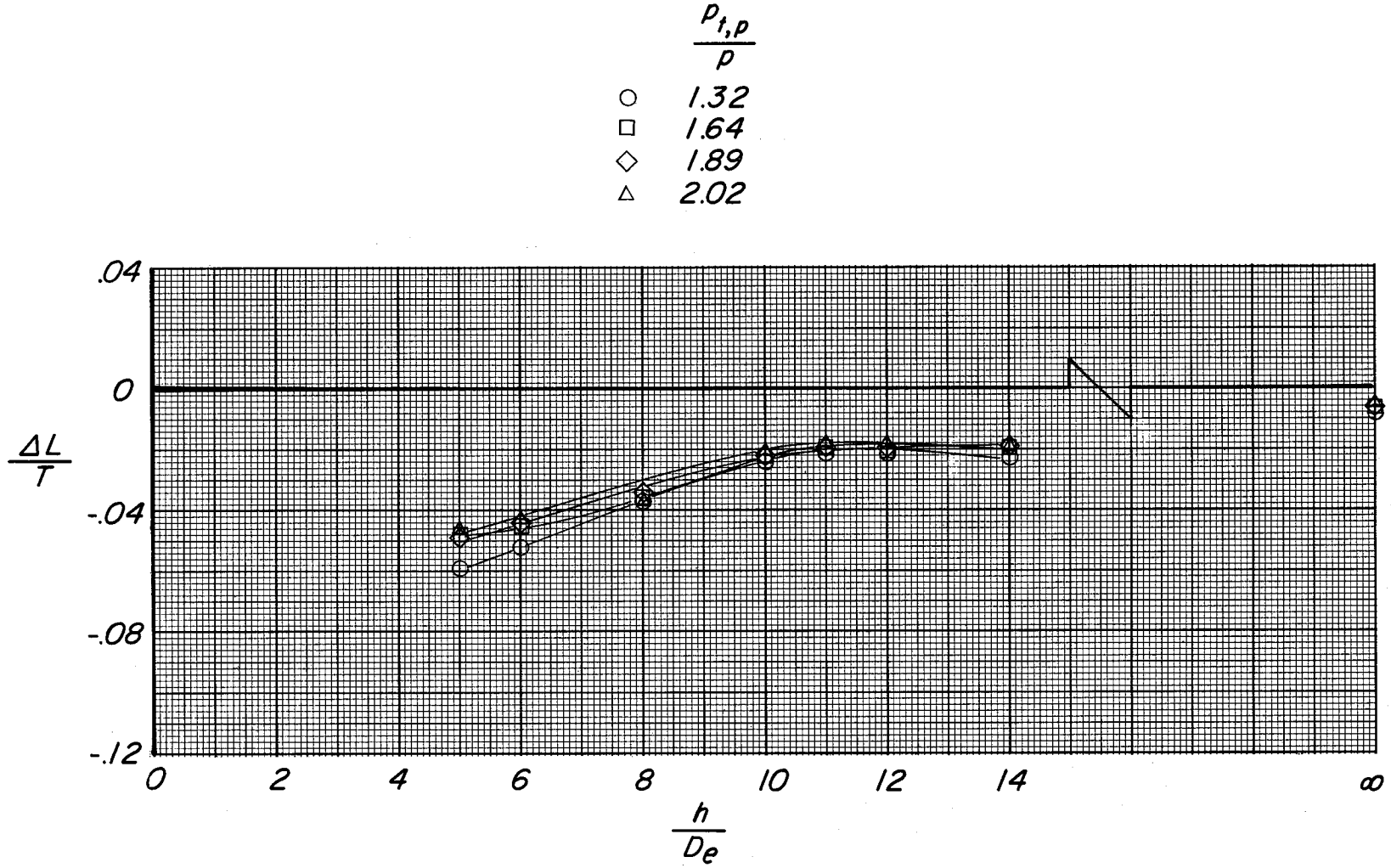

(d) $S/A_j = 69.5$.

Figure 31.- Concluded.

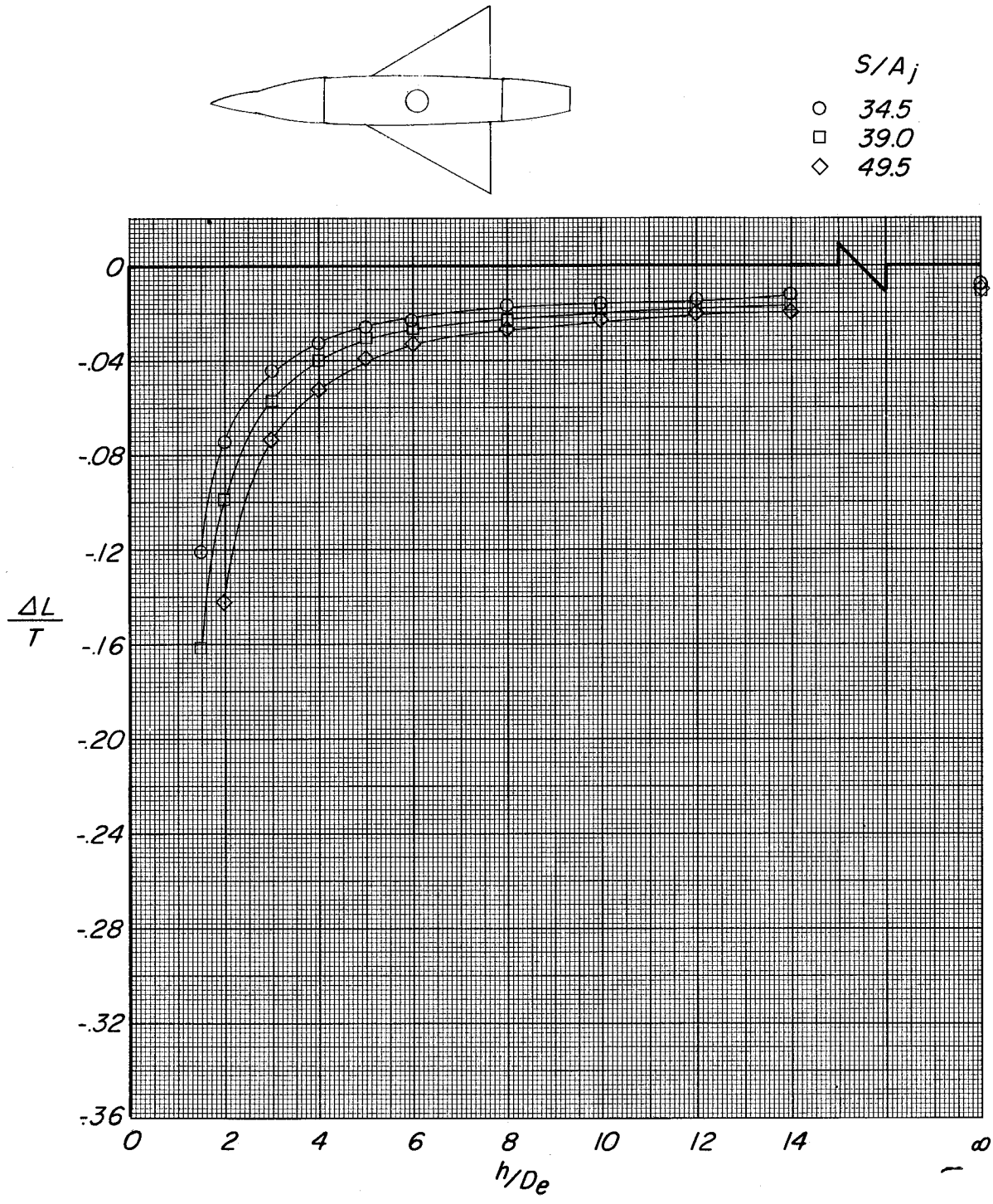

(a) $\frac{p_{t,p}}{p} = 1.34$.

Figure 32.- Effect of height above ground on $\frac{\Delta L}{T}$ as wing area increases on rectangular plenum chamber for single jet.

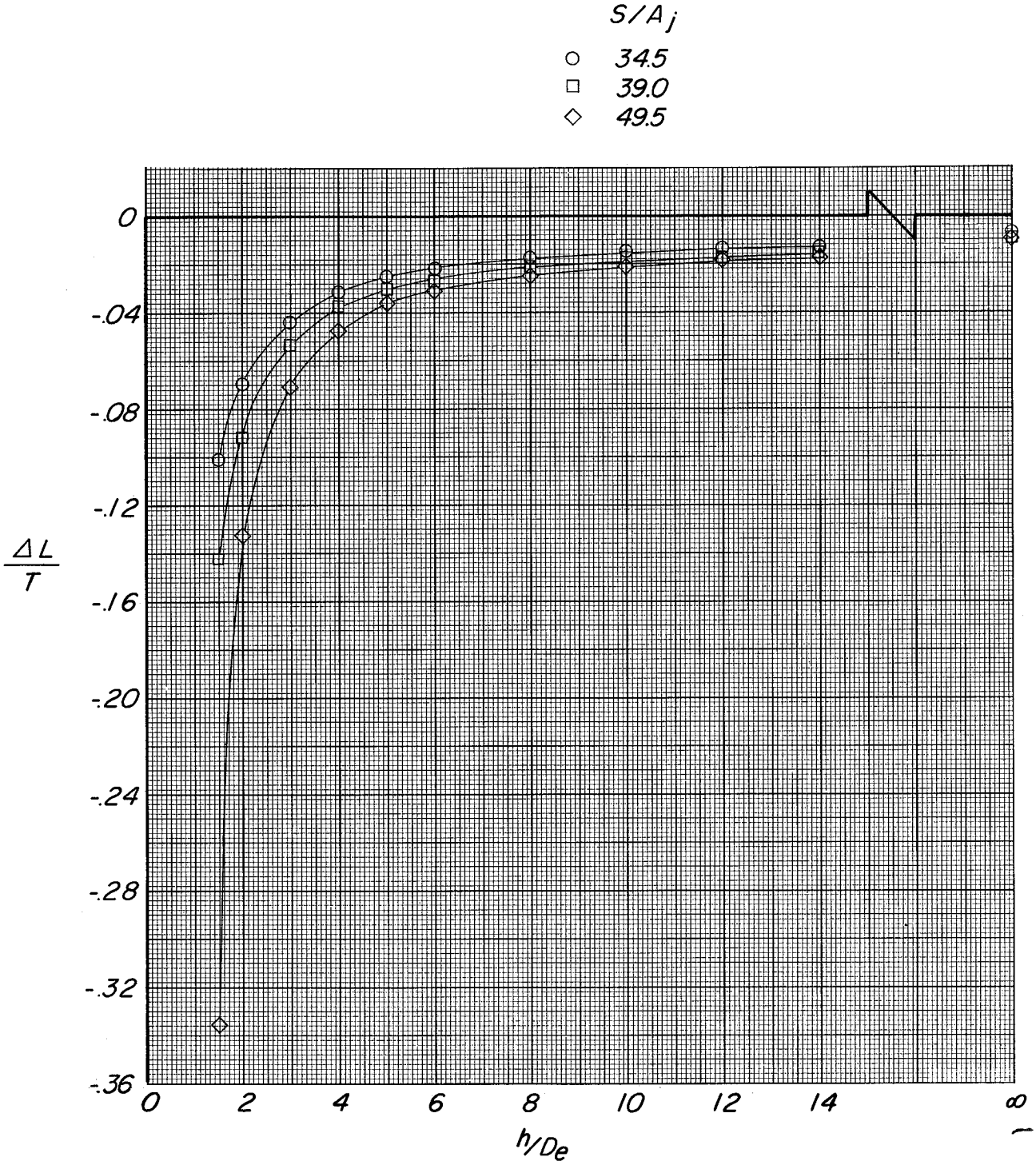

(b) $\frac{p_{t,p}}{p} = 1.68$.

Figure 32.- Continued.

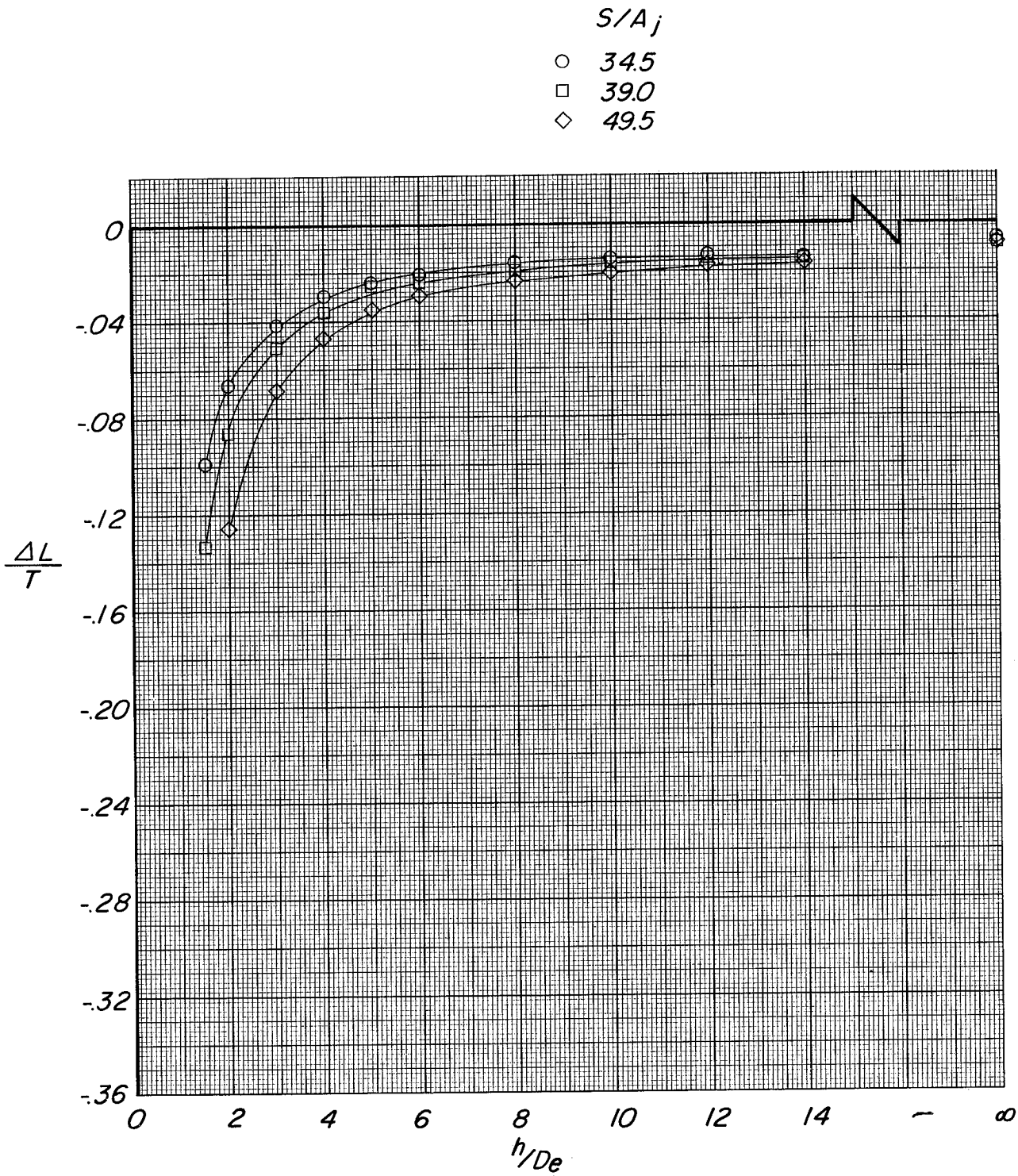

(c) $\frac{p_{t,p}}{p} = 1.89$.

Figure 32.- Continued.

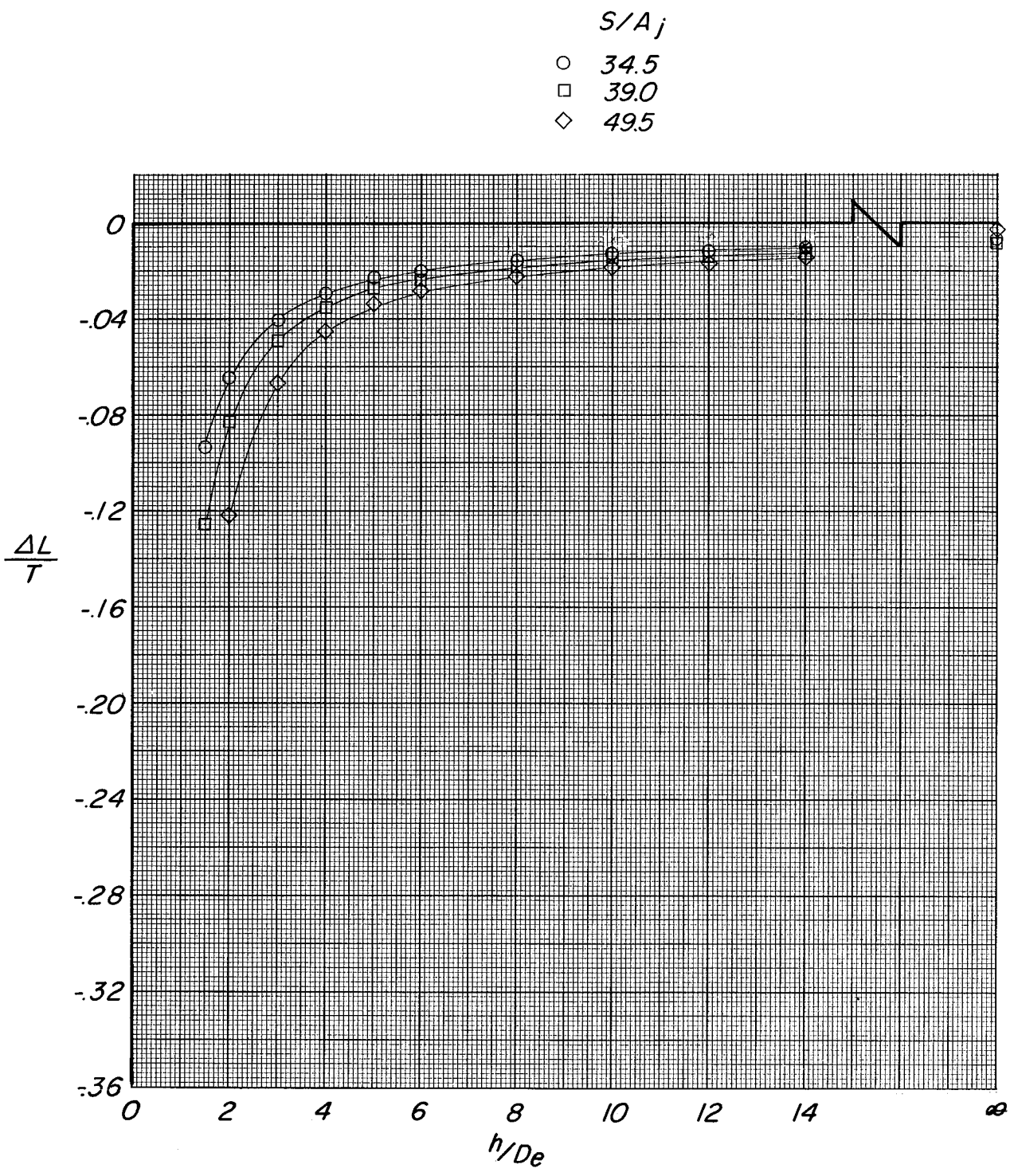

(d) $\frac{p_{t,p}}{p} = 2.08$.

Figure 32.- Continued.

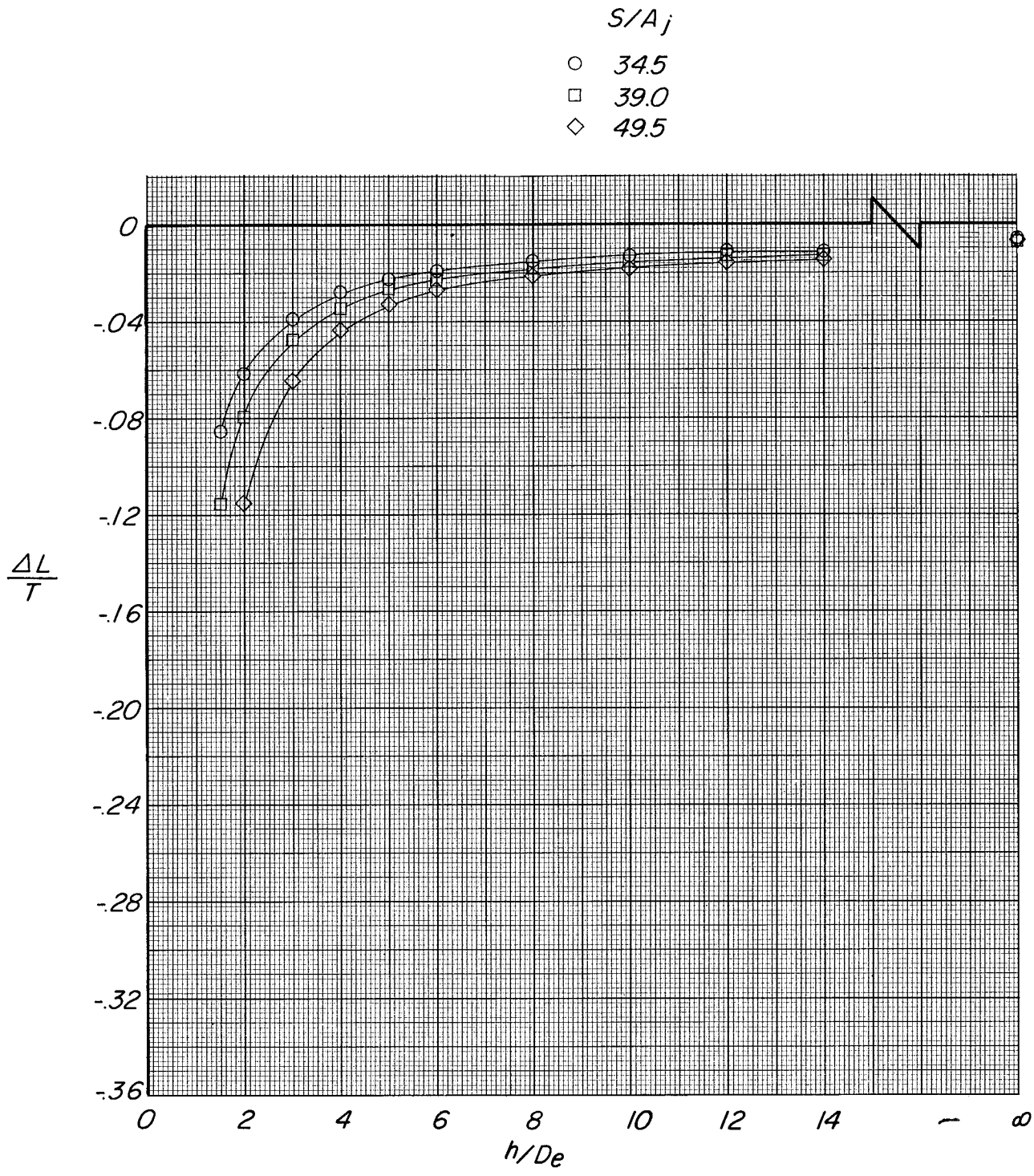

(e) $\frac{p_{t,p}}{p} = 2.35$.

Figure 32.- Concluded.

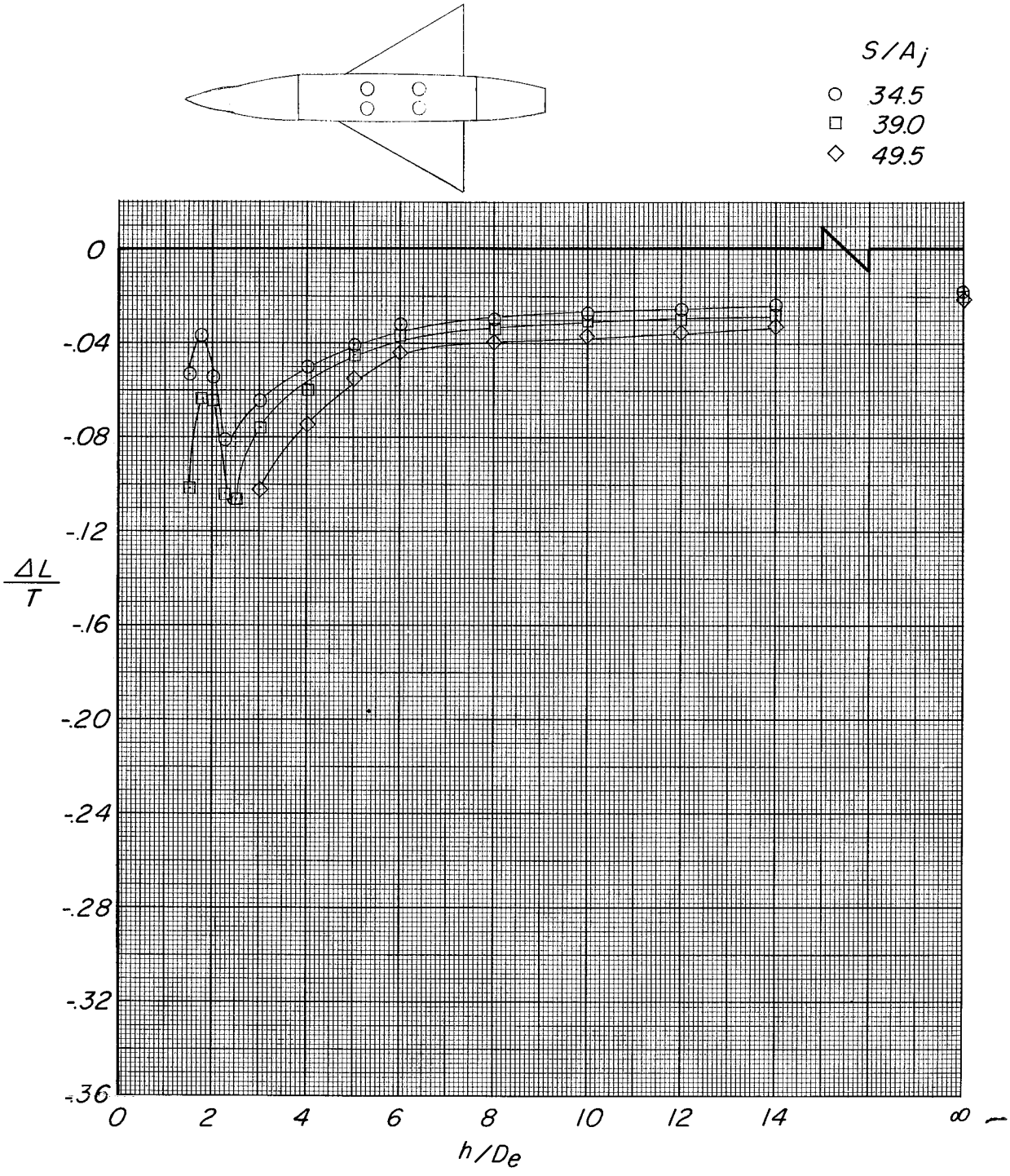

(a) $\frac{p_{t,p}}{p} = 1.338$.

Figure 33.- Effect of height above ground on $\frac{\Delta L}{T}$ as wing size increases for four-jet configuration.

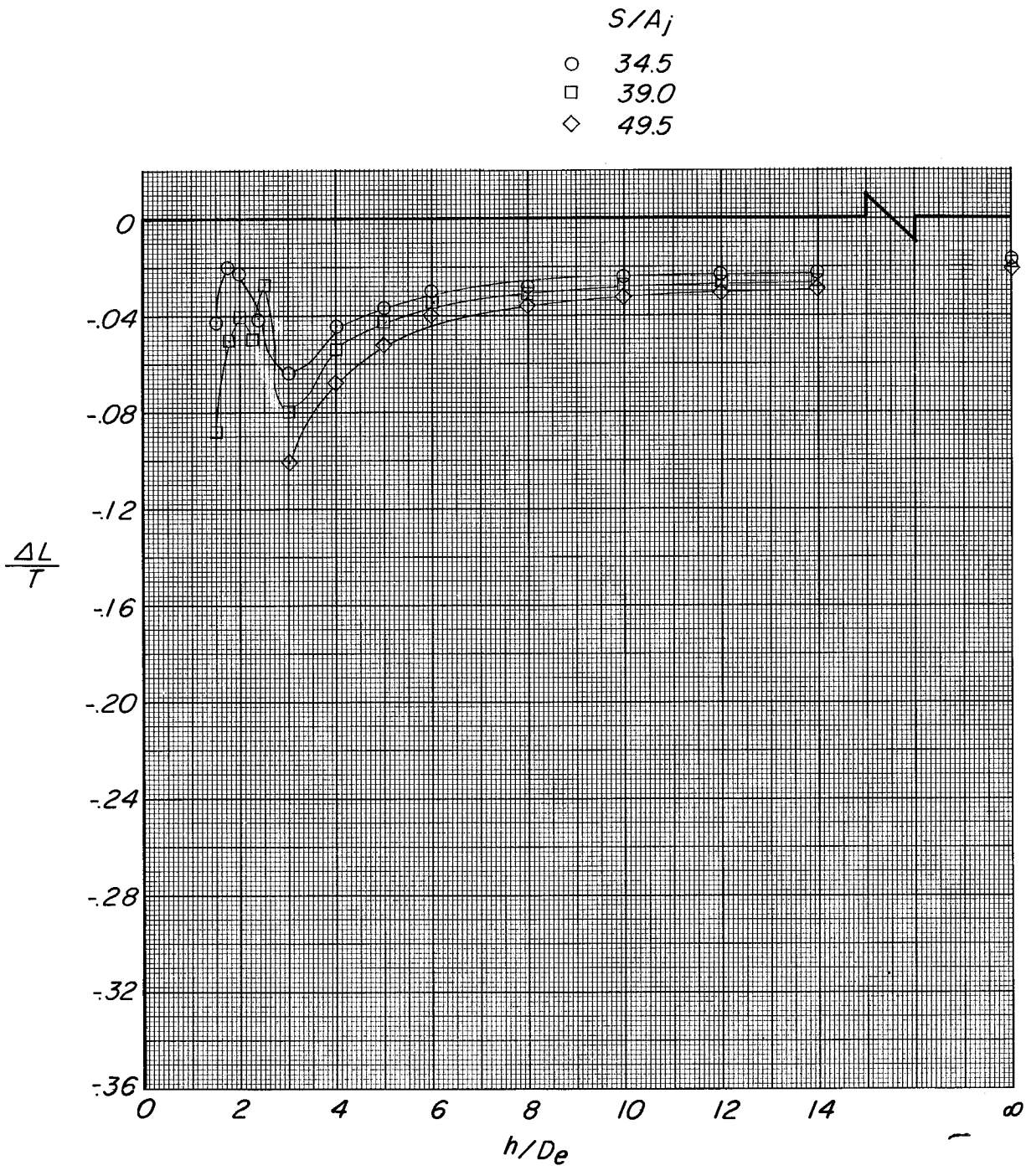

(b) $\frac{p_{t,p}}{p} = 1.677$.

Figure 33.- Continued.

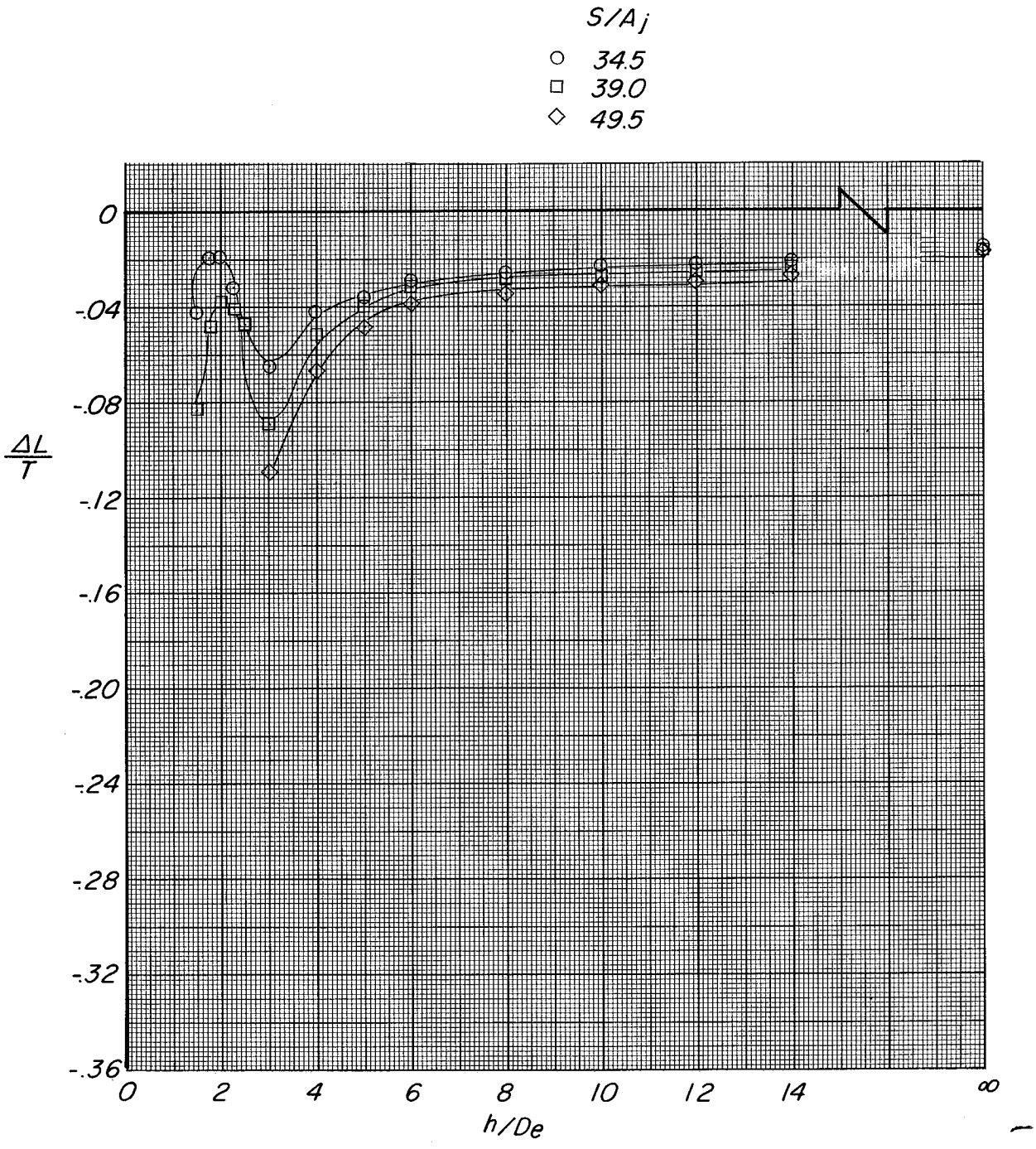

(c) $\frac{p_{t,p}}{p} = 1.89$.

Figure 33.- Continued.

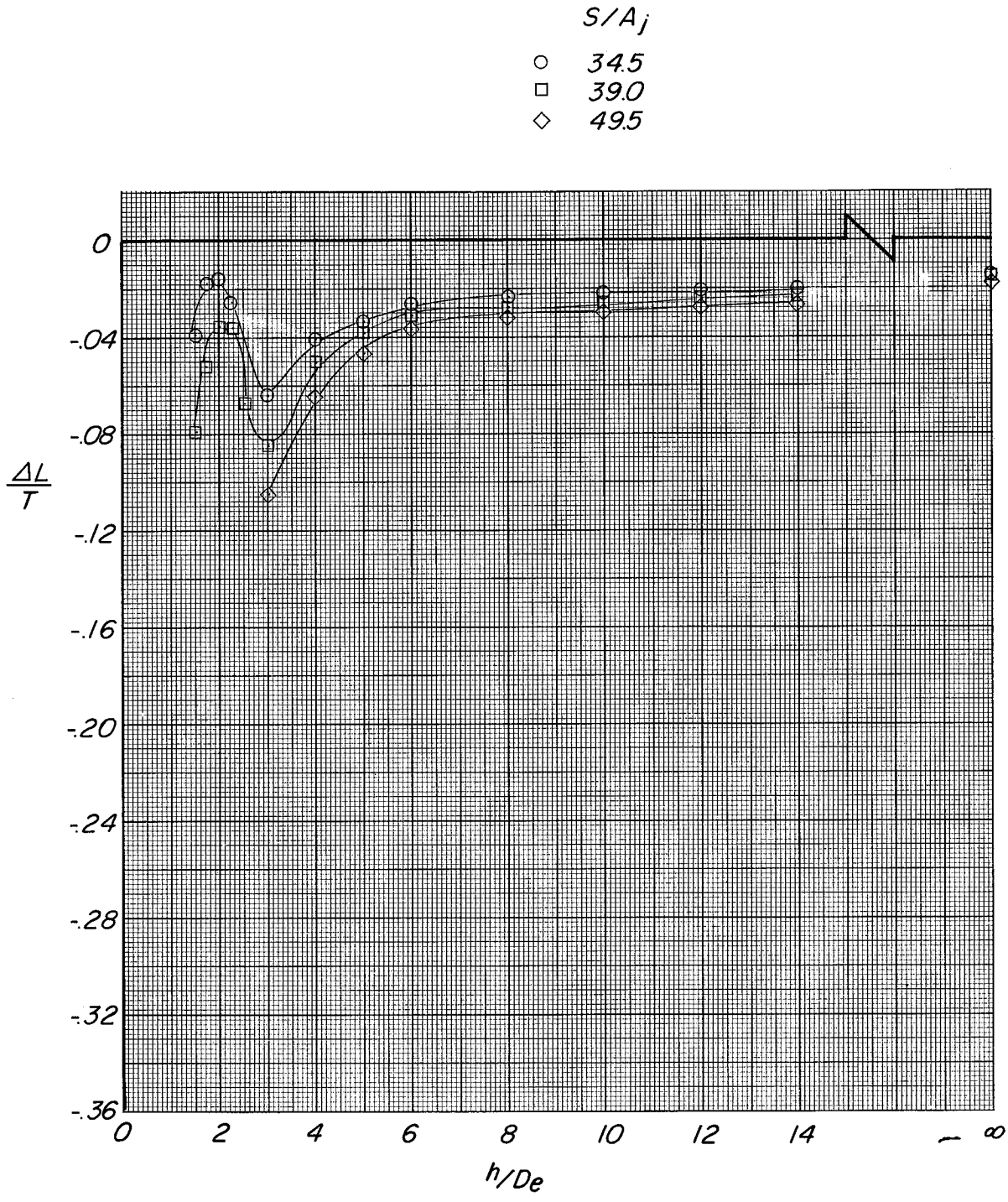

(d) $\frac{p_{t,p}}{p} = 2.08$.

Figure 33.- Continued.

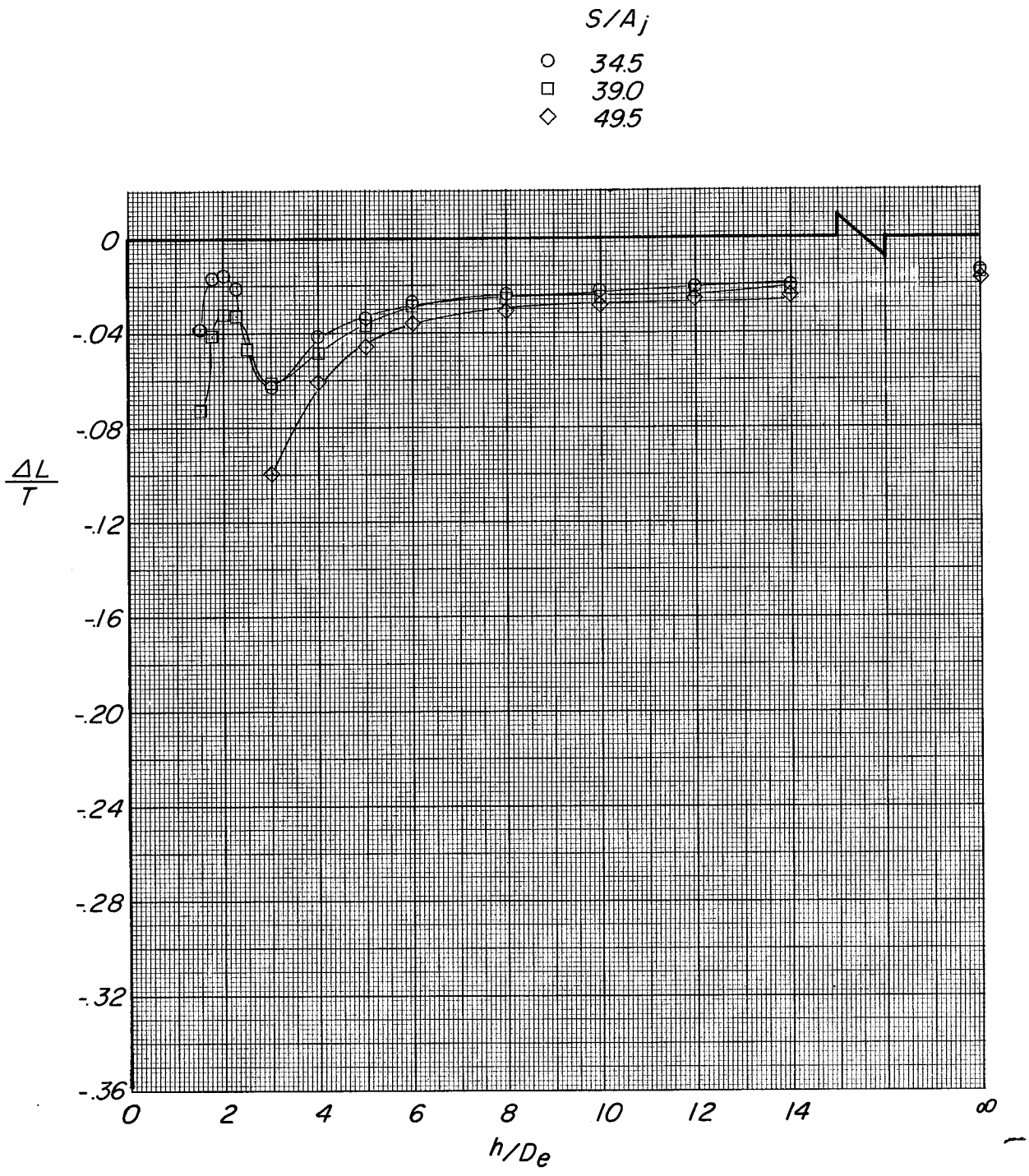

(e) $\frac{p_{t,p}}{p} = 2.355$.

Figure 33.- Concluded.

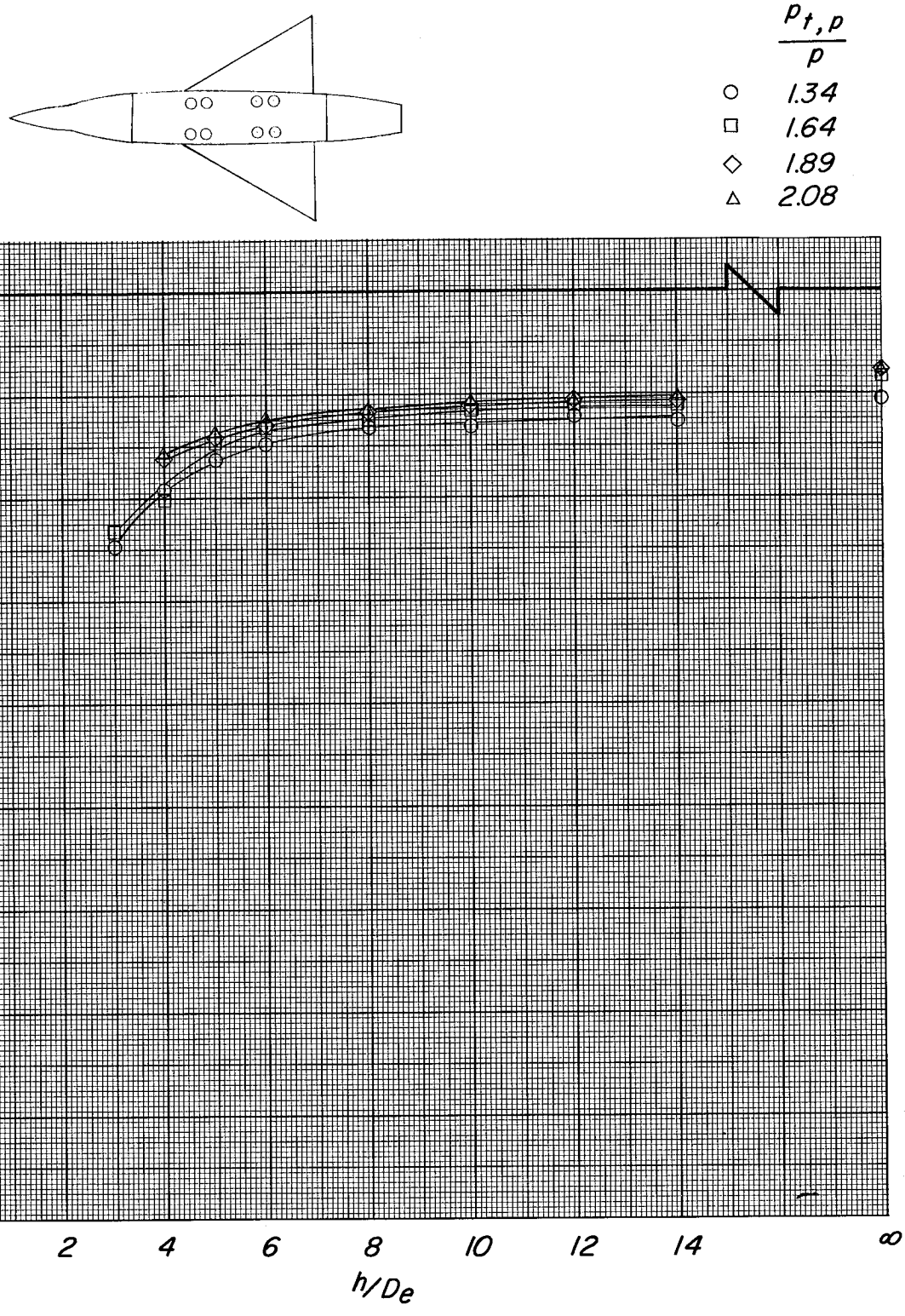

Figure 34.- Effect of height above ground on $\frac{\Delta L}{T}$ as pressure ratio increases for eight-jet configuration. $S/A_j = 49.5$.

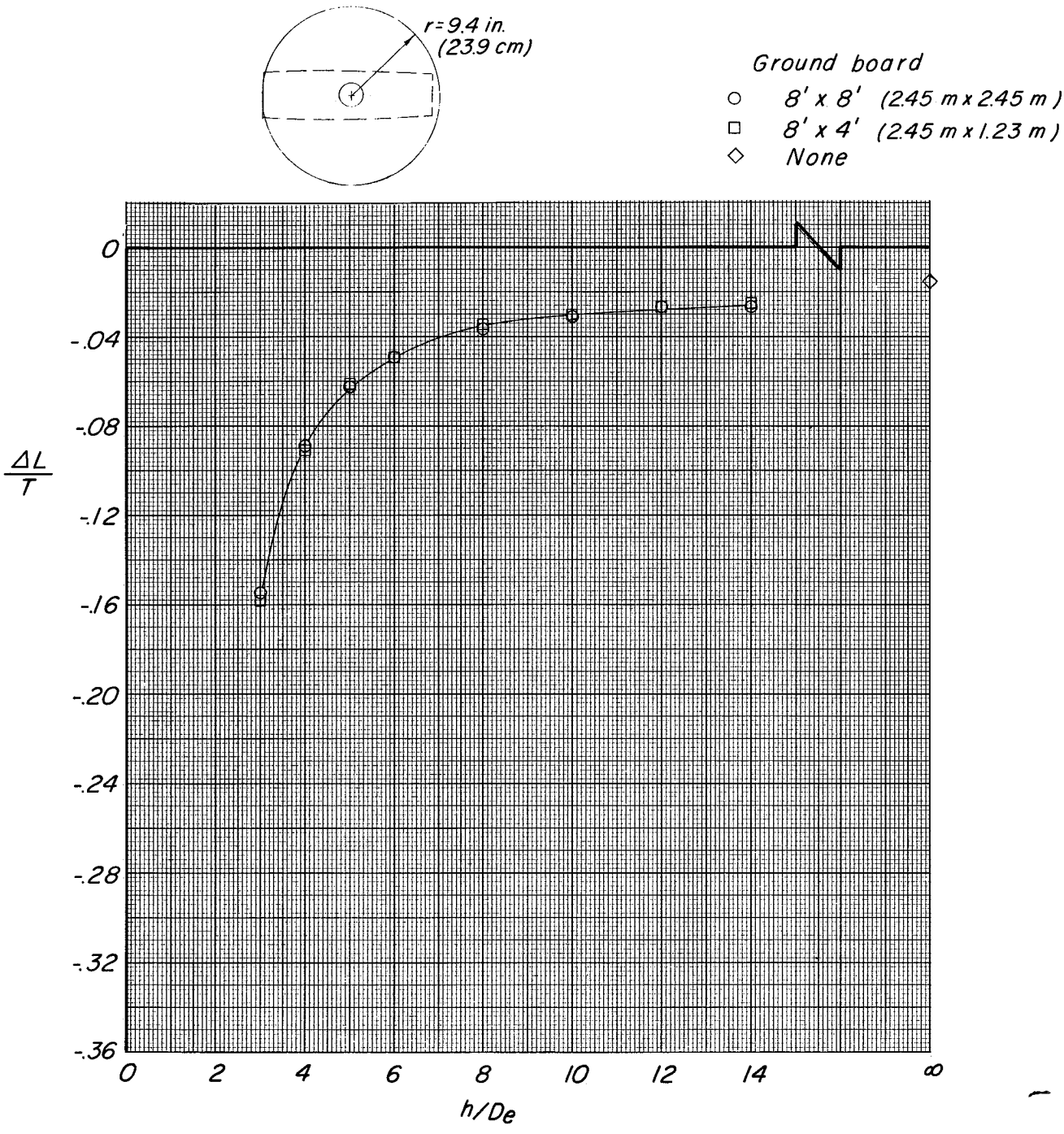

(a) $\frac{p_{t,p}}{p} = 1.34$.

Figure 35.- Effect of platform size used to represent ground. $S/A_j = 69.5$.

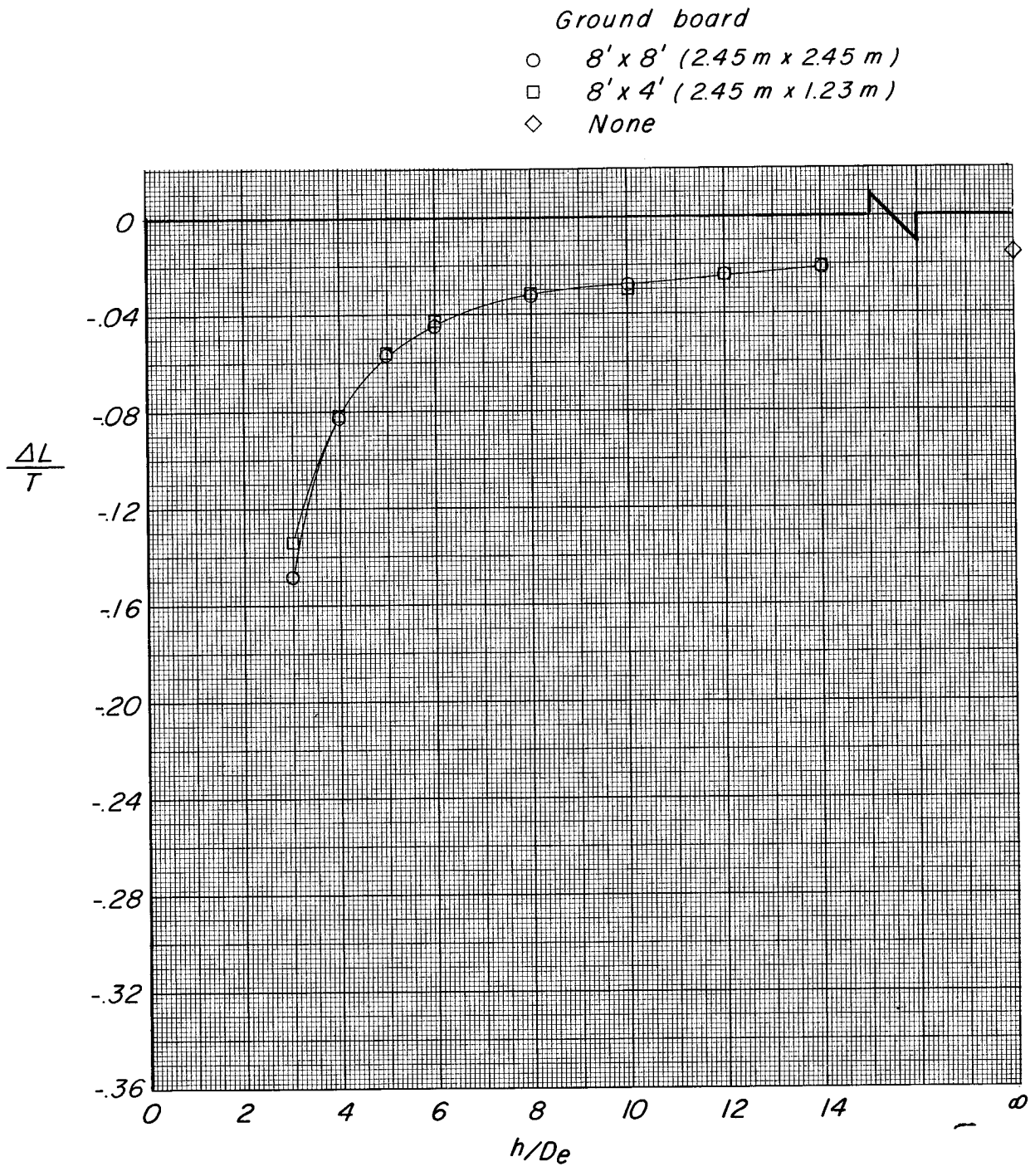

(b) $\frac{p_{t,p}}{p} = 1.89$.

Figure 35.- Continued.

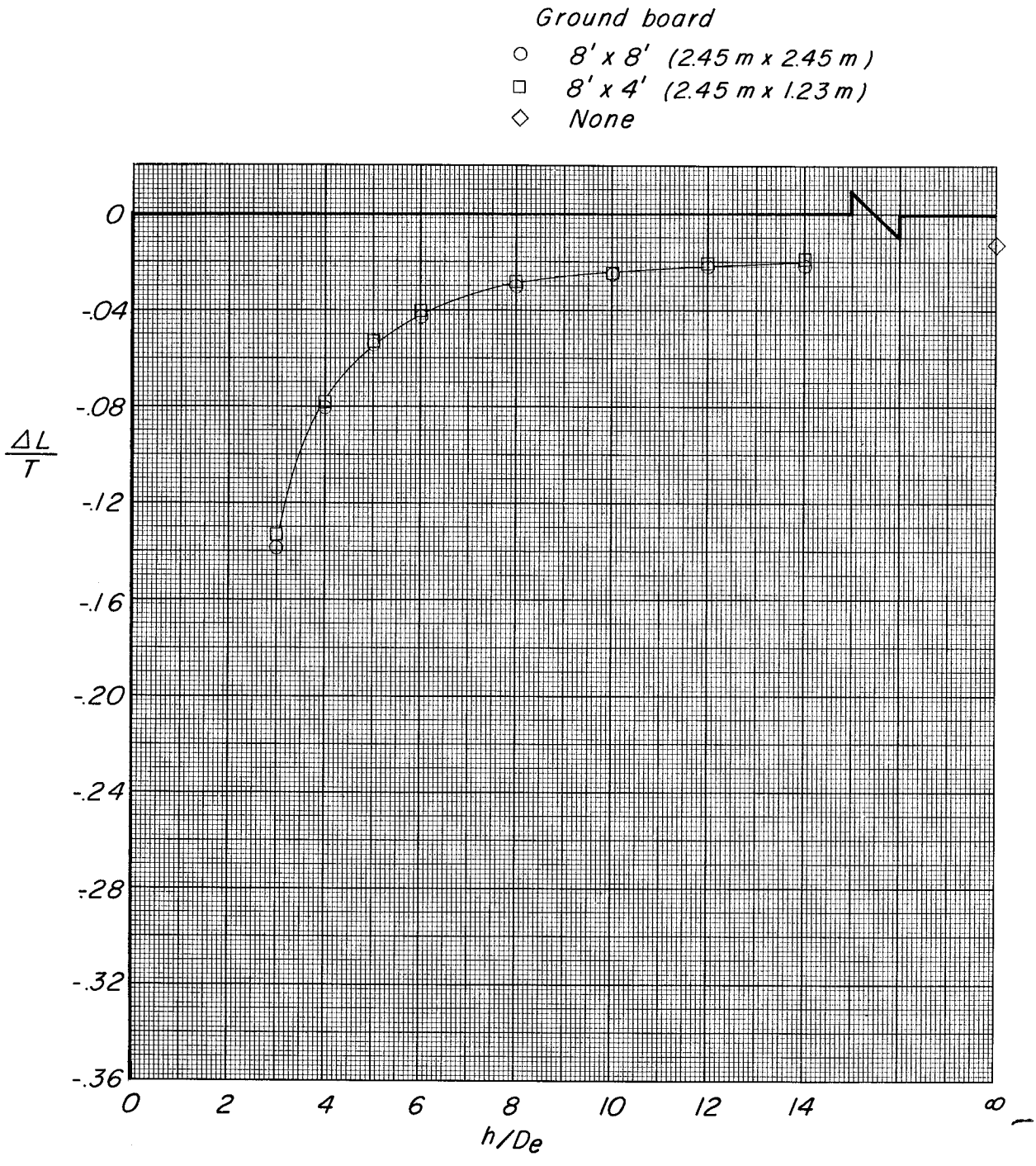

(c) $\frac{p_{t,p}}{p} = 2.36$.

Figure 35.- Concluded.

"The aeronautical and space activities of the United States shall be conducted so as to contribute . . . to the expansion of human knowledge of phenomena in the atmosphere and space. The Administration shall provide for the widest practicable and appropriate dissemination of information concerning its activities and the results thereof."

—NATIONAL AERONAUTICS AND SPACE ACT OF 1958

NASA SCIENTIFIC AND TECHNICAL PUBLICATIONS

TECHNICAL REPORTS: Scientific and technical information considered important, complete, and a lasting contribution to existing knowledge.

TECHNICAL NOTES: Information less broad in scope but nevertheless of importance as a contribution to existing knowledge.

TECHNICAL MEMORANDUMS: Information receiving limited distribution because of preliminary data, security classification, or other reasons.

CONTRACTOR REPORTS: Technical information generated in connection with a NASA contract or grant and released under NASA auspices.

TECHNICAL TRANSLATIONS: Information published in a foreign language considered to merit NASA distribution in English.

TECHNICAL REPRINTS: Information derived from NASA activities and initially published in the form of journal articles.

SPECIAL PUBLICATIONS: Information derived from or of value to NASA activities but not necessarily reporting the results of individual NASA-programmed scientific efforts. Publications include conference proceedings, monographs, data compilations, handbooks, sourcebooks, and special bibliographies.

Details on the availability of these publications may be obtained from:

SCIENTIFIC AND TECHNICAL INFORMATION DIVISION

NATIONAL AERONAUTICS AND SPACE ADMINISTRATION

Washington, D.C. 20546